AD NUMBER
AD509503
CLASSIFICATION CHANGES
TO: **UNCLASSIFIED**
FROM: **CONFIDENTIAL**
LIMITATION CHANGES
TO: **Approved for public release; distribution is unlimited.**
FROM: **Distribution authorized to U.S. Gov't. agencies and their contractors; Administrative/Operational Use; APR 1970. Other requests shall be referred to Naval Facilities Engineering Command, Washington, DC.**
AUTHORITY
USNCEL ltr 10 Jul 1973 ; USNCEL ltr 10 Jul 1973

AD 509.503

SECURITY MARKING

The classified or limited status of this report applies to each page, unless otherwise marked.
Separate page printouts MUST be marked accordingly.

THIS DOCUMENT CONTAINS INFORMATION AFFECTING THE NATIONAL DEFENSE OF THE UNITED STATES WITHIN THE MEANING OF THE ESPIONAGE LAWS, TITLE 18, U.S.C., SECTIONS 793 AND 794. THE TRANSMISSION OR THE REVELATION OF ITS CONTENTS IN ANY MANNER TO AN UNAUTHORIZED PERSON IS PROHIBITED BY LAW.

NOTICE: When government or other drawings, specifications or other data are used for any purpose other than in connection with a definitely related government procurement operation, the U.S. Government thereby incurs no responsibility, nor any obligation whatsoever; and the fact that the Government may have formulated, furnished, or in any way supplied the said drawings, specifications, or other data is not to be regarded by implication or otherwise as in any manner licensing the holder or any other person or corporation, or conveying any rights or permission to manufacture, use or sell any patented invention that may in any way be related thereto.

CONFIDENTIAL

DASA SC318

GROUP 1
Excluded from automatic
downgrading and declassification.

R677

Technical Report

OPTIMUM POSITIONING OF DEEP UNDERGROUND TUNNELS IN ROCK (U)

April 1970

Sponsored by

NAVAL FACILITIES ENGINEERING COMMAND

NAVAL CIVIL ENGINEERING LABORATORY

Port Hueneme, California

CONFIDENTIAL

Sponsored by DASA SC318

OPTIMUM POSITIONING OF DEEP UNDERGROUND TUNNELS IN ROCK (U)

Technical Report

YF 008.08.02.108

by

Joseph Rottgerkamp

ABSTRACT

The objective of this study was to find optimum design features for deep underground protective structures in rock. A computer program was developed to determine survival distance, optimum depth, total construction costs, and costs per usable volume for protective structures in rock. The program was applied to structures with inner radii of 3, 6, and 9 meters; concrete liners 0.5, 1, 2, and 3 meters thick and a steel liner 2.54 centimeters thick were investigated. In the example, the rock field was assumed to be either of sandstone or granite. The influence of the effective longitudinal seismic velocity between the detonation point and the structure was studied. Survival distances, survivabilities, optimum depths, and pertinent costs were found for true surface bursts of 100 and 1,000 kilotons.

It was found that a concrete structure in sandstone can provide full protection against a weapon yield no larger than 100 kilotons, and then only if the structure has a sufficient soil cover. Full protection against a weapon yield of 100 kilotons is provided by a structure with a steel liner in granite irrespective of the composition and stratification of the rock above. Full protection against a weapon yield of 1,000 kilotons can be provided by structures with steel liners in granite, at depths less than 300 meters, only when the effective longitudinal seismic velocity between the detonation point and structure is 2,000 meters per second, or less. In all the cases where full protection cannot be achieved, the optimum depth is between 100 and 300 meters.

CONTENTS

INTRODUCTION

The purpose of this report is to:

1. Obtain, from fundamental solutions of mechanics and available test results, data on the protective ability of structures in rock,

2. Determine the construction costs, and

3. Establish the costs for various levels of protection.

The protective ability of a structure can be measured by the distance between the structure and the point of a nuclear detonation. If the accuracy of the attacking weapon system is taken into account, the protective ability can be expressed by the probability of survival (the survivability). Both the survival distance and the survivability are dependent upon:

1. Characteristics of the attacking weapons,

2. Geological environment, and

3. Structural design.

These factors are embodied in a computer program and an example configuration is used to illustrate the influence of the principal parameters on the survival distance, survivability, and cost effectiveness.

Different optimum configurations exist for underground protective structures because of various weapon characteristics, geological features, and structural geometries. The trend toward optimum conditions has to be found to establish guidelines for site selection and design and to determine the cost effectiveness for underground protective structures in rock, based upon military requirements.

For protection, the guidelines for site selection should contain numerical values for the significance of rock types and tectonic construction patterns. Guidelines for designing underground protective

structures should contain the optimum depth, size of cross section, type of liner material, and liner thickness for the various cases. The economic evaluation should indicate, for a particular protective purpose, whether it is better to have one structure of a higher single-shot survivability and higher unit cost, or to have several structures of lower single-shot survivability and lower costs. An economic evaluation also might determine, to some extent, the most economical direction for further studies. No single source containing solutions or information on the entire problem was found in a survey of available unclassified literature on the design of protective structures in rock. However, many books, reports, and papers together contained all the parts of the problem. The main informational sources for this research were:

1. Reference 1—rock mechanics,

2. Reference 2—statically caused stress distribution around openings, and

3. Reference 3—dynamically caused stress distribution around openings.

Since References 2 and 3 were basic to the information in this report, both static and dynamic load on underground protective structures were considered so the influence of the structural depth could be studied. However, the application of References 2 and 3 placed an important limitation on this investigation; that is, that the liner material and the surrounding rock up to a thickness of 3 cavity diameters is assumed to behave elastically.

In spite of this limitation, the computational procedure based on the elastic behavior of material is of theoretical and practical significance. It is the first step toward improved procedures that may include the plastic range, and it can be used directly for designing protective structures capable of resisting several attacks. The second limitation placed on this study is that only the directly induced ground shock is taken into account. Consequently, this report deals only with protective structures located at depths in which only the directly induced ground shock is critical.

Optimum conditions are ascertained by seven major steps:

1. Determination of the stress distribution around the opening in the liner and in the surrounding rock,

2. Determination of the stress-dependent strength of the liner and the surrounding rock,

3. Determination of the survival distance,

4. Determination of the survivability, based on survival distance between detonation point and structure,

5. Determination of the gross construction costs and costs per usable volume unit, based on the allowable design dimensions of the structures and the construction procedures,

6. Assembly of a computer program, and

7. Determination of optimum design conditions.

THEORY

Determination of Stress Distribution

The load on an underground protective structure consists of residual forces in the rock body, the weight of the overburden, and the ground shock. Since they are unpredictable, residual forces have been neglected for this feature study. However, residual forces may be introduced, as in overburden, into the stress computation if they can be measured in a particular case.

The weight of the overburden is to be considered not only because of its contribution to the stress distribution around the opening but also because of its effects on the strength of rock and liner materials.

Determination of Stresses Caused by Overburden. To compute the stress distribution caused by the static load of the overburden weight, Savin's[2] solution was used. His solution is the only one known that considers a plane distributed load on a lined circular opening in an elastic field. Other solutions, as in Reference 1, are related to a circular distributed load.

The equations of the stresses are given in Appendix A. The influencing factors are depth of the structure, inner radius of the liner, outer radius of the liner, specific gravity of rock, Poisson's ratio of rock, Poisson's ratio of the liner material, elastic modulus of rock, and elastic modulus of the liner material.

The stresses caused by the overburden may reach the yield stresses. Thus, the computer program is organized so that the first computed static stresses are checked against the yield stresses before the dynamic load is brought into play.

Determination of Stresses Caused by Ground Shock. The stresses caused by ground shock are determined in two steps by deriving, first, the impinging pressure pulse and, second, the time-dependent stress distribution.

Determination of Pressure Pulse. The empirically based procedure in Reference 4 is used to calculate the peak radial particle acceleration, peak radial particle velocity, and peak radial displacement of the free field at the location of the structure. According to Hugoniot's Equation, the free-field stresses are approximately proportional to the particle velocity in the elastic range:[4]

$$\sigma = \rho \cdot c_{\alpha} \cdot v$$

where σ = free-field stress

ρ = density

c_{α} = longitudinal seismic velocity

v = particle velocity

The plots of velocity-time dependence and pressure-time dependence can be assumed to be triangles as shown in Figure 1.

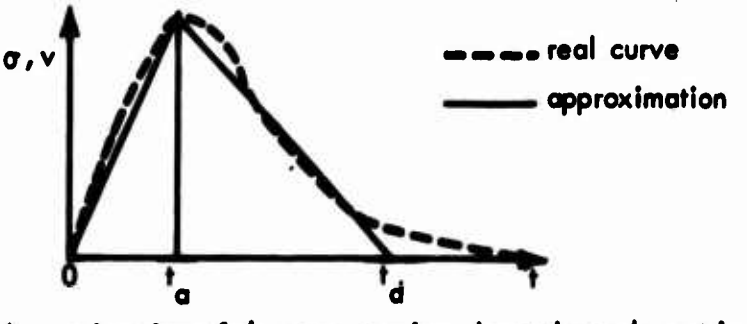

Figure 1. Approximation of the pressure-time dependence by a triangle.

The impinging pressure pulse is fixed with these approximations:

$$\sigma_{max} = \rho \cdot c_{\alpha} \cdot v_{max}$$

$$t_a = \frac{2 \cdot v_{max}}{a_{max}}$$

$$t_d = \frac{2 \cdot d_{max}}{v_{max}}$$

where σ_{max} = peak free field pressure

v_{max} = peak particle velocity

a_{max} = peak particle acceleration

d_{max} = peak radial displacement

Magnitude and history of the pressure pulse are dependent upon the energy coupling of the detonation, weapon yield, energy-conducting property of the rock, and distance from the detonation point. The energy coupling of fully contained bursts, contact surface bursts, and true surface bursts is provided in the computer program. Empirical formulas for the conversion of nominal weapon yields into effective weapon yields pertaining to these three kinds of detonations are given in Reference 4. The procedure for determining the pressure pulse is described in Appendix B.

The energy-conducting ability of the rock mass is represented in the empirical formulas for ground motion by the seismic velocity. In layered rock systems, the seismic velocity and the conductibility changes at each interface. Since the incident wave and all emergent waves are reflected and refracted at each interface, mathematically pursuing the complex energy flow is difficult and time consuming. Reference 5 provides an approximation using an effective seismic velocity for the rock body between detonation point and structure. The effective seismic velocity is defined as the quotient of the distance R_s and the shortest transit time from the point of detonation to the structure (Figure 2):

$$c_p = \frac{R_s}{t_{min}}$$

where c_p = effective seismic velocity

R_s = distance between point of detonation and structure

t_{min} = shortest transit time.

A method for determining the effective seismic velocity is described in Appendix C.

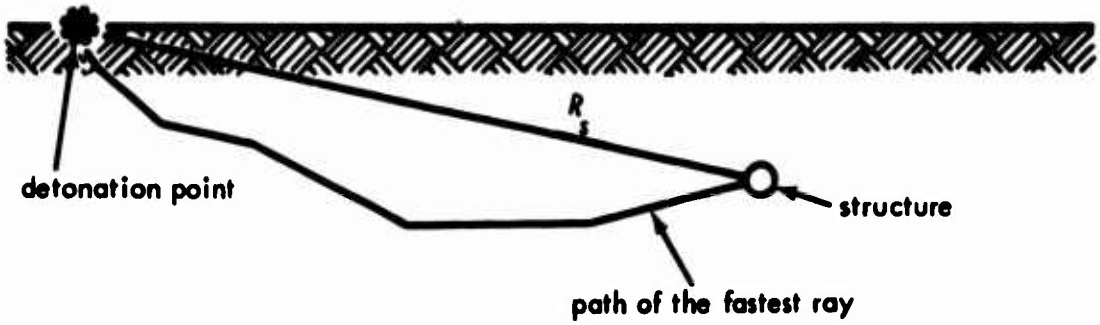

Figure 2. Layout for computing the effective seismic velocity for a layered system.

Determination of Dynamically Caused Stress Distribution. Mow[3] describes a solution for computing the stress distribution caused by a traveling harmonic wave in a liner of arbitrary thickness and in the medium around the liner. In spite of the analysis being limited to homogeneous and isotropic media strained within the elastic range, Mow's method was found to be accurate and promising for further development. Therefore, it was used for the computer program.

The previously mentioned limitation to the elastic range applies only to the medium in the vicinity of the opening (~3 diameters) and to the liner material. The computational treatment of the pulse propagation from the point of detonation to the vicinity of the structure is not based on the elastic behavior of the rock media.

Combining the choice of Mow's method with the assumption of homogeneous, isotropic, and elastic media, less energy-absorbing behavior is indicated than in real materials. This means that the application of Mow's solution regarding stress values is conservative.

The incident wave (Figure 3) is described by its potentials:

longitudinal wave $\phi = \phi_o \cdot e^{i(\alpha x - \omega t)}$

shear wave $\psi = 0$

where ϕ_o = amplitude

ω = circular frequency

α = ω / c_α = wave number

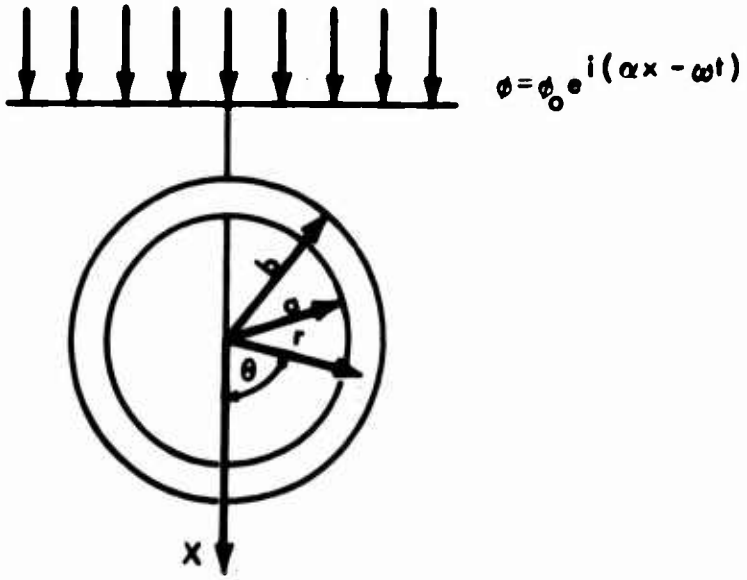

Figure 3. Tunnel liner with impinging stress wave.

The incident wave is reflected and refracted at the interface between rock and liner and is reflected at the inside of the liner. Each reflection and refraction causes a longitudinal and a shear wave that again can be reflected and refracted. All these waves contribute to the particular motions and to the stress distribution.

The boundary conditions that guarantee consideration of these waves are:

1. The radial stresses in the interface between rock and liner are equal,

2. The shear stresses in the interface between rock and liner are equal,

3. The radial displacements in the interface between rock and liner are equal,

4. The circumferential displacement in the interface between rock and liner are equal,

5. The radial stresses at the inner face of the liner are zero, and

6. The shear stresses at the inner face of the liner are zero.

These six boundary conditions are sufficient to solve the problem. The derivation of the stress equations is given in Appendix D.

The approximately triangular-shaped pressure pulse caused by the ground shock can be considered the sum of an infinite number of harmonic waves, as shown in Appendix E. The nonzero potential of the pressure pulse can be formulated by using the Fourier Integral:

$$\varphi(\omega) = \frac{1}{2\pi} \int_{-\infty}^{\infty} \phi(x, t)\, e^{i\omega t} \cdot \alpha t$$

The time-dependent potential ϕ (x, t) and the frequency-dependent potential $\varphi(\omega)$ can be computed for the pressure pulse by a method given in Reference 6. Stresses in terms of the potential are given in Appendix F. Subsequent retransformation of the stresses from the ω-space to the t-space leads to no major difficulties:

$$\sigma(x \cdot t) = \int_{-\infty}^{\infty} \sigma(x, \omega)\, e^{-i\omega t} d\omega$$

Superposition of Static and Dynamic Stresses. The calculation of static and dynamic stresses results in radial normal stresses, circumferential normal stresses, and shear stresses. As is permissible in the linear elastic case, the superposition is accomplished by summing the pertaining stresses:

$$\sigma_{r\,s} = \sigma_{r\ \text{static}} + \sigma_{r\ \text{dynamic}}$$

$$\sigma_{\theta\,s} = \sigma_{\theta\ \text{static}} + \sigma_{\theta\ \text{dynamic}}$$

$$\tau_{r\theta s} = \tau_{r\theta\ \text{static}} + \tau_{r\theta\ \text{dynamic}}$$

For further use, an advantage is having the principal stresses available. For the static, dynamic, and superimposed case, the principal stresses are determined by the equation:

$$\sigma_{1,2} = \frac{\sigma_r + \sigma_\theta}{2} \pm \frac{1}{2} \sqrt{4\tau_{r\theta}^2 + \left(\sigma_r - \sigma_\theta\right)^2}$$

Determination of Rock Strength and Liner Material

Mohr's Theory of Failure was chosen as failure criteria for both the rock and the liner material. The Air Force Special Weapons Center[7] and the Geological Society of America[8] published test results proving that the envelopes of Mohr's circles for most rocks can be considered straight lines. This simple relationship between the state of stress and the strength of rock, known as the Mohr-Coulomb-Navier's Theory, was accepted for the computer program. The equation for the allowable maximum principal stress is derived in Appendix G. The value of the allowable maximum principal stress is influenced positively by the minimum principal stress, the cohesive strength of the rock, and the angle of internal friction. The American Society for Testing Materials[9] recommends a curved line as Mohr's envelope for concrete. Following this proposal and information given by the Concrete Division of the Waterways Experiment Station in Vicksburg, Miss., the allowable maximum principal stress is taken as:

$$\sigma_{allowable} = \left[\frac{\sigma_2 - L}{M}\right]^{\frac{1}{N}}$$

where σ_2 = minimum principal stress

N = constant = 1.37

$L = f_t$ = tensile strength of concrete

$$M = \frac{f_t}{f_c^N}$$

f_c = compressive strength of concrete

In steel construction, the increase of strength with increasing confinement is not used for designing construction members. Information about Mohr's envelope of steel is given in Reference 10. The published test results do not show an angle of internal friction for steel. The envelope is parallel to the major stress axis; steel is considered a "von Mises" material. For computational convenience, the equation of Mohr's envelope for steel was written in the form of the corresponding equation for concrete:

$$\sigma_{1\ \text{allowable}} = \left[\frac{\sigma_2 - L}{M}\right]^{\frac{1}{N}}$$

where $N = M = 1$

$L = \phi F_y$ = yield stress of steel

Determination of Survival Distance

Since the strength of the rock and liner material depends on the state of stress in these media, a strength distribution as well as a stress distribution will occur around the underground opening. Therefore, it is necessary to check the state of stress against the state of strength around the opening. Should stress exceed strength anywhere at any time, the underground protective structure is considered a violation of the prerequisite condition of elastic behavior of all materials. As previously mentioned, the check of stress against strength is made twice for each point and time:

1. The state of stress caused by the overburden is checked against the strength, and

2. The state of stress caused by overburden and ground shock is checked against the strength.

If the first check is negative, the calculation will be stopped before the dynamic stresses are considered. The calculation also will be stopped if the second check is negative. A negative result for this second check means that the structure failed during ground shock. The computer program is organized in such a manner that the weapon, geology, and structure values, and the depth of the structure are kept constant for each calculation while the horizontal distance from the detonation point to the structure increases for each loop as long as the structure does not fail. The result of one calculation cycle is the horizontal survival distance for a preselected structure with given values of cross-sectional size, liner material, liner thickness, depth, geology condition, and threat attack procedures.

Determination of Survivability

The effectiveness of a protective structure is denoted by the single-shot survivability. Single-shot survivability means the probability

of survival of a protective structure undergoing a single attack.

For this determination of survivability, the entire structure is assumed to fail even if failure will occur only in one of its cross sections. The survivability is influenced by weapon values and system parameters. The main weapon values are the hit accuracy and the damage range. The hit accuracy is introduced into the computation of the survivability by the standard deviations of the weapons system in the longitudinal and transverse direction, respectively. If the standard deviations are the same in both directions, the accuracy of the weapon system is expressed by the Circular Error Probable (CEP). The relationship between standard deviation and CEP is:

$$\sigma = 0.84932 \text{ CEP}$$

The horizontal damage range of a weapon for a particular structure equals the horizontal survival distance of the structure calculated in the design computation. The horizontal survival distance R determines the aim area of the underground structure at the surface (Figure 4).

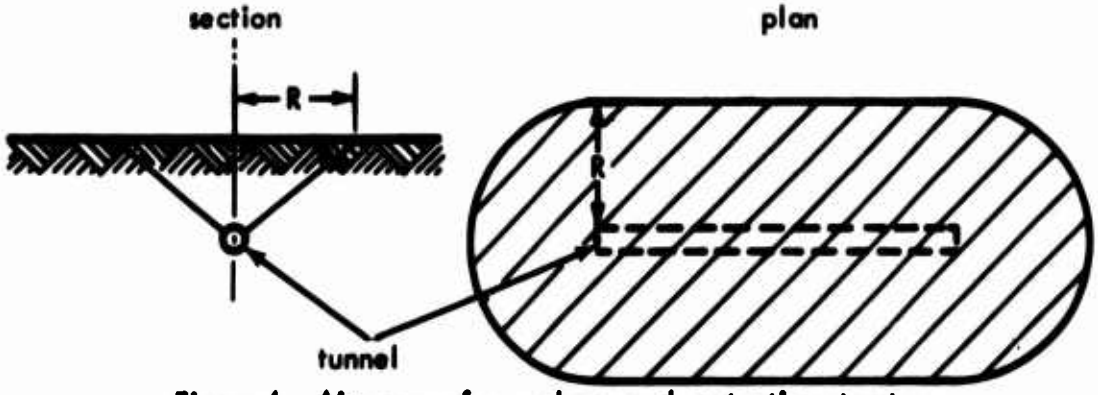

Figure 4. Aim area of an underground protective structure.

If the design weapon hits inside this area, the structure will fail. The calculation of the survivability is derived in Appendix H. For this derivation, References 11, 12, and 13 were used.

Determination of the Gross Construction Costs and Costs Per Usable Volume Unit

Information about estimating costs for tunnels in rock was given by the Department of Water Resources of the State of California[12] and the Metropolitan Water District of Southern California (unpublished guidelines). The information given by the Department of Water Resources

is based upon data compiled from 99 tunnel projects around the world. For the most part, this information was used in the computer program. The guidelines of the Metropolitan Water District were used as basic information about the costs of steel liner and for checking and updating the figures furnished by the Department of Water Resources.

The cost estimation procedure is due specifically to conventional tunneling methods. Under certain limitations, machine excavating costs for tunneling are estimated at 60% of the costs of conventional excavating. This estimate is based on information given in Reference 15.

The total construction costs are the sum of the costs for a main tunnel, access tunnels, and access shafts. The total cost for each structure comprises liner costs and excavation costs. The liner costs are calculated by "unit costs in place." The excavation costs are specified in costs of labor, equipment, energy, explosives, drill bits, and rods. The specified costs are classified according to the size of tunnel sections and according to rock strength. The rock strength has been described thus:

Type 1: Dry, massive, moderately jointed or dry intact rock

Type 2: Dry, stratified or schistose rock

Type 3: Dry, moderately blocky and seamy rock

Type 4: Dry, very blocky and seamy rock.

This classification has to be expressed numerically to be used in the computer program. The approximate numerical classification assumed for the program is based on the cohesive strength of rock:

Type 1: $K \geq 200\ kp/cm^2$

Type 2: $200\ kp/cm^2 > K \geq 100\ kp/cm^2$

Type 3: $100\ kp/cm^2 > K \geq 50\ kp/cm^2$

Type 4: $50\ kp/cm^2 > K$.

Besides the variables of tunnel length and radius, the provision of machine tunneling depends upon the kind of rock. The limits[15] of machine tunneling are assumed as:

$$180 \text{ kp/cm}^2 > K > 60 \text{ kp/cm}^2$$

$$L > 2000 \text{ m}$$

$$b < 5 \text{ m}$$

where L = length of the tunnel

b = outer radius of the tunnel

Comparable unit construction costs are obtained by dividing the total construction costs by the usable volume of the main tunnel. A measure of the cost effectiveness of the protective structures is the quotient of unit construction costs per unit of survivability:

$$C_{eff} = \frac{C}{V_{us} \cdot S}$$

where C_{eff} = cost effectiveness

C = total construction costs

V_{us} = usable volume

S = survivability

Since $n = 1/S$, the number of structures necessary to provide 100% survivability for one of them, the cost effectiveness quotient can be interpreted as the costs for sure protection of one unit. The cost computation procedure is derived in Appendix I. In all the cost equations, an adjustment factor is provided for updating and transforming into foreign currencies.

COMPUTER PROGRAM

Many portions of the analysis do not require the effective seismic velocity between detonation point and structure location. So, in the interest of economy and clarity, two separate programs were written. The main program computes the survival distance, the survivability, and the economic features. The second program determines the effective seismic velocity between detonation point and structure location in a layered rock system. The second program can be introduced easily into the main program as a subroutine.

Both programs are written in FORTRAN IV language. The time necessary for one run of the main program using the CDC 6600 is 40 seconds. The description, the flow chart, and the listing of the main program is given in Appendix J. The flow chart and the listing of the program for computing the effective seismic velocity of a layered rock system is given in Appendix K.

DETERMINATION OF OPTIMUM DESIGN CONDITIONS

Example of Protective Structure

The total structure consists of the main tunnel, the two access tunnels, and the two shafts (Figure 5) with lengths:

Length of the main tunnel	100.0 m
Total length of the access tunnels	100.0 m
Inner radius of the access tunnels	2.0 m
Inner radius of the shafts	2.0 m
Inner radius of the main tunnel	Variable

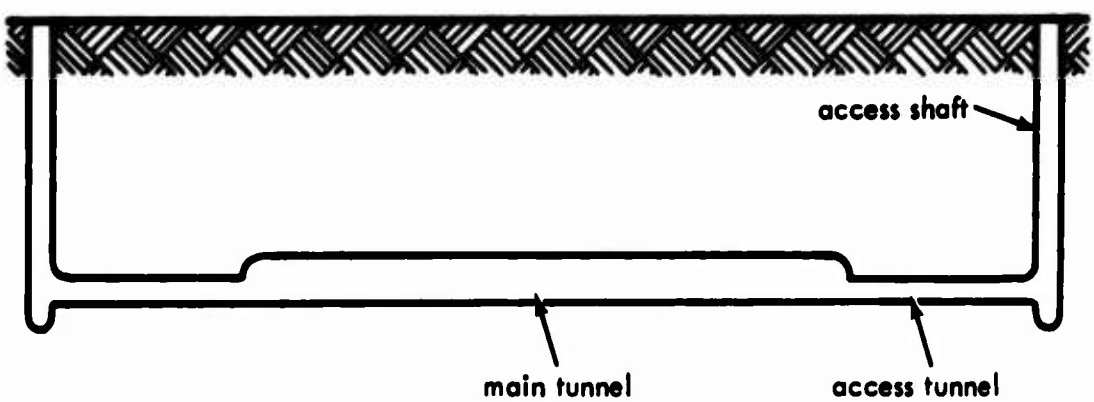

Figure 5. Configuration sample for an underground protective structure in rock.

The main tunnel, access tunnels, and access shafts are lined by the same material, either reinforced concrete or steel. The liner thickness T_a of the access tunnels is:

$$T_a = \frac{T_m \cdot R_a}{R_m}$$

and at least 15.0 centimeters for concrete of 1.27 centimeters for steel where T_m = liner thickness of the main tunnel

R_m = inner radius of the main tunnel

R_a = inner radius of the access tunnels

The thickness of the shaft T_s liner is:

$$T_s = 1.5 \cdot T_a$$

and at least 20.0 centimeters for concrete or 1.91 centimeters for steel. These determinations are based on rules of conventional mining and engineering. For reinforced concrete liner, these properties are assumed.

Compressive strength	350 kp/cm^2 (5,000 psi)
Reinforcement ratio	1%
Tensile strength	50 kp/cm^2
Specific gravity	2.4
Poisson's ratio	0.19
Elastic modulus	$3.5 \cdot 10^5$ kp/cm^2

The properties for the steel liner are:

Yield stress	$2.52 \cdot 10^3$ kp/cm^2 (36,000 psi)
Specific gravity	7.85
Poisson's ratio	0.25
Elastic modulus	$2.05 \cdot 10^6$ kp/cm^2

Two conditions for the rock were assumed:

1. The entire rock body between detonation point and structure location consists of the same rock type.
2. The earth body under consideration consists of different rock types or upper layers of soil.

For both cases, a particular sandstone and a particular granite were selected as the directly surrounding structure. The properties of the sandstone are:

Specific gravity	2.5
Poisson's ratio	0.15
Elastic modulus	$3.0 \cdot 10^5$ kp/cm^2

Longitudinal seismic velocity	3,525 msec
Factor of internal friction	1.5
Cohesive strength	100 kp/cm^2
Tensile strength	30 kp/cm^2

The properties of the granite are:

Specific gravity	2.6
Poisson's ratio	0.20
Elastic modulus	$4.0 \cdot 10^5$ kp/cm^2
Longitudinal seismic velocity	4,100 m/s
Factor of internal friction	1.5
Cohesive strength	140 kp/cm^2
Tensile strength	60 kp/cm^2

The detonation is assumed to be a true surface burst. Computations are made for 100- and 1,000-kiloton weapon yields. The protective structure is considered to be the target itself; the middle of its target area is Desired Ground Zero. The CEP of the attacking system is assumed to be 402.25 meters (quarter of a mile). In subsequent comparisons, the influence of rock type, liner material, liner thickness, and cross-sectional size are presented.

Optimum Design Conditions in a Rock Body of the Same Rock Type

Protective Structures with Concrete Liner in Sandstone. For an inner radius of the main tunnel of 6 meters and a weapon yield of 100 kilotons, the concrete liner thickness was varied from 0.5 to 3 meters as a function of survivability. The survivability, which is dependent upon the structure depth, is shown in Figure 6. The increasing liner thickness does not affect significantly the survival distance for values between 110 and 120 meters and a survivability of about 92%.

The curves of Figure 6 show that only in the depth range from 50 to 100 meters does the survival distance decrease with an increase of depth. Further increases in depths beyond 100 meters are not advantageous. Figure 7 illustrates the total costs for protection. The lower parts of the curves represent the depth range from 50 to 100 meters. Increased expenditure in this range results in more protection, in a decrease of survival distance, and in an increase of survivability.

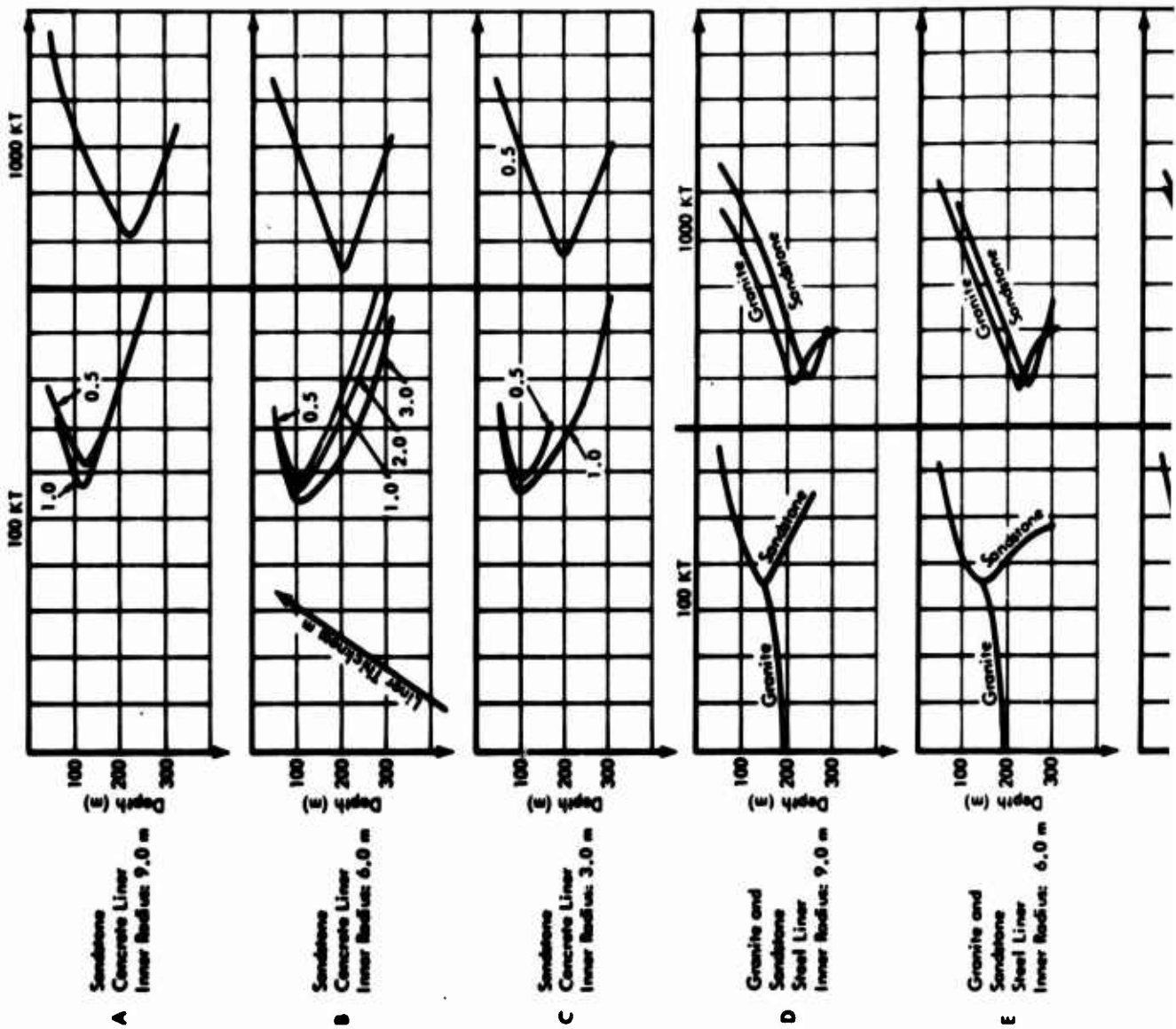

Figure 6 (C). Survival distance in a rock body of the same rock type (U).

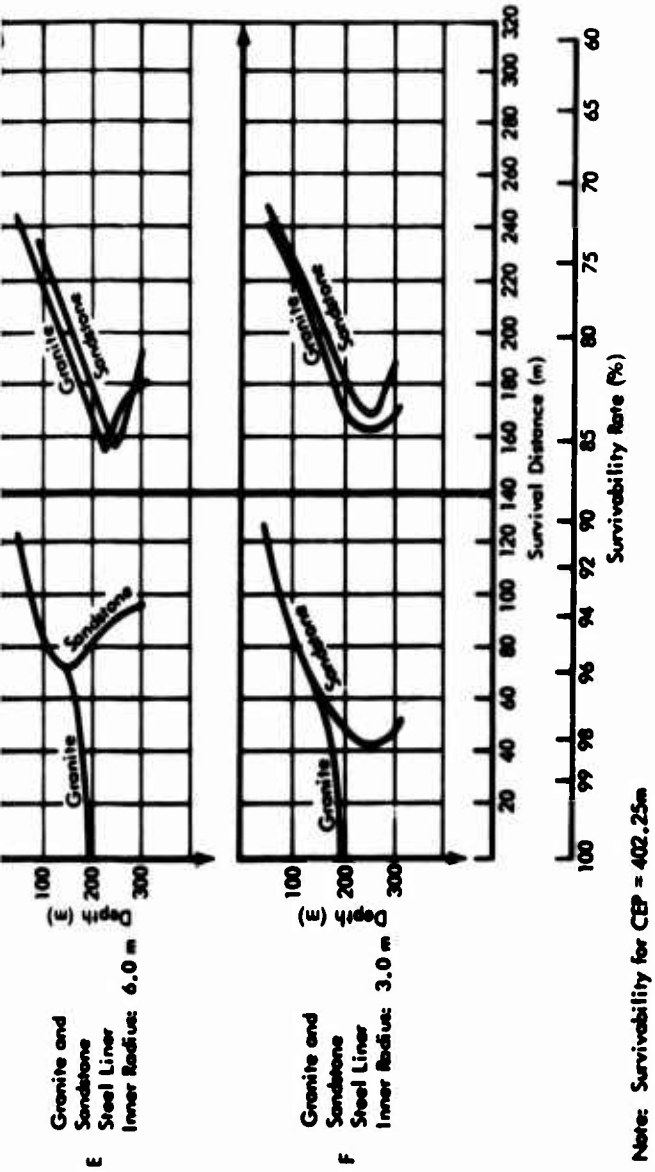

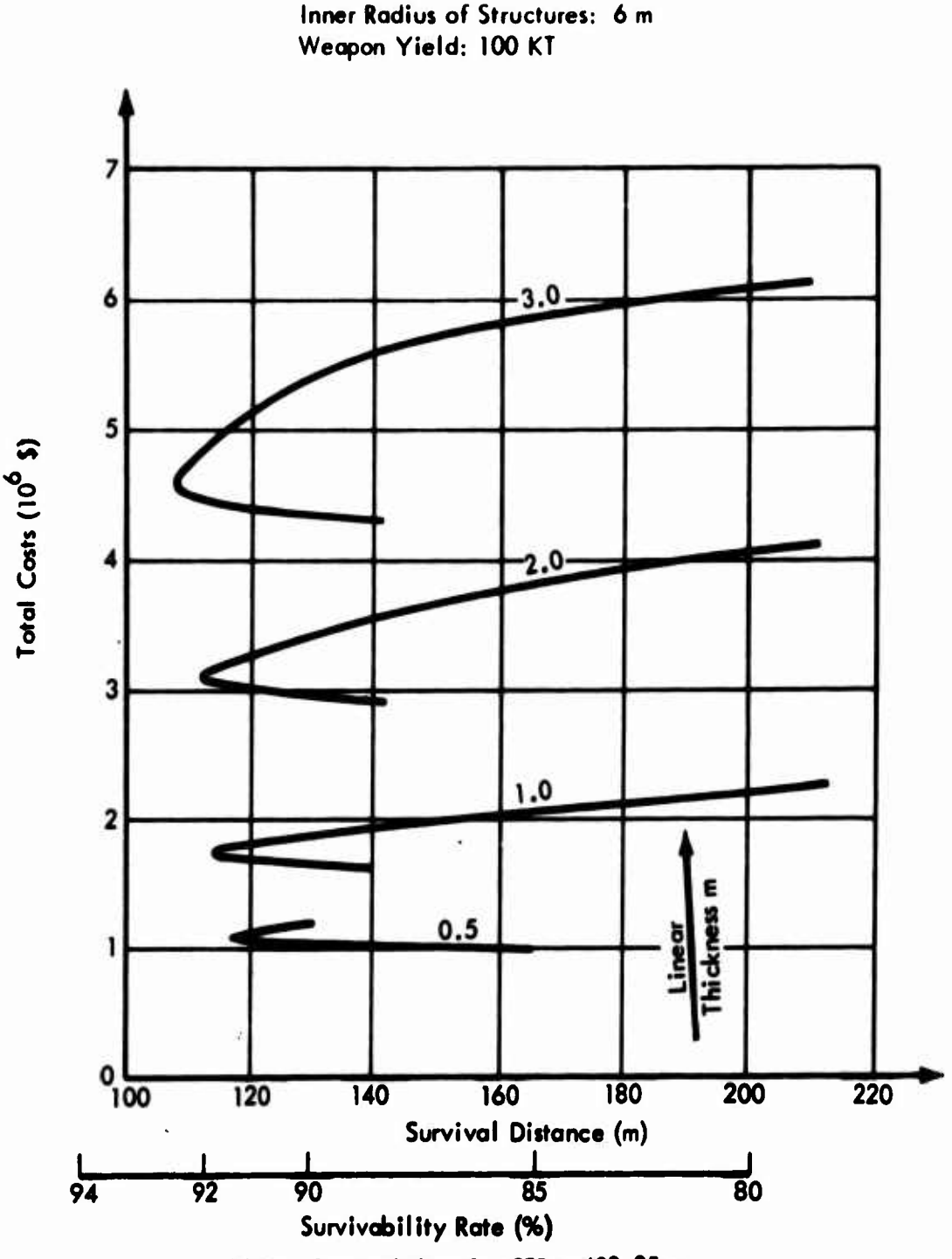

Note: Survivability for CEP = 402.25 m

Figure 7 (C). Total costs for concrete structures in sandstone with different liner thicknesses (U).

Obviously, the slope of the curve for the liner thickness of 0.5 meter is less than the others. This means:

1. For the same amount of additional money, the structure with the smaller liner thickness offers more additional protection.

2. Planning concrete structures with a liner thickness of 0.5 meters for a survivability of 50% is not economically reasonable since a relatively small increase in the cost increases the survivability to 91%.

Figure 8 exhibits the cost per usable volume and the costs per usable volume related to the survivability. The difference between these two cost values is smallest for the liner thickness of 0.5 meter and thus demonstrates the economic superiority of this design feature as compared to the others. Considering the previously mentioned advantages, only the liner thickness of 0.5 meter was chosen for a comparative study of the cross-sectional sizes of concrete structures having inner radii of 3, 6, and 9 meters.

Figure 6 shows that within the range considered, the section radius does not have a substantial influence on the survival distance and survivability. The figure also shows that the optimum depth (optimum in relation to the survival distance and survivability) changes only slightly with the cross-sectional size (the optimum depth values for the inner radii of 6 and 3 meters can be considered the same). The optimum depth for the inner radius of 9 meters is about 120 meters for a weapon yield of 100 kilotons and about 220 meters for a weapon yield of slightly 1,000 kilotons deeper than the others having a depth of 100 and 200 meters, respectively. Figure 6 makes numerically comprehensible the influence of the weapon yield on the survival distance and survivability. The survival distance of concrete structures increases from 120 meters for 100 kilotons to 220 meters for 1,000 kilotons. Assuming the CEP equals 402.25 meters, the survivability decreases from about 92 to 77%. This means a change from a high to a medium survivability. The difference in the survivability becomes even larger when the CEP of the attacking system is smaller.

Figure 6 illustrates that the larger weapon yields require a greater depth for optimum survival distance. The economic aspects of varying the cross-sectional size is illustrated in Figures 9 and 10. Considering the total cost, the structure with the inner radius of 3

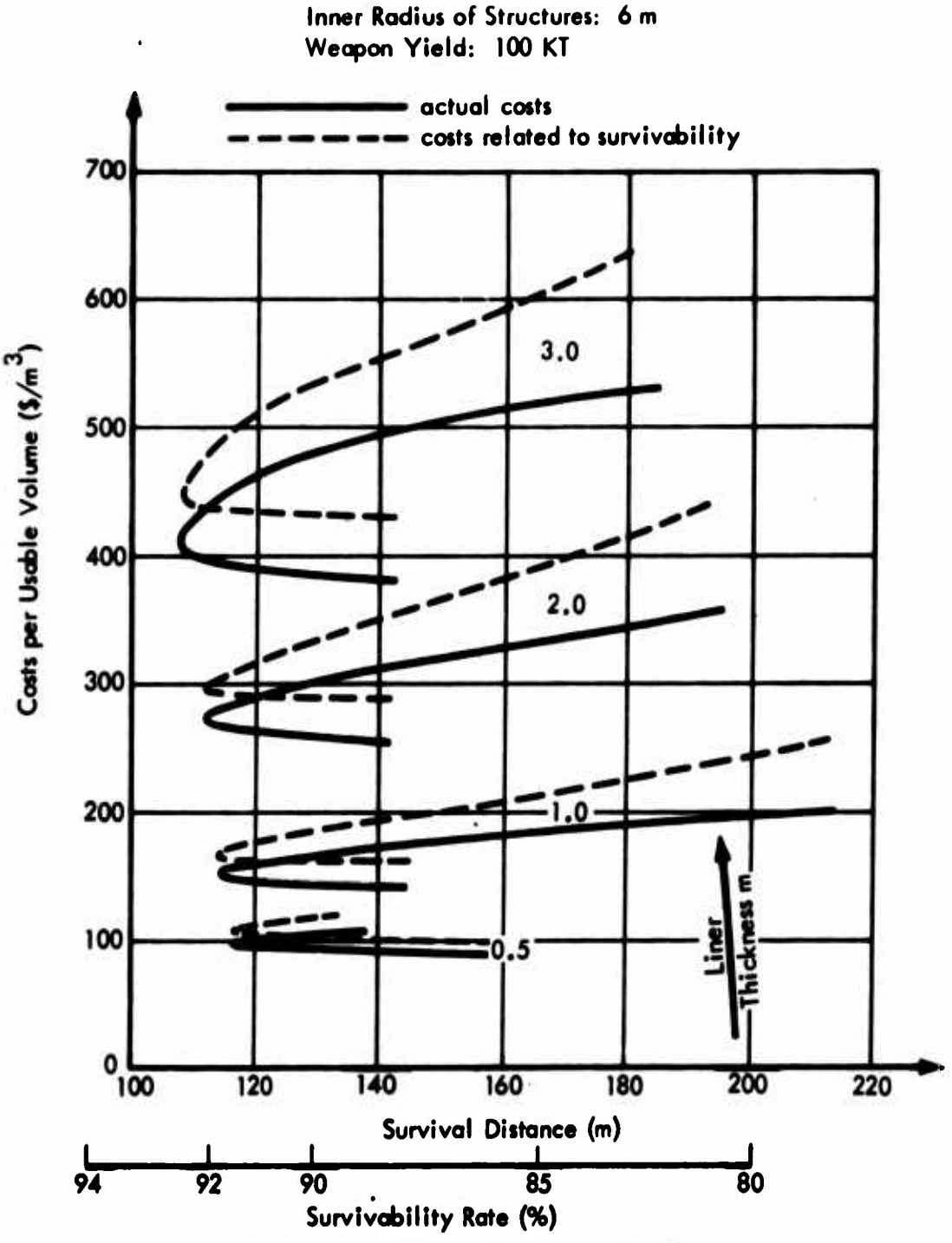

Note: Survivability for CEP = 402.25 m

Figure 8 (C). Costs per usable volume for concrete structures in sandstone with different liner thicknesses (U).

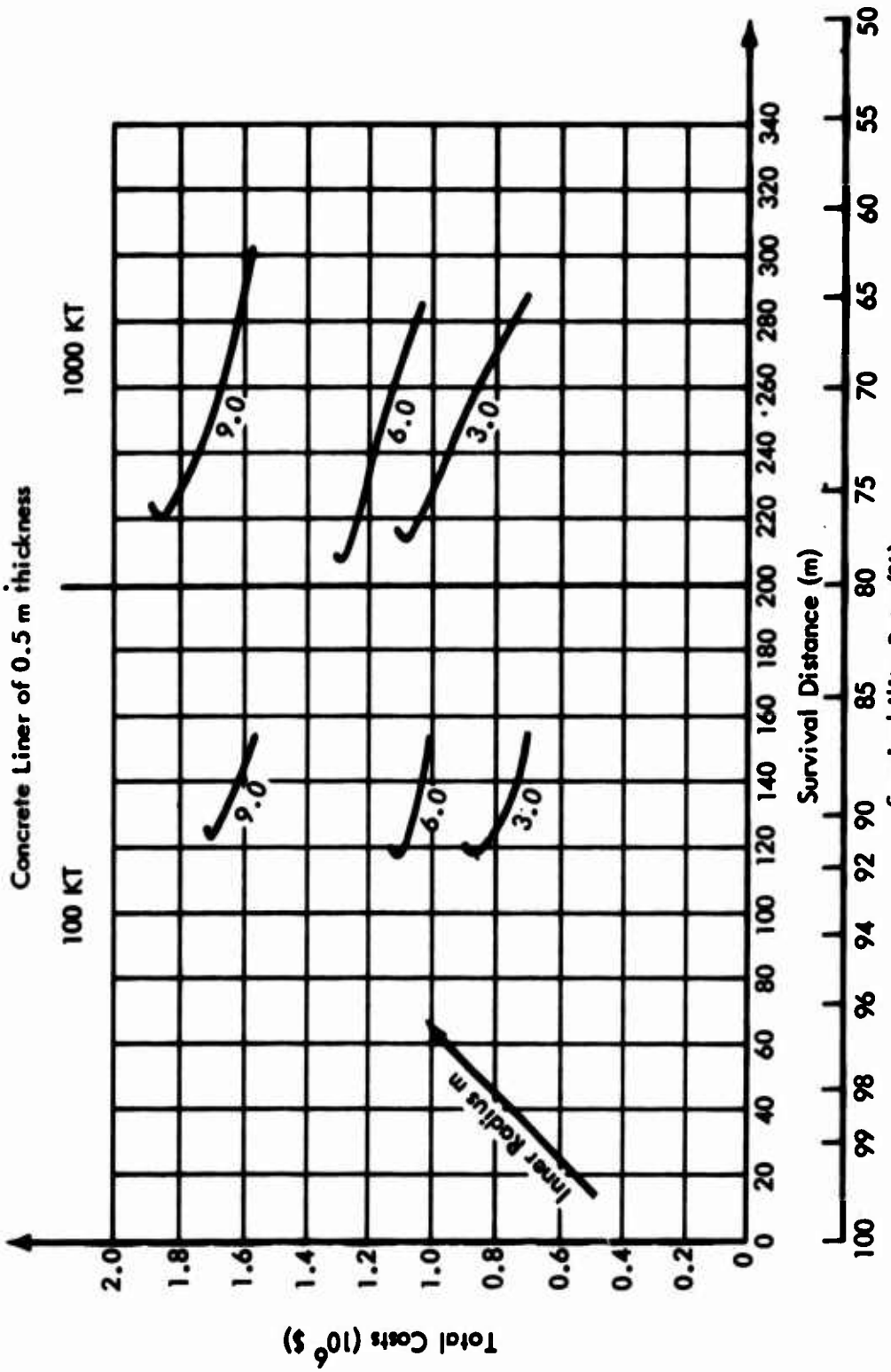

Figure 9 (C). Total costs for structures in sandstone with different inner radii (U).

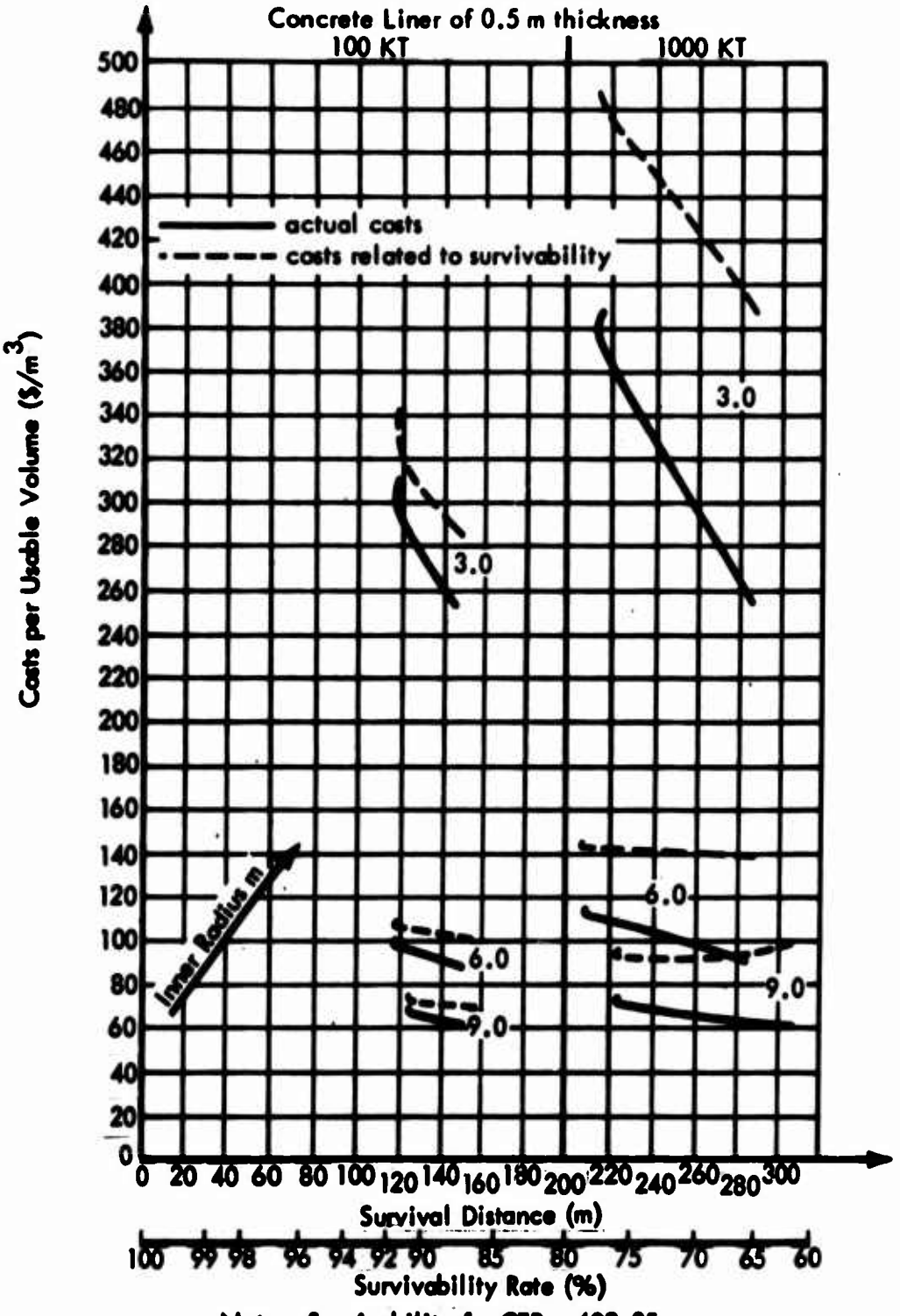

Note: Survivability for CEP = 402.25 m

Figure 10 (C). Costs per usable volume for structures in sandstone with different inner radii (U).

meters is least expensive; however, structures of larger radii yield favorable costs per usable volume. These economic considerations indicate:

1. Small cross-sectional sizes should be preferred for the protection of installations with small space requirements.

2. For volume-oriented installations (for instance, as depots), a smaller number of structures of larger cross-sectional size is, even considering survivability, more economical than a larger number of structures of smaller cross-sectional size.

Protective Structure with Steel Liner in Sandstone. The steel liner is assumed to be a tube of equal thickness. And the space between the rock and steel liner is filled with concrete. For the scope of this study, consideration of a liner thickness of 2.54 centimeters (1 inch) was sufficient.

Figure 6 shows the survival distance is dependent upon the structure depth and the weapon yield. For both the cross-sectional sizes with inner radii of 9 and 6 meters, the survival distance decreases with increasing depth to the optimum depth of 150 meters for a weapon yield of 100 kilotons and to 250 meters for a weapon yield of 1,000 kilotons. The cross-sectional size with an inner radius of 3 meters has an optimum depth of about 250 meters for 100 kilotons and offers a smaller survival distance and higher survivability. This size effect, however, is lost for the 1,000-kiloton weapon yield. With the higher values, the weapon yield becomes the more dominant influencing factor.

The comparison between concrete and steel liner demonstrates the superiority of steel liner. The survival distance for the considered steel liner is about 50 meters less than that for a concrete liner. The superiority of a steel liner is corroborated by its economical features, as given in Figures 11 and 12. In spite of the higher material unit costs, steel liner is less expensive than concrete (Figures 13, 14, and 15) because expensive excavation costs can be reduced.

Protective Structure with Steel Liner in Granite. The curves for the survival distance of structures in granite with a steel liner (Figure 6) show that full protection against a 100-kiloton weapon yield can be provided for the three considered cross-sectional sizes at a depth of about 190 meters. The surrounding granite provides better protection than sandstone from a 100-kiloton weapon. However, the superiority of granite to sandstone almost vanishes during a shock wave of a 1,000-kiloton weapon. The optimum survival distance is about 160 meters.

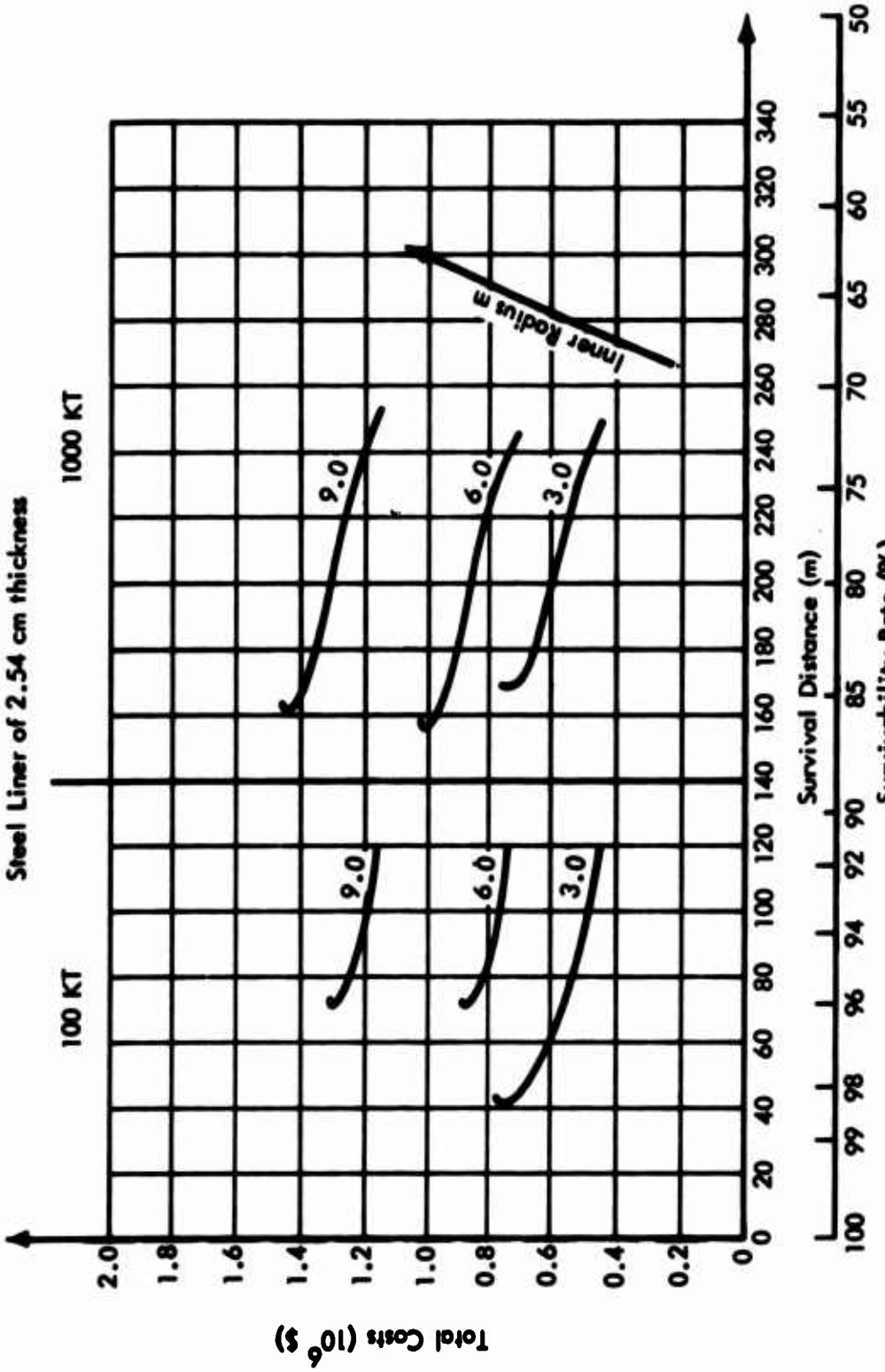

Figure 11 (C). Total costs for structures in sandstone with different inner radii (U).

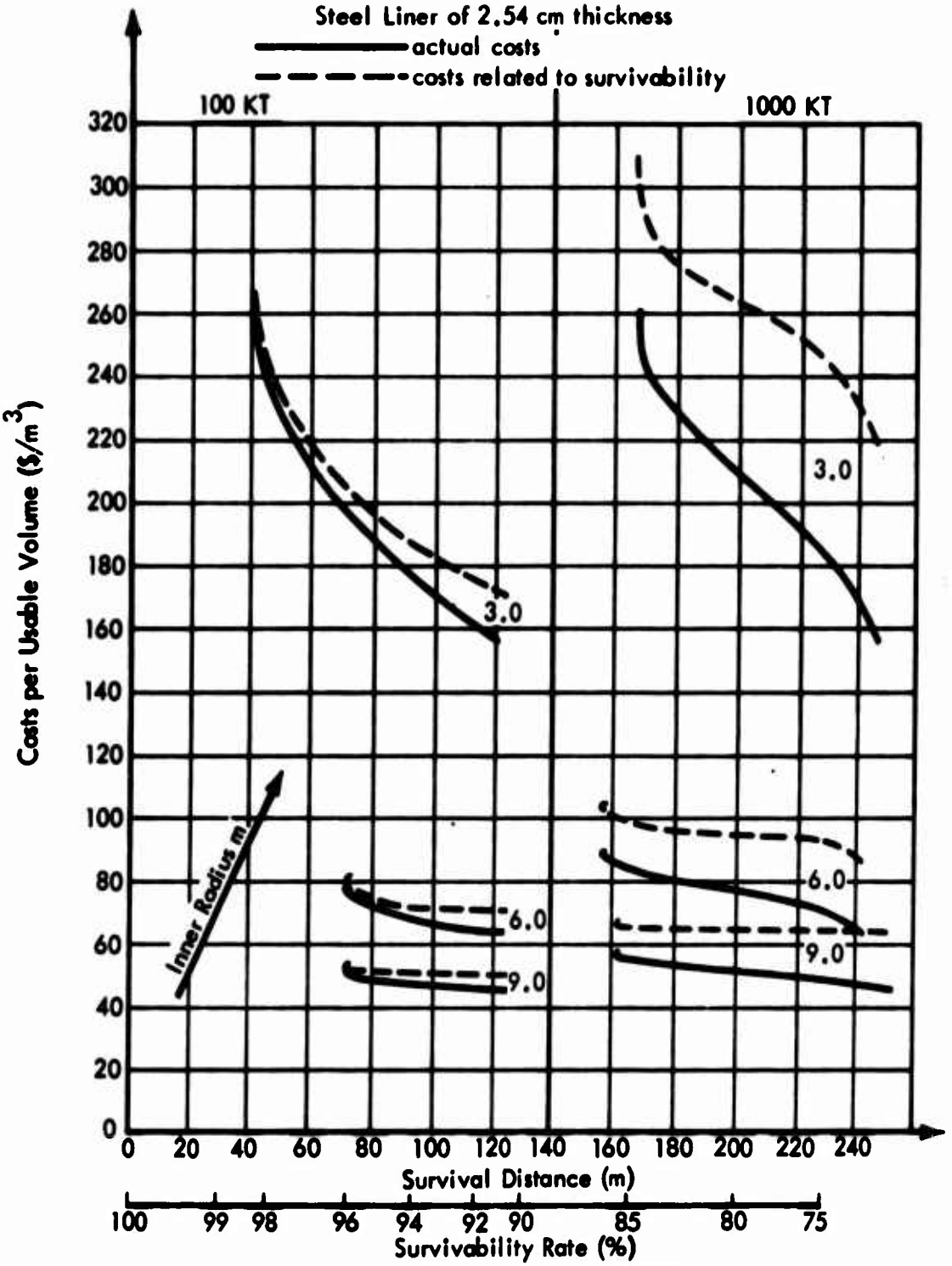

Note: Survivability for CEP = 402.25 m

Figure 12 (C). Costs per usable volume for structures in sandstone with different inner radii (U).

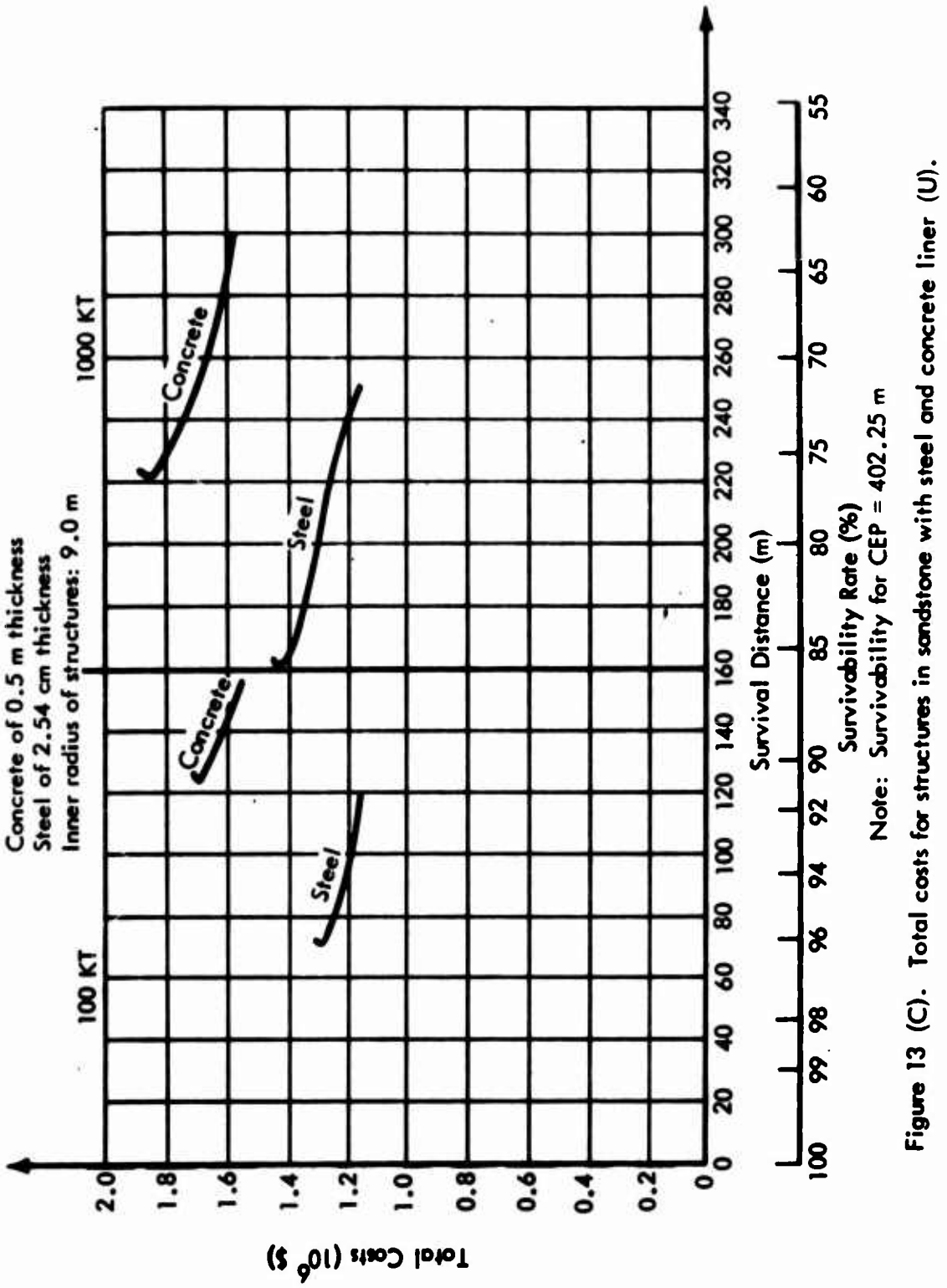

Figure 13 (C). Total costs for structures in sandstone with steel and concrete liner (U).

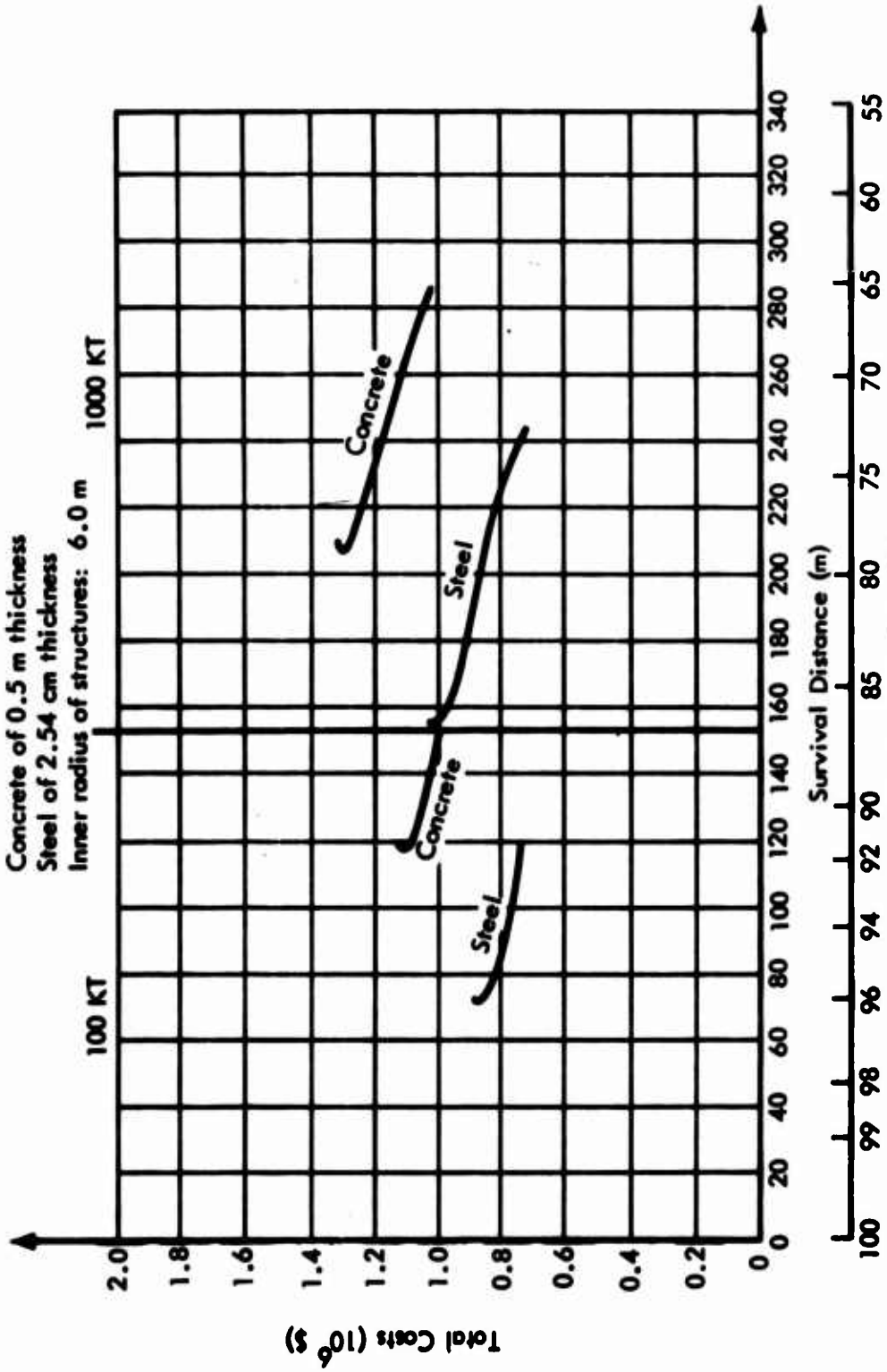

Figure 14 (C). Total costs for structures in sandstone with steel and concrete liner (U).

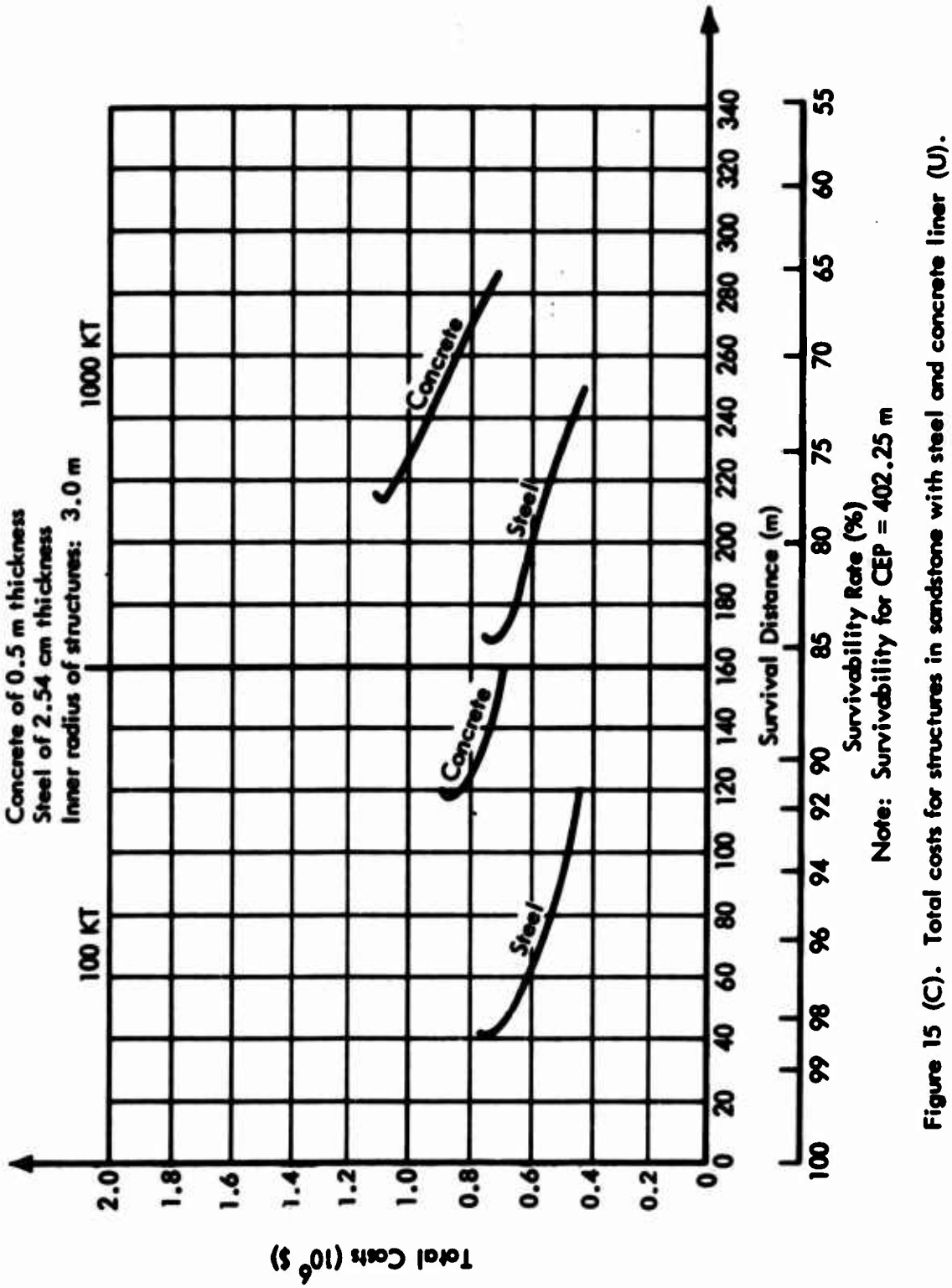

Figure 15 (C). Total costs for structures in sandstone with steel and concrete liner (U).

The optimum depth for granite is slightly less than that for sandstone. The economic features of structures in granite with a steel liner are shown in Figures 16 and 17. They emphasize that full protection can be obtained against a 100-kiloton weapon yield with the same amount of money that is necessary to provide high, but limited, protection in sandstone.

Optimum Design Conditions in a Rock Body Consisting of Different Types of Rocks

Structures are assumed in this part of the study to be embedded in either the same sandstone or granite as in the previous section. However, the rock faces make changes in the rock body between the detonation point and the structure location. Figure 18 illustrates two possibilities of such structures.

Two cases are investigated: a structure of an inner radius of 6 meters embedded in: (1) sandstone with a concrete liner and (2) granite with a steel liner. For both cases, the effective longitudinal seismic velocity between detonation point and structure location is varied in 1,000-meter-per-second steps from 1,000 to 6,000 meters per second.

Protective Structure with Concrete Liner in Sandstone. The survival distance and the survivability are graphed in Figure 19. For the weapon values of 100 and 1,000 kilotons, the survival distance increases with increasingly effective seismic velocity. Accordingly, the survivability decreases with increasingly effective seismic velocity. Full protection is given for an effective seismic velocity of 1,000 meters per second and a weapon yield of 100 kilotons. The optimum structure depth increases slightly with decreasingly effective seismic velocity. This increase of the optimum depth is more distinct in Figure 6 for the case with a 1,000-kiloton weapon yield.

Figures 20, 21, and 22 show the economic features. The curves demonstrate that the expenditures for protective structures in a rock body of different types of rocks produce greater protection if the effective seismic velocity is small. This result shows numerically the significance of proper site selection.

In the case of a 1,000-kiloton weapon yield, the curves of the costs per usable volume as related to the survivability have minimum values for the seismic velocities of 2,000, 4,000, 5,000, and 6,000 meters per second. The cost effectiveness is the highest for the survival distances and depths pertaining to these minimum values.

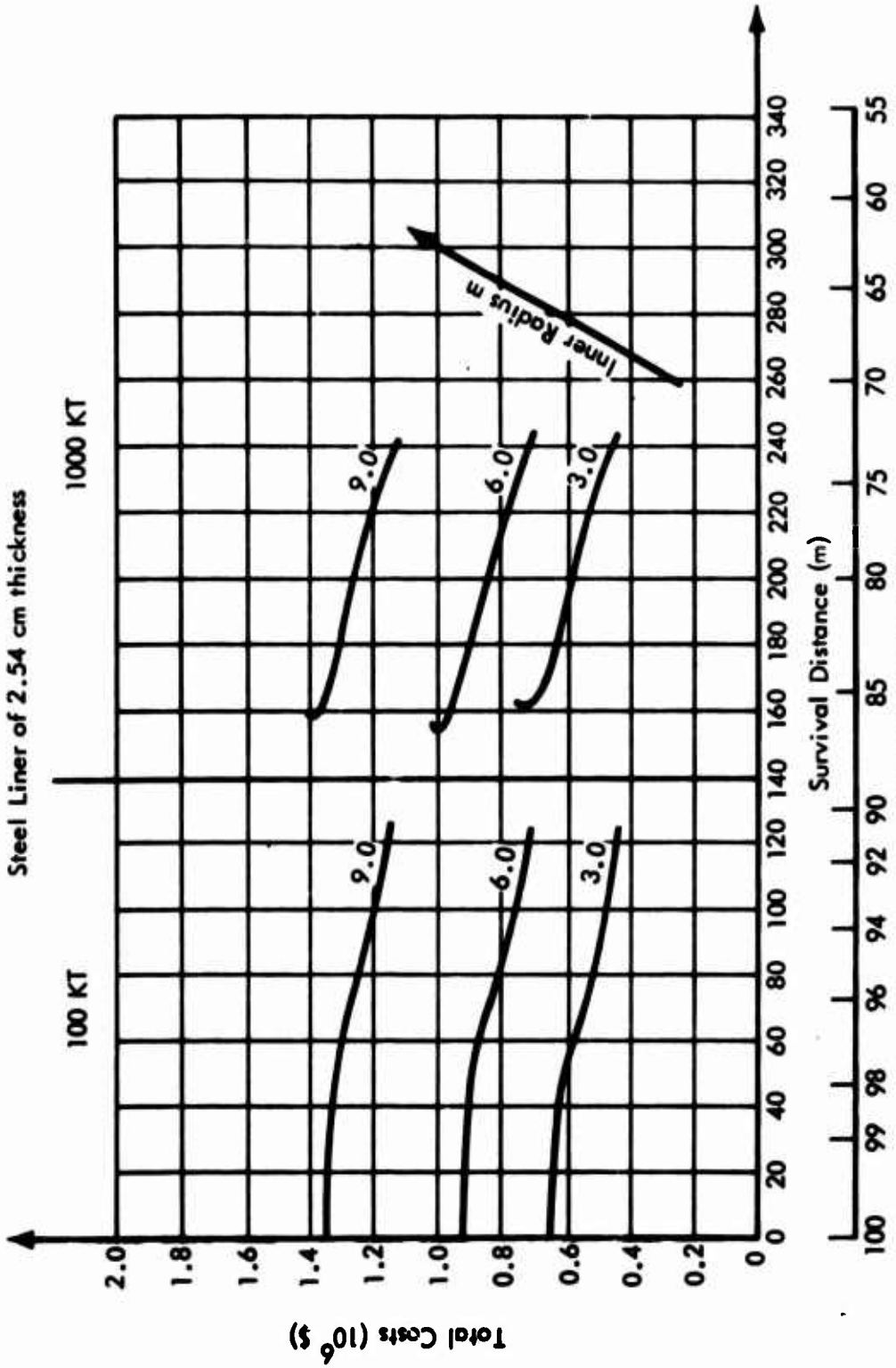

Note: Survivability for CEP = 402.25 m

Figure 16 (C). Total costs for structures in granite with different inner radii (U).

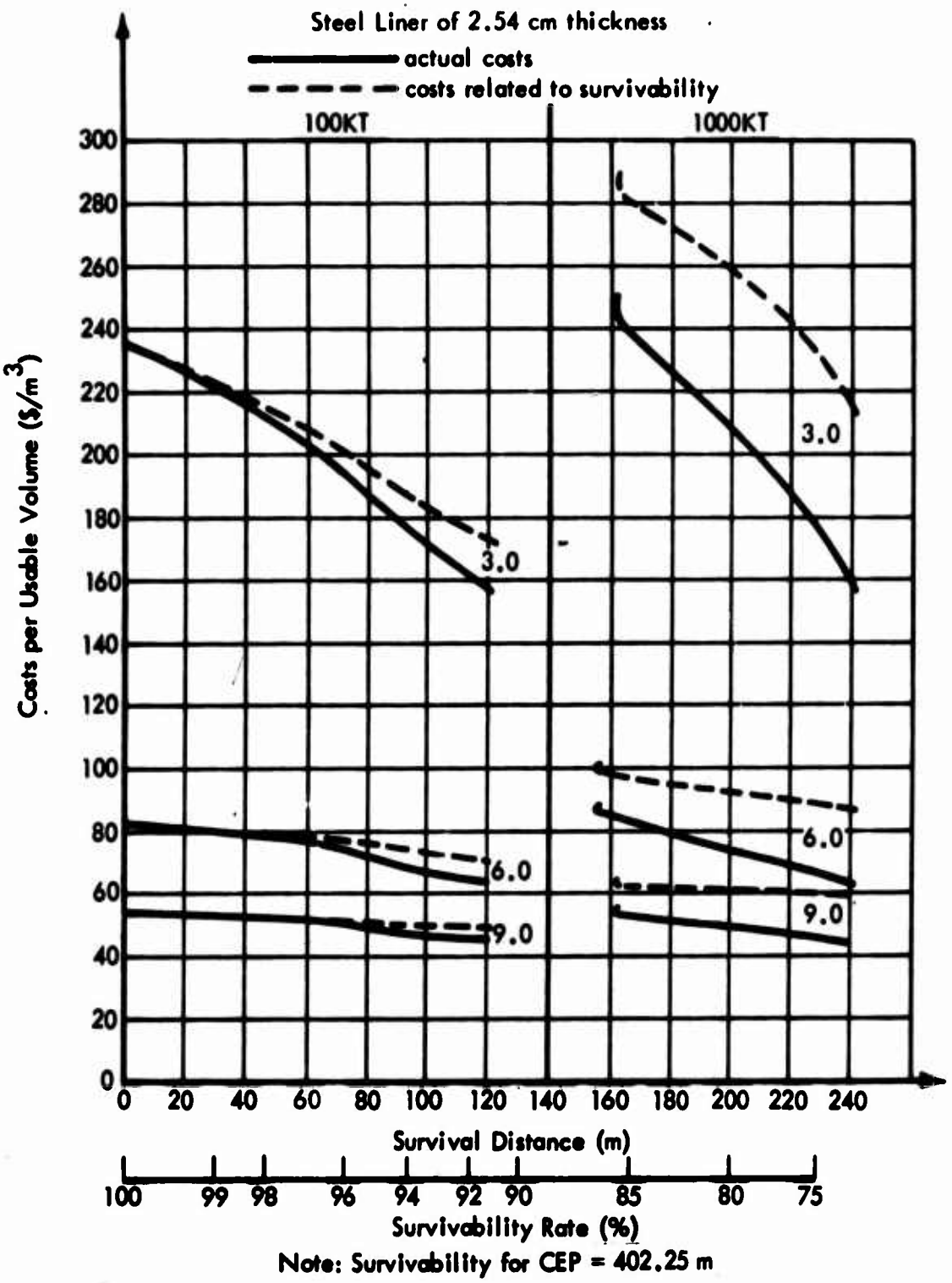

Note: Survivability for CEP = 402.25 m

Figure 17 (C). Costs per usable volume for structures in granite with different inner radii (U).

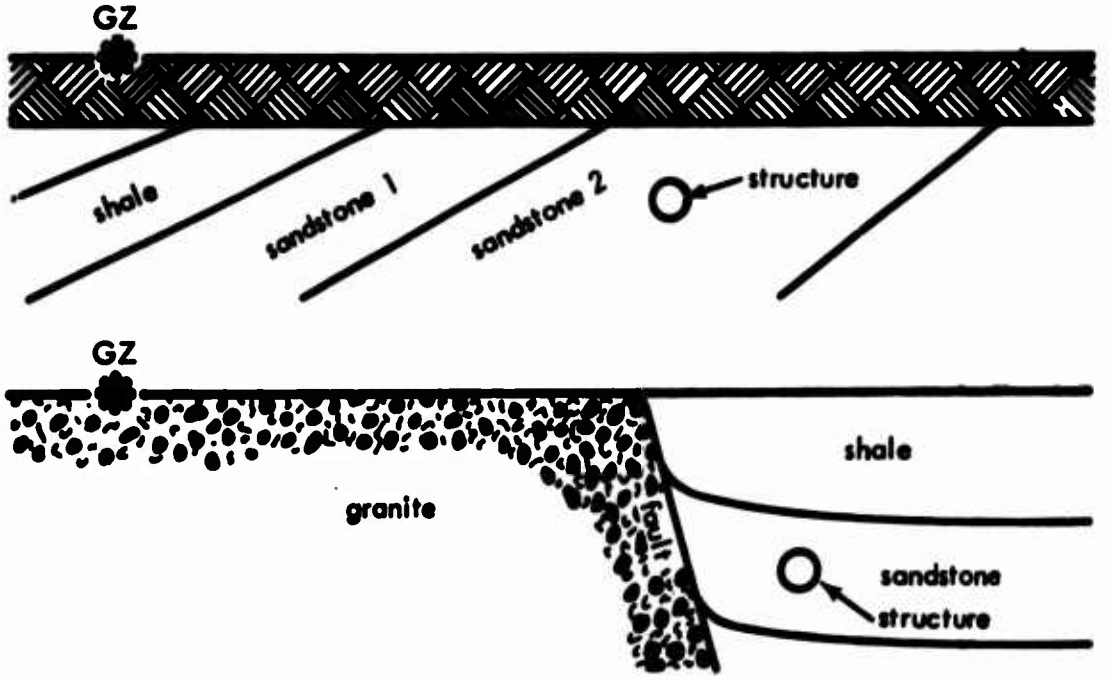

Figure 18. Rock bodies consisting of different types of rock.

Protective Structure with Steel Liner in Granite. Figure 19 shows that full protection can be reached against a 100-kiloton weapon yield for all values of the effective seismic velocity. However, a small seismic velocity is advantageous here, too, because full protection can be realized for less depth and, therefore, for less cost. In the case of a 1,000-kiloton weapon yield (Figure 19), full protection is given for values of the effective seismic velocity of 1,000 and 2,000 meters per second. The curves for the other values of the effective seismic velocity show more explicitly that the optimum depth decreases with increasingly effective seismic velocity. The cost curves in Figures 20, 21, and 22 show that structures in granite with steel liners are more economical than structures in sandstone with concrete liners.

FINDINGS

1. Deep underground protective structures can be designed for high degrees of survivability and even for full protection.

2. Steel is a better liner material than concrete for protective structures in rock. A liner 2.54 centimeters (1 inch) thick satisfies the requirements for protection against a true surface burst of 1,000 kilotons.

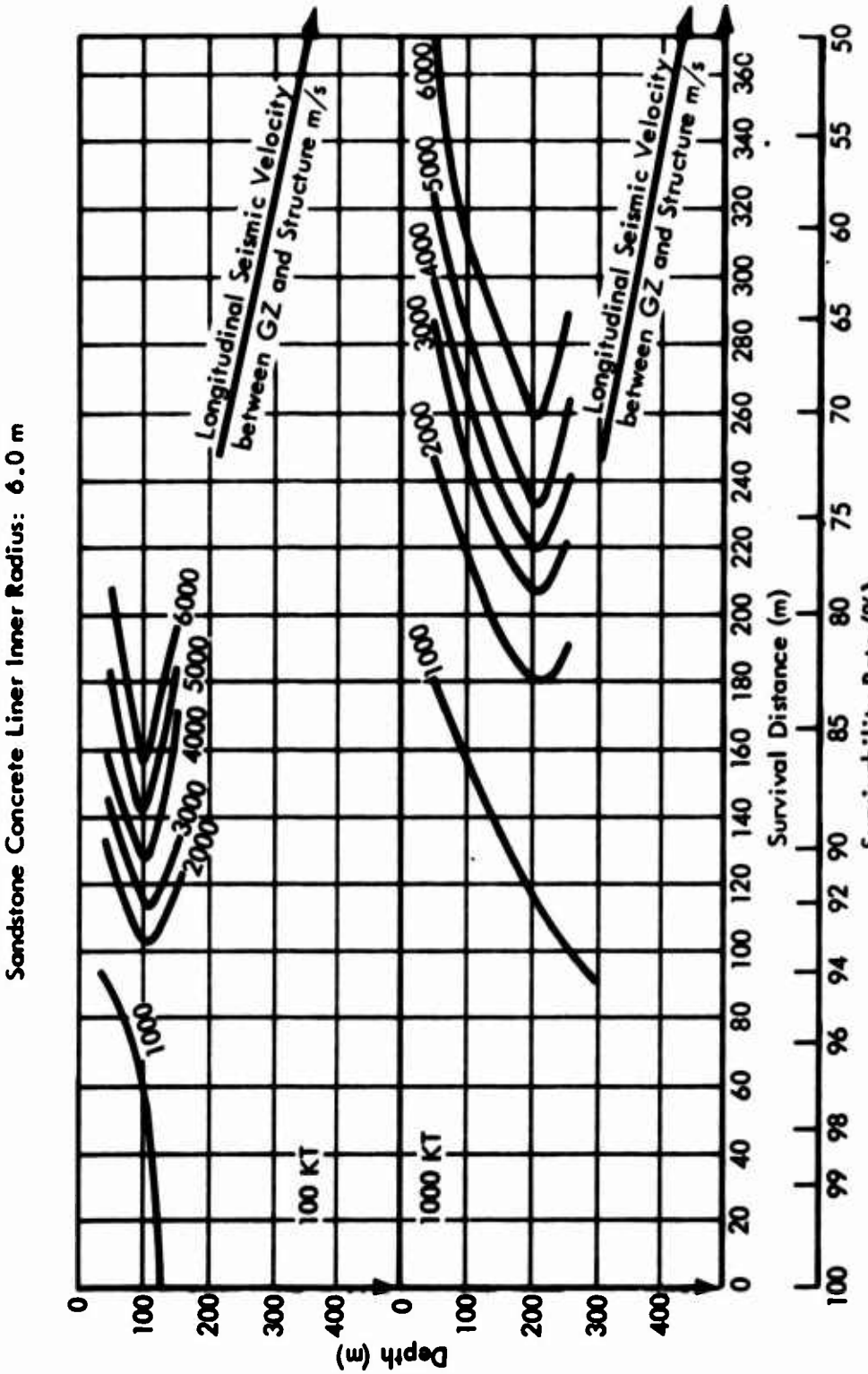

Figure 19 (C). Survival distance in a rock body with different rock types (U).

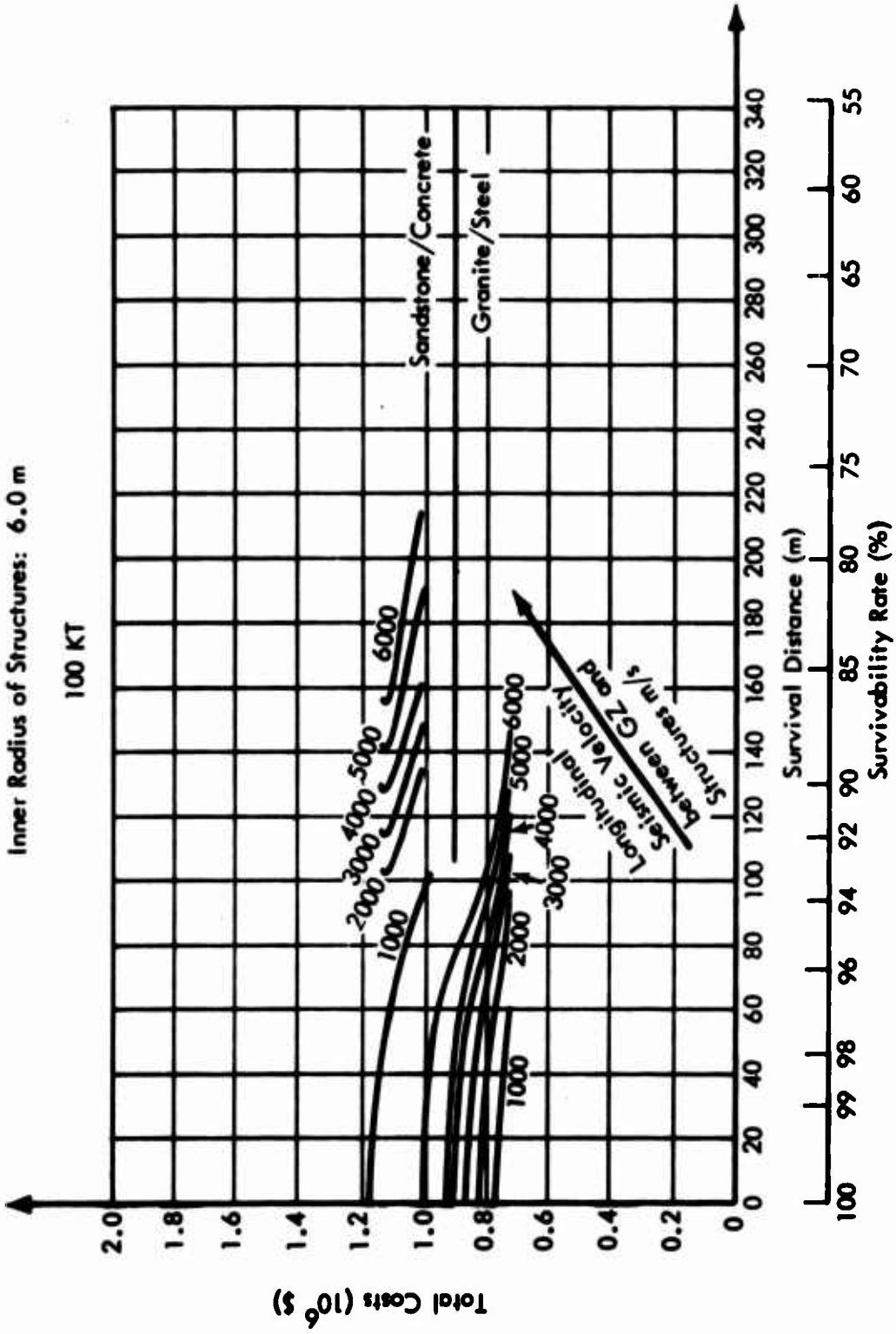

Note: Survivability for CEP = 402.25 m

Figure 20 (C). Total costs for structures in sandstone and granite in cases of different rock types between detonation point and surrounding structure (U).

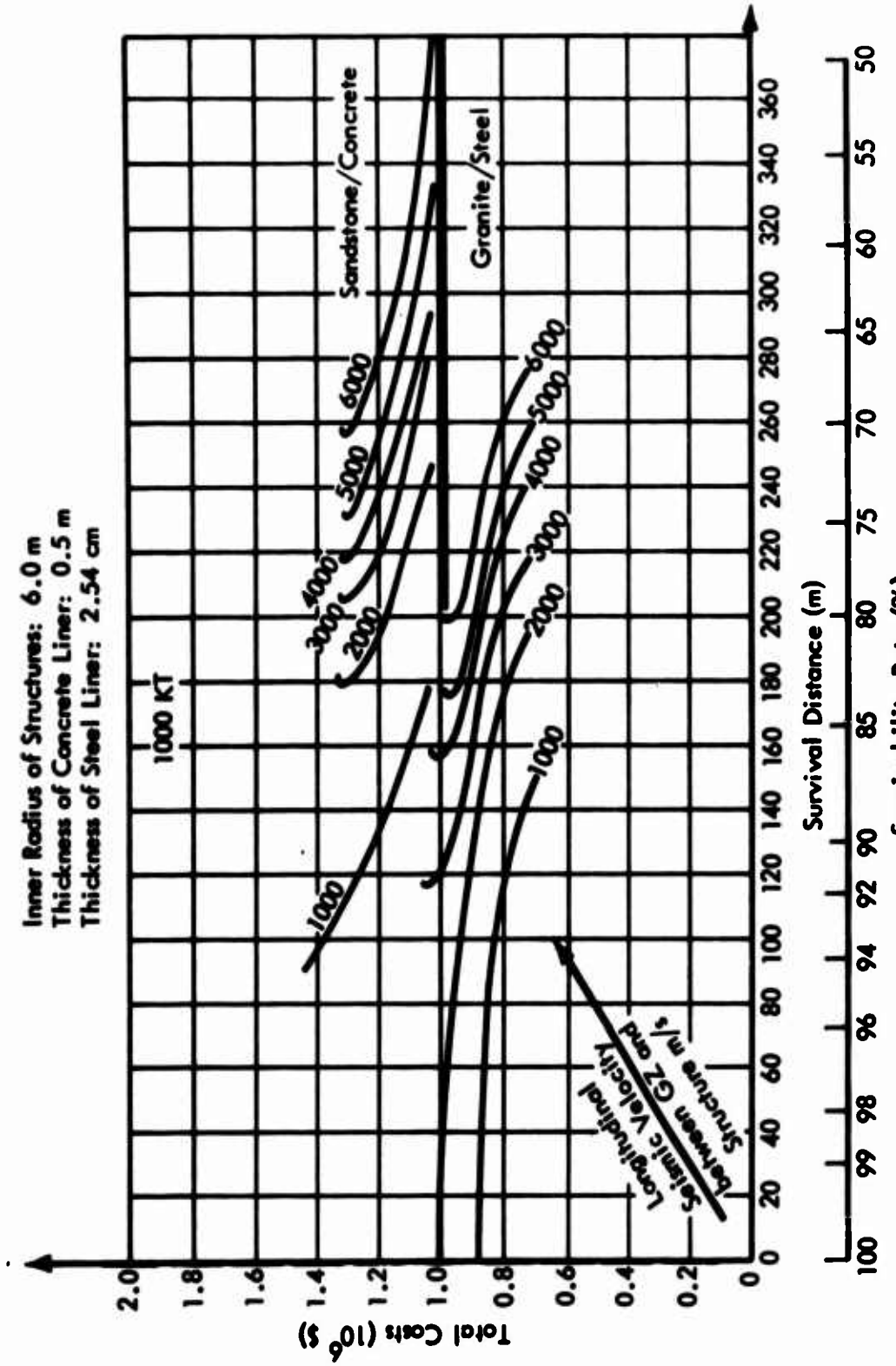

Note: Survivability for CEP = 402.25 m

Figure 21 (C). Total costs for structures in sandstone and granite in cases of different rock types between detonation point and surrounding structure (U).

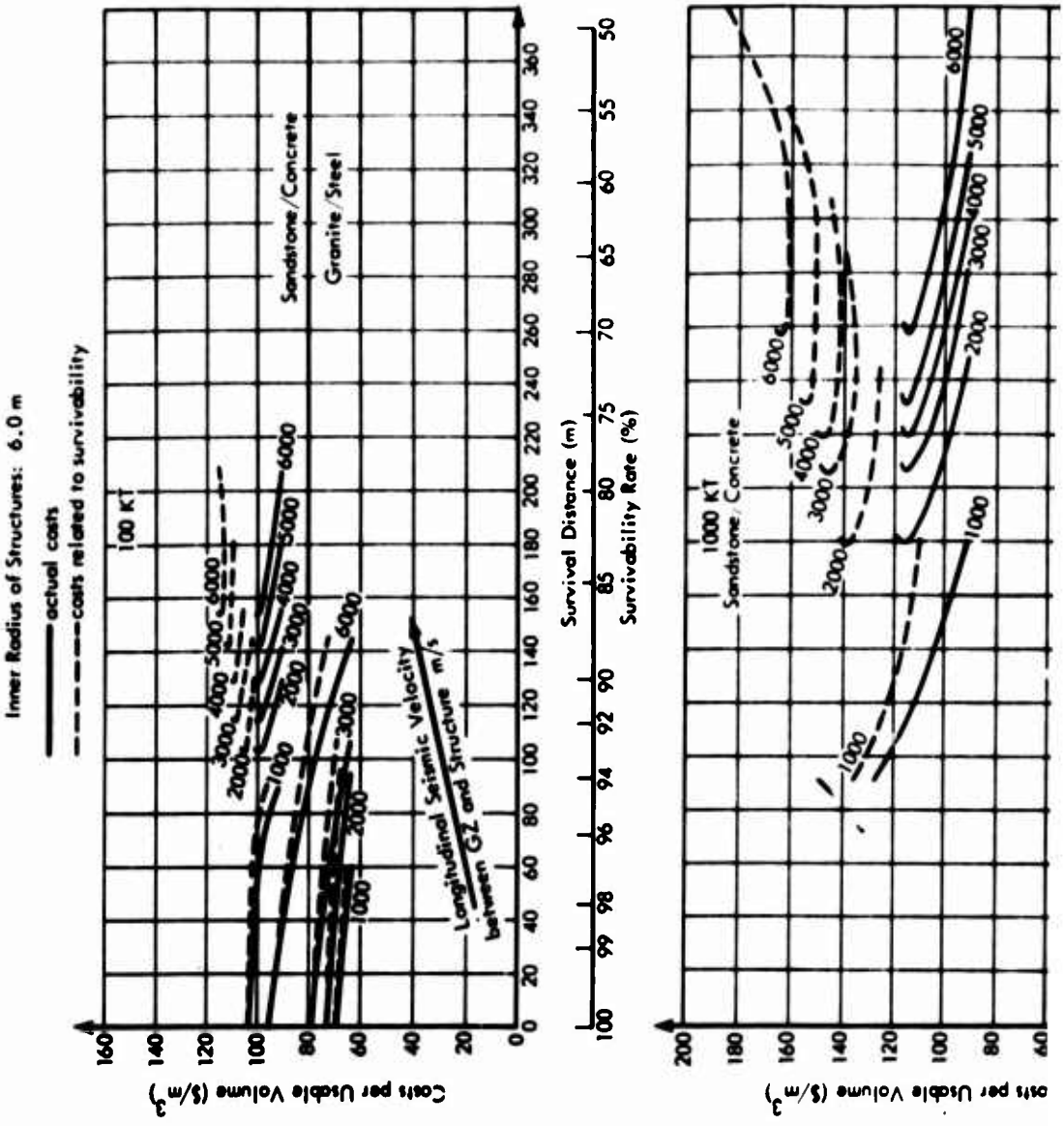

Figure 22 (C). Costs per usable volume for structures in sandstone and granite in different rock types between detonation point and surrounding stru

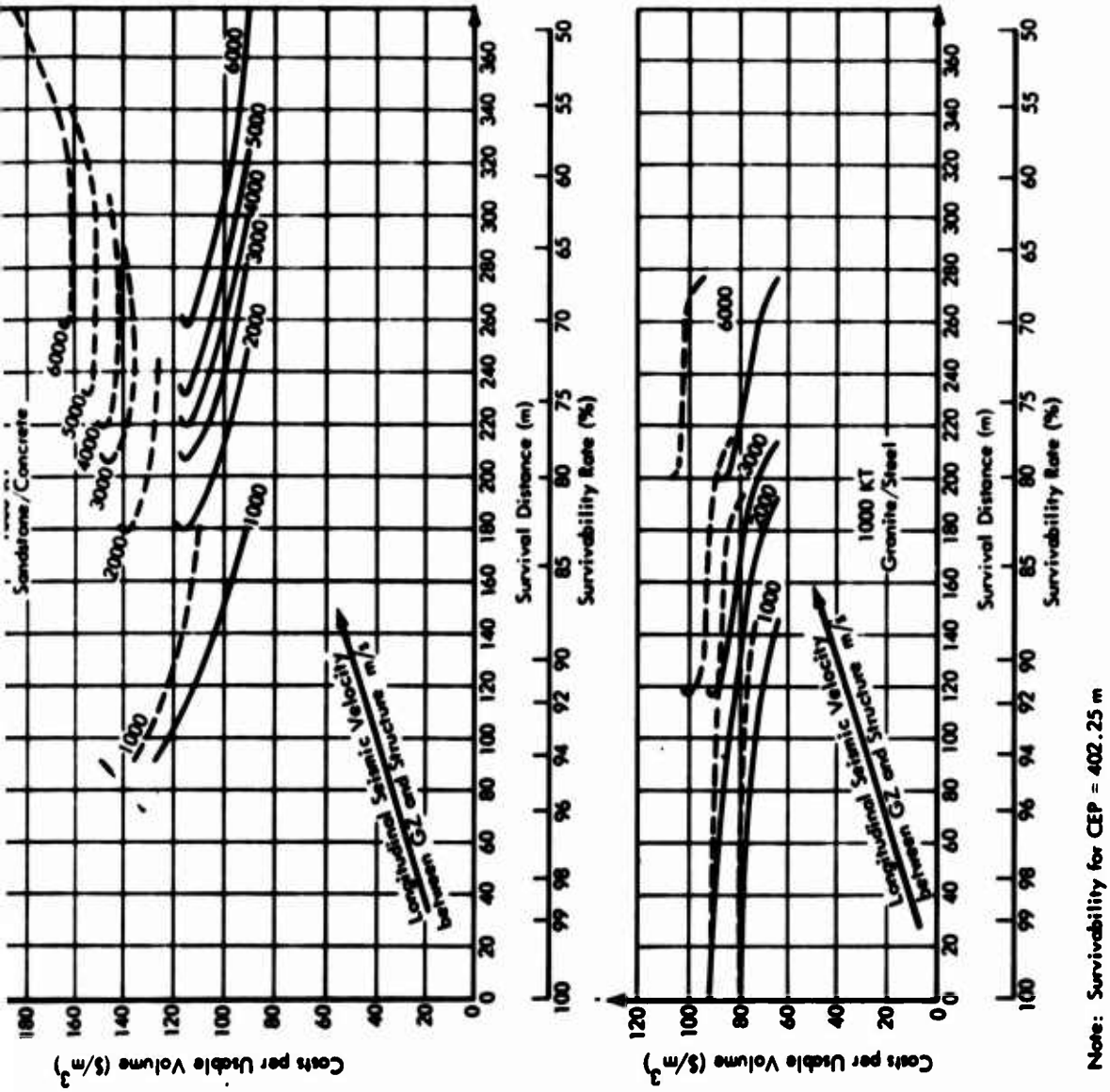

Note: Survivability for CEP = 402.25 m

n sandstone and granite in cases of
point and surrounding structure (U).

3. The weapon yield is the dominant factor influencing the survival distance and optimum depth. Its influence was determined numerically for the 100- and 1,000-kiloton values. The results are shown in Figures 6 and 19.

4. The influence of the type of enveloping rock appears to be more significant for the smaller weapon yield of 100 kilotons.

5. The rock interfaces between the detonation point and the structure are of great importance since the survivability increases greatly when the effective seismic velocity of the rock body decreases. The influence of the rock interfaces, represented here by the seismic velocity, is shown numerically in Figure 19.

6. No significant influence of the cross-sectional size on the survivability could be found for structures with concrete liners.

7. For structures with concrete liners, the increase in resistance of liner thicknesses greater than 0.5 meter was found to be insignificant.

8. With a steel liner, tunnels having an inner radius of 3 meters provided greater survivability than those with inner radii of 6 and 9 meters.

9. Steel liners provide greater survivability than concrete liners.

10. Structures with steel liners are less expensive than those with concrete liners.

CONCLUSIONS

From the foregoing study of deep underground tunnels in rock, it can be concluded that:

1. An increase in the depth of cover does not always lead to an increase in survivability. There are optimum depths which, if exceeded, will increase the survival distance and decrease the survivability.

2. The optimum site profile consists of a thick soil layer over a strong basement rock.

The computer program described herein gives the location, with respect to ground zero, of a tunnel with a preselected survivability. It also provides unit and total costs.

ACKNOWLEDGMENTS

The work on this study was started at the Nuclear Weapons Effects Division of the Waterways Experiment Station in Vicksburg, Mississippi. Dr. R. Froelich and Mr. J. L. Drake of the Waterways Experiment Station gave advice on the theoretical development. Mr. R. E. Walker of WES checked the adequacy of the theory and the mathematics. Mr. F. L. Switzer programmed the equation system for the determination of the survival distance and composed the entire program. Mr. M. L. Eaton and Mr. N. F. Shoemaker of NCEL gave advice on the probability computations. Mrs. R. M. Brooks programmed the sections concerning the effective seismic velocity of the probability and the cost estimation.

REFERENCES

1. Leonard Obert and Wilbur J. Duvall. Rock mechanics and design of structures in rock. New York, London, Sydney; John Wiley and Sons, Inc., 1967.

2. G. N. Savin. Stress concentration around holes. New York, Oxford, London, Paris, 1961, pp. 234–259.

3. The Rand Corporation. Memorandum RM - 3962 - PR: Dynamic response of lined and unlined underground openings, by C. C. Mow. Santa Monica, Calif., March 1964.

4. Air Force Systems Command Manual AFSCM 500-8: System applications of nuclear technology; effects of air blast, ground shock, and cratering on hardened structures. Washington, D. C., March 1967.

5. Air Force Special Weapons Center AFSWC-TDR-62-138: Air Force Design Manual; Principles and practices for design of hardened structures. Kirtland Air Force Base, N. Mex., December 1962, p. 4-62.

6. U. S. Army Engineer Waterways Experiment Station. Miscellaneous paper No. 1-962: Data reduction techniques for analysis of wave propagation; in dissipative materials, by Jim L. Drake. Vicksburg, Miss., January 1968.

7. Air Force Special Weapons Center. AFSWC-TDR-61-93: Geologic structure stability and deep protection construction. Kirtland Air Force Base, N. Mex., November 1961.

8. The Geological Society of America, Inc., Memoir 97: Handbook of physical constant, by Sydney P. Clark, Jr., editor. Yale University, New Haven, Conn., 1966.

9. Glenn Balmer. "A general analytic solution for Mohr's Envelope," in American Society for Testing Materials, Proceedings, Volume 52, ed. by American Society for Testing Materials. Philadelphia, 1952, pp. 1260–1271.

10. Eidgenössische Materialprüfungs- und Versuchsanstalt für Industrie, Bauwesen und Gewerbe; Bericht Nr. 172: Die Bruchgefahr festes Körper bei ruhender-statischer Beanspruchung, by M. Rös and A. Eichinger. Zurich, Switzerland, September 1949.

11. National Bureau of Standards. Official Project No. 65-2-97-33: Tables of probability functions, Volume I and II. Washington, D. C., 1941 and 1948.

12. Emanuel Parzen. Modern probability theory and its application, 3rd printing. New York, London, John Wiley & Sons, Inc., 1962.

13. A. Hald. Statistical Tables and Formulas, 7th printing. New York, London, Sydney, John Wiley & Sons, Inc., 1967.

14. State of California, Department of Water Resources. Bulletin No. 78, Appendix C: Procedure for estimating costs of tunnel construction. Sacramento, Calif., September 1959.

15. George Hill. "What's ahead for tunneling machines?" in Journal of the Construction Division, Proceedings of the American Society of Civil Engineers, Volume 94, October 1968, pp. 211-231.

APPENDIX A

STRESS DISTRIBUTION CAUSED BY THE OVERBURDEN

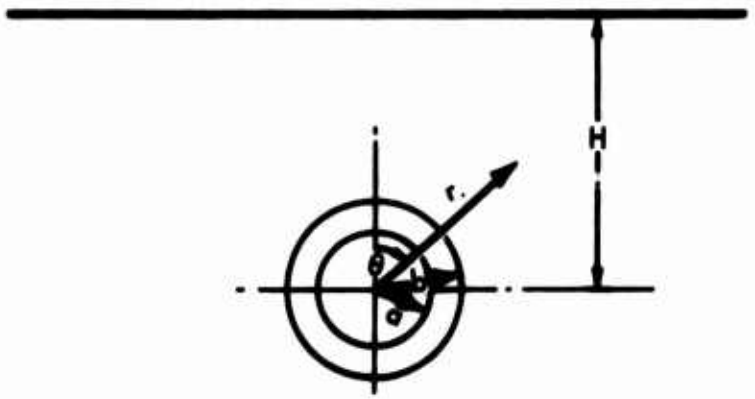

Figure 23. Tunnel configuration.

Notation:

H = depth of the structure in meters

a = inner radius of the liner in meters

b = outer radius of the liner in meters

r = coordinate radius in meters

θ = coordinate angle in degrees

γ = specific weight of the overburden in Mp/m^3

E_1 = elastic modulus of surrounding rock in kp/m^2

E_2 = elastic modulus of liner material in kp/m^2

ν_1 = Poisson's ratio of surrounding rock

ν_2 = Poisson's ratio of liner material

$\sigma_{r(1)st}$ = radial stress in rock caused by the overburden in kp/m^2

$\sigma_{\theta(1)st}$ = circumferential stress in rock caused by the overburden in kp/m^2

$\tau_{r(1)st}$ = shear stress in rock caused by the overburden in kp/m^2

$\sigma_{r(2)st}$ = radial stress in liner caused by the overburden in kp/m^2

$\sigma_{\theta(2)st}$ = circumferential stress in liner caused by the overburden in kp/m^2

$\tau_{r\theta(2)st}$ = shear stress in liner caused by the overburden in kp/m^2

The specific weight is the average specific weight divided by the entire depth H. The elastic properties E_1 and ν_1 of the surrounding rock are the respective values of the rock body, within 3 cavity diameters, around the structure. The stress equations are:

$$\sigma_{r(1)st} = \frac{\gamma \cdot H}{2} \left\{ \left[1 - \frac{1}{2} \ell_{-1} \left(\frac{b}{r} \right)^2 \right] + \left[1 - 2S_{-1} \left(\frac{b}{r} \right)^2 - \frac{3}{2} \ell_{-3} \left(\frac{b}{r} \right)^4 \right] \cos 2\theta \right\}$$

$$\sigma_{\theta(1)st} = \frac{\gamma \cdot H}{2} \left\{ \left[1 + \frac{1}{2} \ell_{-1} \left(\frac{b}{r} \right)^2 \right] - \left[1 - \frac{3}{2} \ell_{-3} \left(\frac{b}{r} \right)^4 \right] \cos 2\theta \right\}$$

$$\tau_{r\theta(1)st} = -\frac{\gamma \cdot H}{2} \left[1 + S_{-1} \left(\frac{b}{r} \right)^2 + \frac{3}{2} \ell_{-3} \left(\frac{b}{r} \right)^4 \right] \cdot \sin 2\theta$$

$$\sigma_{r(2)st} = \frac{\gamma \cdot H}{2} \left\{ \left[d_1 - \frac{f_{-1}}{2} \left(\frac{b}{r} \right)^2 \right] + \left[\frac{f_1}{2} - 2d_{-1} \left(\frac{b}{r} \right)^2 - \frac{3}{2} f_{-3} \left(\frac{b}{r} \right)^4 \right] \cos 2\theta \right\}$$

$$\sigma_{\theta(2)st} = \frac{\gamma \cdot H}{2}\left\{\left[d_1 + \frac{f_{-1}}{2}\left(\frac{b}{r}\right)^2\right] - \left[\frac{f_1}{2} - 6d_3\left(\frac{r}{b}\right)^2 - \frac{3}{2}f_{-3}\left(\frac{b}{r}\right)^4\right]\cos 2\theta\right\}$$

$$\tau_{r\theta(2)st} = \frac{\gamma \cdot H}{2}\left[3d_3\left(\frac{r}{b}\right)^2 - \frac{f_1}{2} - d_{-1}\left(\frac{b}{r}\right)^2 - \frac{3}{2}f_{-3}\left(\frac{b}{r}\right)^4\right]\sin 2\theta$$

where

$$f_1 = \frac{2(1+\kappa_1)}{G_1}\left\{\left(\frac{\mu_1}{\mu_2} - 1\right)\left[4 - 3\left(\frac{b}{a}\right)^2\right] + \left(\frac{b}{a}\right)^6\left(1 + \kappa_2\frac{\mu_1}{\mu_2}\right)\right\}\left(\frac{b}{a}\right)^2$$

$$f_{-1} = \frac{2(1+\kappa_1)}{2\left(\frac{\mu_1}{\mu_2} - 1\right) - \left(\frac{b}{a}\right)^2\left[\left(\frac{\mu_1}{\mu_2} - 1\right) - \left(1 + \kappa_2\frac{\mu_1}{\mu_2}\right)\right]}$$

$$f_{-3} = -\frac{2(1+\kappa)}{G_1}\left[\left(\frac{\mu_1}{\mu_2} - 1\right) + \left(\frac{b}{a}\right)^4\left(1 + \kappa_2\frac{\mu_1}{\mu_2}\right)\right]$$

$$\ell_{-1} = 2 - \frac{2\left[\left(\frac{b}{a}\right)^2 - 1\right](1+\kappa_1)}{2\left(\frac{\mu_1}{\mu_2} - 1\right) - \left(\frac{b}{a}\right)^2\left[\left(\frac{\mu_1}{\mu_2} - 1\right) - \left(1 + \kappa_2\frac{\mu_1}{\mu_2}\right)\right]}$$

$$\ell_{-3} = -2 + \frac{2(1+\kappa_1)}{G_1}\left\{\left(\frac{\mu_1}{\mu_2} - 1\right)\left[4\left(\frac{b}{a}\right)^6 - 7\left(\frac{b}{a}\right)^4 + 4\left(\frac{b}{a}\right)^2 - 1\right] + \left(\frac{b}{a}\right)^4\left[\left(\frac{b}{a}\right)^4 - 1\right]\left(1 + \kappa_2\frac{\mu_1}{\mu_2}\right)\right\}$$

$$d_1 = \frac{\left(\frac{b}{a}\right)^2 \left(1 + \kappa_1\right)}{2\left(\frac{\mu_1}{\mu_2} - 1\right) - \left(\frac{b}{a}\right)^2 \left[\left(\frac{\mu_1}{\mu_2} - 1\right) - \left(1 + \kappa_2 \frac{\mu_1}{\mu_2}\right)\right]}$$

$$d_{-1} = \frac{2\left(1 + \kappa_1\right)}{G_1}\left[\left(\frac{\mu_1}{\mu_2} - 1\right) + \left(\frac{b}{a}\right)^6 \left(1 + \kappa_2 \frac{\mu_1}{\mu_2}\right)\right]$$

$$d_3 = -\frac{2\left(1 + \kappa_1\right)}{G_1}\left(\frac{b}{a}\right)^4 \left[\left(\frac{b}{a}\right)^2 - 1\right]\left(\frac{\mu_1}{\mu_2} - 1\right)$$

$$S_{-1} = 2 - \frac{2\left(1 + \kappa_1\right)}{G_1}\left[\left(\frac{\mu_1}{\mu_2} - 1\right)\left[3\left(\frac{b}{a}\right)^6 - 6\left(\frac{b}{a}\right)^4 + 4\left(\frac{b}{a}\right)^2 - 1\right]\right.$$

$$\left. + \left(\frac{b}{a}\right)^6 \left[\left(\frac{b}{a}\right)^2 - 1\right]\left(1 + \kappa_2 \frac{\mu_1}{\mu_2}\right)\right]$$

$$G_1 = \left(\kappa_1 + \frac{\mu_1}{\mu_2}\right)\left(\frac{b}{a}\right)^2 \left[\left(\frac{\mu_1}{\mu_2} - 1\right)\left[3\left(\frac{b}{a}\right)^4 - 6\left(\frac{b}{a}\right)^2 + 4\right]\right.$$

$$\left. + \left(\frac{b}{a}\right)^6 \left(1 + \kappa_2 \frac{\mu_1}{\mu_2}\right)\right] + \left(\kappa_2 \frac{\mu_1}{\mu_2} - \kappa_1\right)\left[\left(\frac{\mu_1}{\mu_2} - 1\right)\right.$$

$$\left. + \left(\frac{b}{a}\right)^6 \left[1 + \left(\kappa_2 \frac{\mu_1}{\mu_2}\right)\right]\right.$$

when

$$\kappa_1 = \frac{3 - \nu_1}{1 + \nu_1} \qquad \mu_1 = \frac{E_1}{1 + \nu_1}$$

$$\kappa_2 = \frac{3 - \nu_2}{1 + \nu_2} \qquad \mu_2 = \frac{E_2}{1 + \nu_2}$$

APPENDIX B

DETERMINATION OF THE PRESSURE PULSE

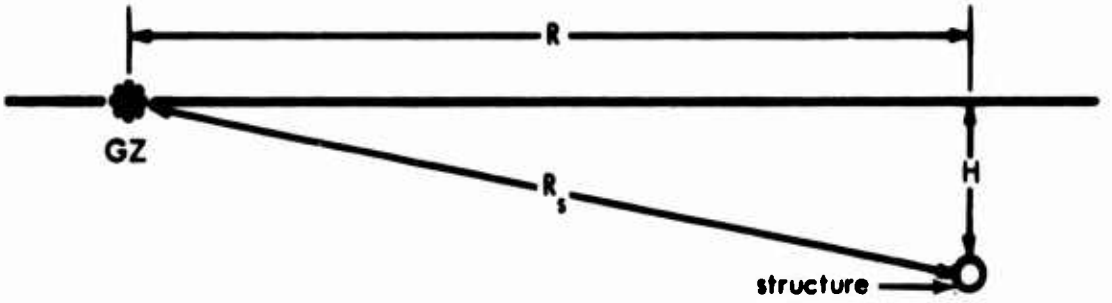

Figure 24. Tunnel location with respect to ground zero.

Notation:

H = depth of the structure in meters

R = horizontal distance between detonation point and structure in meters

R_s = slant distance between detonation point and structure in meters

C_p = effective longitudinal seismic velocity for the rock body between the point of detonation and the structure in meters per second

$C_\alpha = c_\alpha$ = longitudinal seismic velocity of the rock body of three tunnel diameters around the structure in meters per second

a_{max} = free rock field peak radial particle acceleration in g's

v_{max} = free rock field peak radial particle velocity in meters per second

d_{max} = free rock field peak radial displacement in meters

t_a = rise time of the pressure pulse in seconds

t_d = duration of the pressure pulse in seconds

t_b = decay time of the pressure pulse in seconds

W_n = nominal weapon yield in kilotons

Three kinds of atomic weapon bursts are distinguished and considered. The fully contained burst is assumed to have an energy coupling for the ground shock of 100%. The effective weapon yield W_e is equal to the nominal weapon yield W_n:

$$W_e = W_n$$

The contact surface burst detonates a small but finite distance above the ground surface:

$$W_e = W_n(0.02 - \frac{0.018}{5} \log W_n)$$

The true surface burst detonates coincident with the ground surface:

$$W_e = 0.01\ W_n(6.00 - \log W_n) \ .$$

The true distance between the detonation point and the center of the structure is:

$$R_s = \sqrt{R^2 + H^2}$$

The true distance is converted into the scaled distance:

$$R_e = \frac{R_s}{(W_e)^{1/3}}$$

The scaled distance is the variable in the equations for free-field peak radial particle acceleration, velocity, and displacement. These equations are obtained from the graphs in Reference 4:

Peak radial particle acceleration.

$$a_{max} = \begin{cases} \dfrac{a_{max_i}}{1525^2}(C_p)^2 & \text{if} \quad C_p \leq 1800 \text{ m/s} \\ \dfrac{a_{max_i}}{2440^2}(C_p)^2 & \text{if} \quad 1800 \text{ m/s} < C_p \leq 3600 \text{ m/s} \\ \dfrac{a_{max_i}}{4880^2}(C_p)^2 & \text{if} \quad 3600 \text{ m/s} < C_p \end{cases}$$

where a_{max_i} depends upon C_p and R_e, thus:

C_p	R_e	$\log a_{max_i}$
$C_p \leq 1800$ m/s	$R_e \leq 130$ m	$-4.4064 \log R_e + 9.1425$
$C_p \leq 1800$ m/s	$R_e > 130$ m	$-1.9991 \log R_e + 4.0456$
$1800 \text{ m/s} < C_p \leq 3600$ m/s	$R_e \leq 200$ m	$-3.9798 \log R_e + 9.3843$
$1800 \text{ m/s} < C_p \leq 3600$ m/s	$R_e > 200$ m	$-1.8143 \log R_e + 4.4104$
$3600 \text{ m/s} < C_p$	$R_e \leq 105$ m	$-2.6394 \log R_e + 6.9549$
$3600 \text{ m/s} < C_p$	$R_e > 105$ m	$-4.8804 \log R_e + 11.4999$

Peak radial particle velocity.

$$V_{max} = \begin{cases} \frac{V_{max_i}}{1525}(C_p) & \text{if } C_p \leq 1800 \text{ m/s} \\ \frac{V_{max_i}}{2440}(C_p) & \text{if } 1800 \text{ m/s} < C_p \leq 3600 \text{ m/s} \\ \frac{V_{max_i}}{4880}(C_p) & \text{if } 3600 \text{ m/s} < C_p . \end{cases}$$

where V_{max_i} depends upon C_p and R_e, thus:

C_p	R_e	$\log V_{max_i}$
$C_p \leq 1800$ m/s	$R_e \leq 105$ m	$-3.6860 \log R_e + 6.8244$
$C_p \leq 1800$ m/s	$R_e > 105$ m	$-1.3497 \log R_e + 2.0926$
$1800 \text{ m/s} < C_p \leq 3600$ m/s	$R_e \leq 75$ m	$-2.9822 \log R_e + 6.0408$
$1800 \text{ m/s} < C_p \leq 3600$ m/s	$R_e > 75$ m	$-1.6660 \log R_e + 3.5528$
$3600 \text{ m/s} < C_p$	$R_e \leq 120$ m	$-2.4134 \log R_e + 5.2966$
$3600 \text{ m/s} < C_p$	$R_e > 120$ m	$-1.2544 \log R_e + 2.8790$

Peak radial particle displacement.

Likewise, d_{max} depends upon C_p and R_e, thus:

C_p	R_e	$\log d_{max}$
$C_p \leq 1800$ m/s	$R_e \leq 100$ m	$-3.7901 \log R_e + 5.7939$
$C_p \leq 1800$ m/s	$R_e > 100$ m	$-1.3722 \log R_e + 0.9520$
$1800 \text{ m/s} < C_p \leq 3600$ m/s	$R_e \leq 150$ m	$-1.4312 \log R_e + 1.7842$
$1800 \text{ m/s} < C_p \leq 3600$ m/s	$R_e > 150$ m	$-1.1358 \log R_e + 1.1393$
$3600 \text{ m/s} < C_p$		$-1.6436 \log R_e + 2.1860$

The free-field stresses are approximately proportional to the particle velocity (Hugoniot Equation):

$$\sigma = \rho \cdot C_\alpha \cdot v \text{ , and}$$

$$\sigma_{max} = \rho \cdot C_\alpha \cdot v_{max}$$

where σ = free-field radial stress in kp/m^2 ,

ρ = mass density = $\frac{\gamma}{9.807} \cdot 1000$

For the triangular-shaped load impulse (Figure 25), the rise time is

$$t_a = \frac{2 \cdot v_{max}}{a_{max} \cdot 9.81}$$

and the pulse duration is

$$t_d = \frac{2 \cdot d_{max}}{V_{max}}$$

For further computations, it is convenient to have the decay time expressed as:

$$t_b = t_d - t_a \ .$$

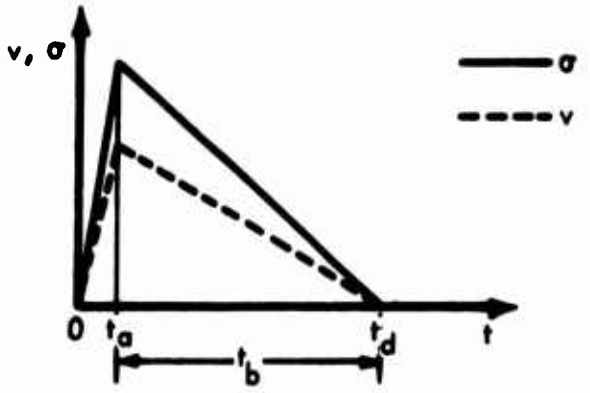

Figure 25. Stress and velocity pulse.

APPENDIX C

DETERMINATION OF THE EFFECTIVE SEISMIC VELOCITY OF A LAYERED ROCK SYSTEM

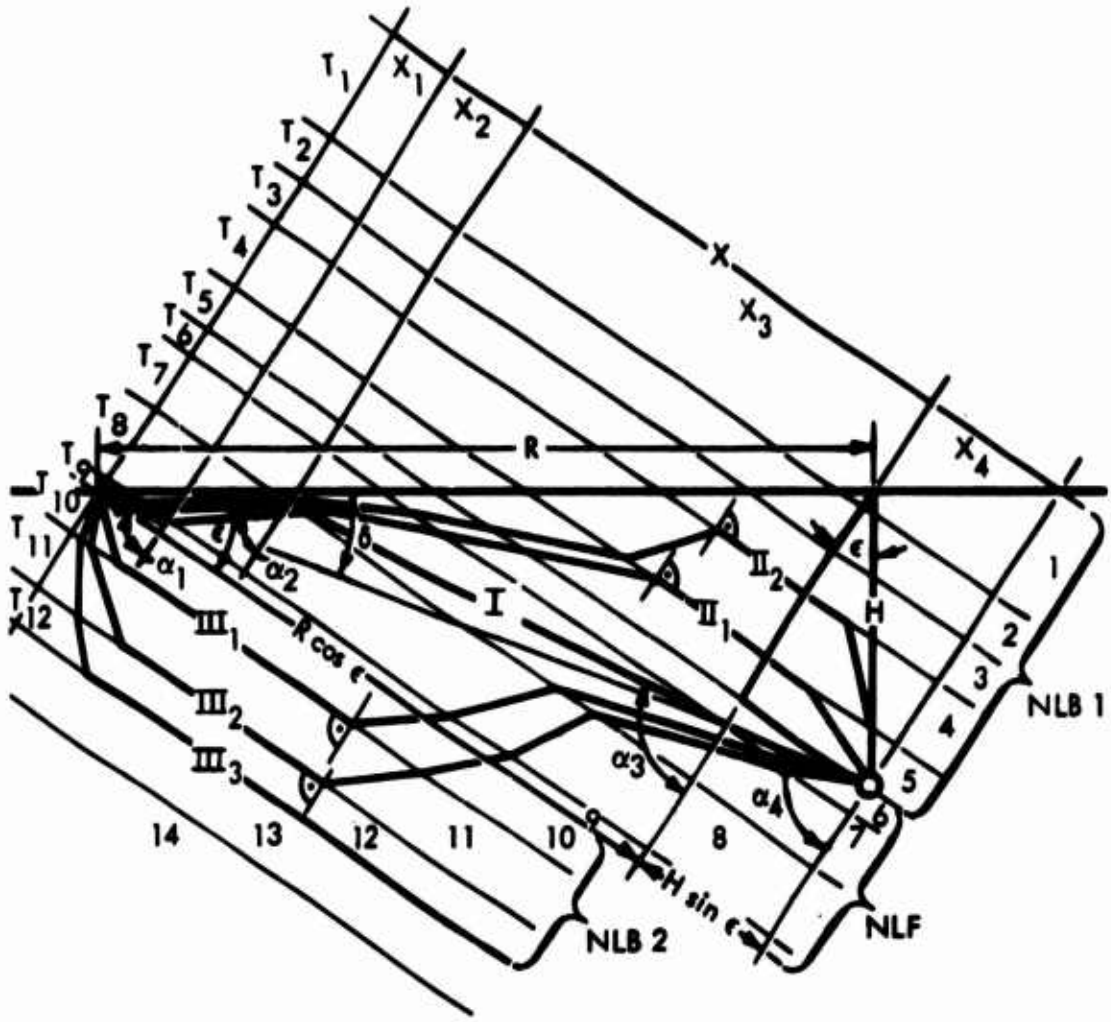

Figure 26. Direct and indirect rays from the point of detonation to the structure.

Notation:

H = depth of the structure in meters

R = horizontal distance between detonation point and structure in meters

R_s = slant distance between detonation point and structure in meters

T_k = thickness of layer k in meters

T_D = thickness of layer package between point of detonation and structure in meters

L_{max} = maximum thickness of the layer packages penetrated by the indirect rays in meters

α = acute angle between ray and the normal of the refracting plane in degrees

ϵ = angle of layer inclination

δ = angle between horizontal distance (R) and slant distance (R_s) in degrees

C_k = seismic velocity of layer k in meters per second

C_p = effective seismic velocity for the distance between point of detonation and structure location in meters per second

k = ordinal number of the layers

The effective longitudinal seismic velocity is the quotient of the slant distance from the point of detonation to the structure and the shortest time necessary to travel this distance:

$$C_p = \frac{\sqrt{R^2 + H^2}}{t_{min}}$$

The structure can be hit directly by a pressure ray (ray group I through layers 6, 7, 8, and 9) going through the layers between the point of

detonation and the structure, indirectly by ray group II which penetrates into layers above the structure and returns after having traveled parallel in one of the layers above, and indirectly by ray group III which penetrates into layers below the detonation point and propagates to the structure after having traveled parallel in one of the layers below. The travel times of the direct ray and all the indirect rays are computed and compared. By Snell's Law, the direct ray has to yield these conditions:

$$\frac{\sin \alpha_k}{\sin \alpha_{k+1}} = \frac{C_k}{C_{k+1}}$$

and

$$\sum_{m}^{n} X_k = X$$

where

$$X = R \cdot \cos \epsilon + H \cdot \sin \epsilon$$

$$X_k = T_k \cdot \mathrm{tg}\alpha_k$$

The path of the direct ray must be found by iteration. The loop is initiated by the ray that starts into the straight-line direction from the detonation point to the structure:

$$\alpha_1 = 90 - (\epsilon - \delta) .$$

A direct pressure ray does not exist if its path leaves the surface of the half space (Figure 27).

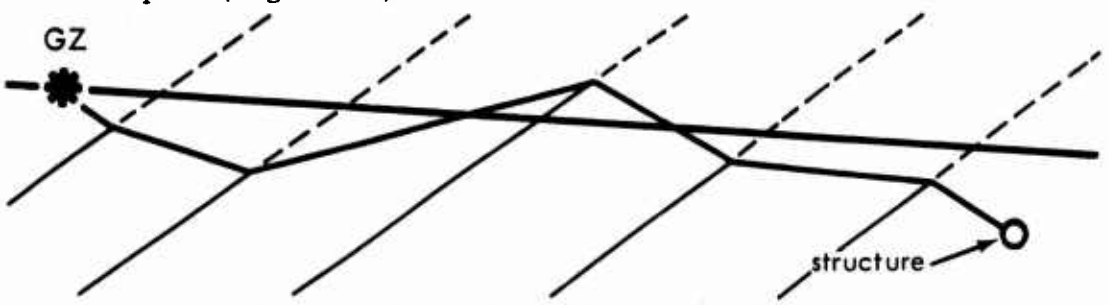

Figure 27. Path of ray leaving the half space.

The travel time is:

$$t = \sum_{k=m}^{k=n} \frac{T_k}{\cos \alpha_k \cdot C_k}$$

In the example of Figure 27, m = 9 and n = 6.

The computation of the refraction angles α_k, since the indirect rays start with the one that is 90 degrees, is:

$$\alpha_r = 90°$$

$$\sin \alpha_r = 1$$

$$\sin \alpha_k = \frac{C_k}{C_r} .$$

The path length traveled parallel to the layers is:

$$X_s = X - \sum_{k=m}^{k=j} X_k - \sum_{k=j}^{k=n} X_k$$

For ray group III_2 in Figure 26, m = 10, j = 11, and n = 6. If an assumed ray's length, X_s, is negative, that ray never can be the fastest one and is to be ignored.

The travel time for an indirect ray is:

$$t = \frac{X_s}{C_r} + \sum_{k=m}^{k=j} \frac{T_k}{\cos \alpha_k \cdot C_k} + \sum_{k=j}^{k=n} \frac{T_k}{\cos \alpha_k \, C_k}$$

For computational convenience, the detonation point and the structure locations are assumed to divide their particular layers by an imaginary cut into two layers of the same seismic velocity.

To simplify the computation and the use of the program, the half space is considered to consist of four areas as shown in Figure 28. The areas are limited by the relations:

Area A: ϵ is positive and $0 \leq \delta < (90 - \epsilon)$

Area B: ϵ is positive and $(90 - \epsilon) \leq \delta < 90$

Area C: ϵ is negative and $|\epsilon| \leq \delta \leq 90$

Area D: ϵ is negative and $0 \leq \delta < |\epsilon|$.

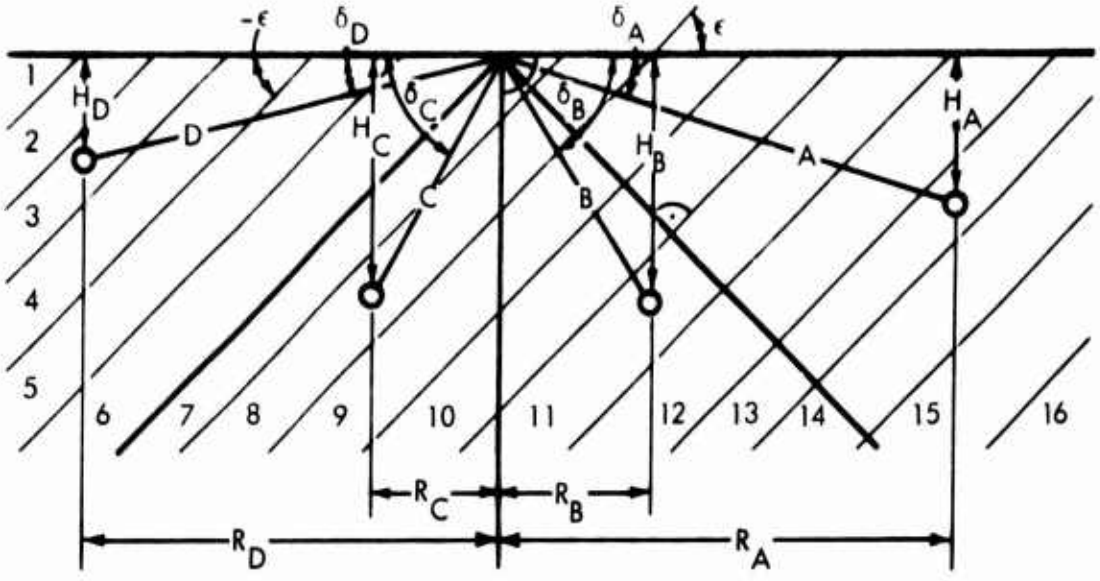

Figure 28. Partition of the half space in areas related to layers' inclination and structure location.

This distinction is based on the following sign convention:

Distance R is always positive.

Depth H is always positive.

Location angle δ is always positive.

Layer inclination ϵ is positive if the detonation point is located "above the layers" and is negative if the detonation point is located "below the layers."

"Above the layers" means that an observer moving into the direction of R meets lower, in general earlier sedimented, layers. "Below the layers" means that the observer meets higher, in general later sedimented, layers (Figure 28).

With this area and sign convention, the previously given expressions for this distance X and for the first approximate angle change to:

Area A: $X = R_A \cdot \cos \epsilon - H_A \cdot \sin \epsilon$

$\alpha_1 = 90 - \epsilon - \delta_A$

Area B: $X = R_B \cdot \cos \epsilon - H_B \cdot \sin \epsilon$

$\alpha_1 = \delta_B + \epsilon - 90$

Area C: $X = R_C \cdot \cos \epsilon + H_C \sin \epsilon$

$\alpha_1 = 90 + \epsilon - \delta_C$

Area D: $X = R_D \cdot \cos \epsilon + H_D \sin \epsilon$

$\alpha_1 = 90 - \epsilon + \delta_D$

All the rays that are supposed to hit the structure travel between the perpendiculars from the point of detonation or the location of the structure to the layers. A ray traveling beyond a perpendicular cannot cross the perpendicular because the signs of both sides of the basic law:

$$\sin \alpha_{i+1} = \frac{C_{i+1}}{C_1} \sin \alpha_1$$

are the same and, in the case of refraction, the angles are allowed to change only from 0 to 90 degrees.

Because of these relations, ray group II does not exist for area A. To penetrate the first layer above the detonation point, the rays would have to travel beyond the perpendicular in area D and from there they cannot return to area A by refraction.

Besides the layer package between the detonation point and the location of the structure, layers above and below this package are significant in selecting the shortest travel time. The program user will want to know how many layers above and below to consider (Figure 29). The maximum thickness of the layer package above may be determined by the assumption that the layers penetrated do have the minimum seismic velocity for rock of 1,000 meters per second and that the layer in which the ray travels parallel does have the maximum seismic velocity in rock of 6,500 meters per second.

From Figure 29 it can be seen that:

$$t_{direct} = \frac{\sqrt{R^2 + H^2}}{1000}$$

$$t_{indirect} = \frac{L}{1000 \cdot \cos \alpha_1} + \frac{X_s}{6500} + \frac{L + T_D}{1000 \cdot \cos \alpha_1}$$

$$\sin \alpha_1 = \frac{C_1}{C_2} = \frac{1000}{6500} = 0.1539$$

$$\cos \alpha_1 = 0.9881$$

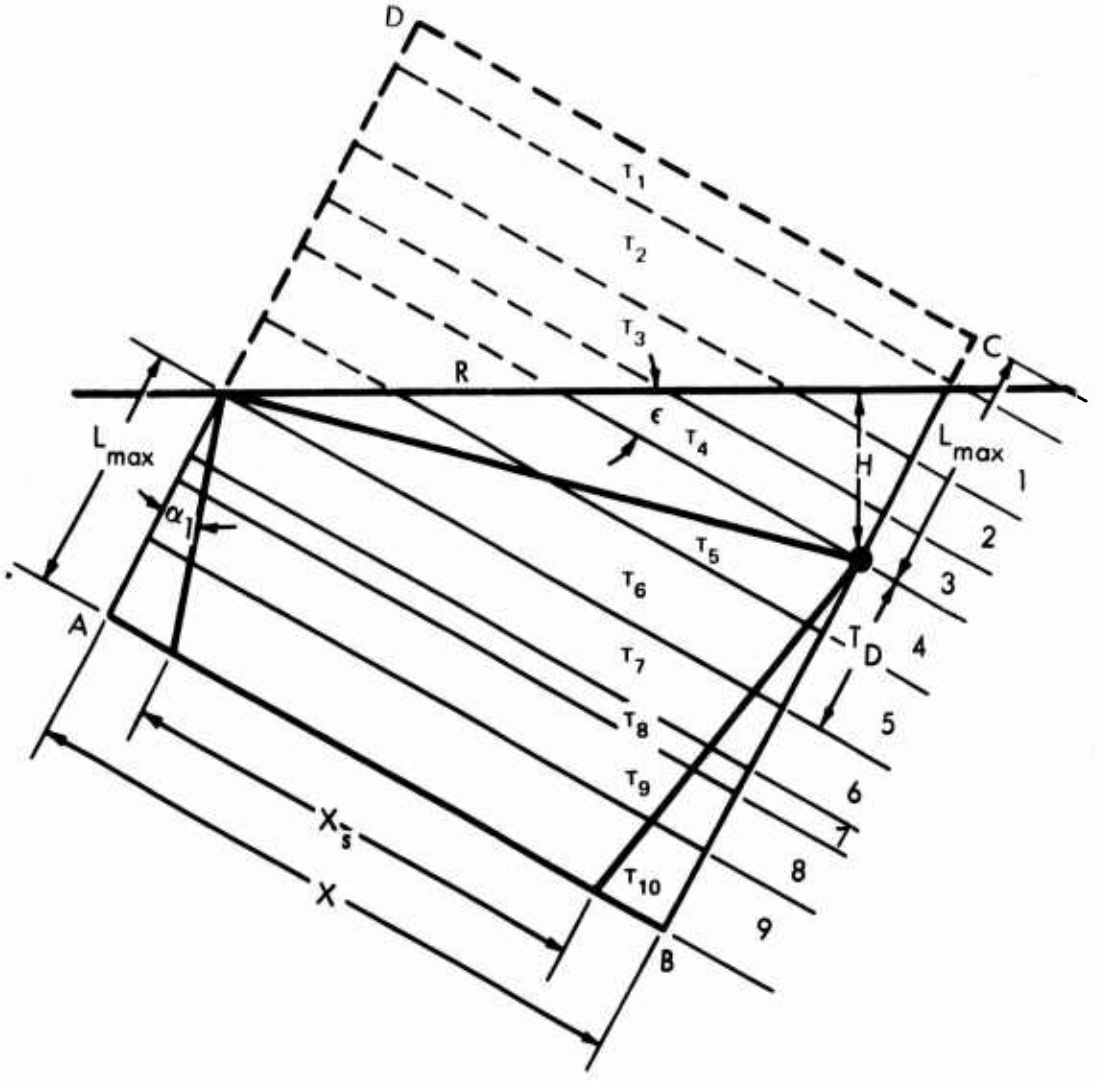

Figure 29. Maximum thickness of the layer package above and below the directly penetrated layers.

$\tan \alpha_1 = 0.1557$

$X = R \cdot \cos \epsilon + H \sin \epsilon$

$X_s = (R \cdot \cos \epsilon + H \sin \epsilon) - L \cdot \tan \alpha_1 - (L + T_D) \cdot \tan \alpha_1$

$= (R \cdot \cos \epsilon + H \sin \epsilon) - 0.1557(2 \cdot L + T_D)$

$t_{direct} = t_{indirect}$

$$\frac{\sqrt{R^2 + H^2}}{1000} = \frac{L}{1000 \cdot 0.9881} + \frac{X_s}{6500} + \frac{L + T_D}{1000 \cdot 0.9881}$$

$$L = \sqrt{\frac{R^2 + H^2}{1.974}} + \frac{R \cdot \cos \epsilon + H \cdot \sin \epsilon}{1.974 \cdot 6.5} + \frac{0.987 \cdot T_D}{1.974}$$

Since $-R \cdot \sin \epsilon + H \cdot \cos \epsilon = 0$

$$L' = \frac{-R \cdot \sin \epsilon + H \cdot \cos \epsilon}{1.974 \cdot 6.5} = 0$$

$$\tan \epsilon = \frac{H}{R}$$

$$L'' = \frac{-R \cdot \cos \epsilon - H \sin \epsilon}{1.974 \cdot 6.5}$$

If $0 \leq \epsilon \leq 90$

$$L'' < 0$$

$$L_B \left(\epsilon = \arctan \frac{H}{R}\right) = L_{max}$$

$$\cos \epsilon = \frac{1}{\sqrt{\tan^2 \epsilon + 1}} = \frac{R}{\sqrt{R^2 + H^2}}$$

$$\sin \epsilon = \frac{\tan \epsilon}{\sqrt{\tan^2 \epsilon + 1}} = \frac{H}{\sqrt{R^2 + H^2}}$$

$$L_{max} = \sqrt{\frac{R^2 + H^2}{1.974}} + \frac{R^2 + H^2}{1.974 \cdot 6.5 \sqrt{R^2 + H^2}} + \frac{T_D}{2}$$

$$L_{max} = 0.585 \cdot R_S + 0.5 \cdot T_D$$

$$L_{max} \approx 0.6 \cdot R_S + 0.5 \cdot T_D$$

Parallels to the layers in the distance L_{max} from either the detonation point or the location of the structure determine the lower and upper boundary of the rock body which has to be taken into consideration (A, B, C, and D in Figure 29). In the demonstration case of Figure 29, however, the distance L_{max} on the perpendicular into the upper layers exceeds the ground surface. Therefore, the real upper boundary is the ground surface itself. So layer T_2 is the upper boundary layer and layer T_{10} is the lower boundary layer.

The direct rays in areas A and D and the indirect rays of group II in areas B, C, and D have to be checked against leaving the half space. For the check, a critical X_A of each layer is computed (Figure 29).

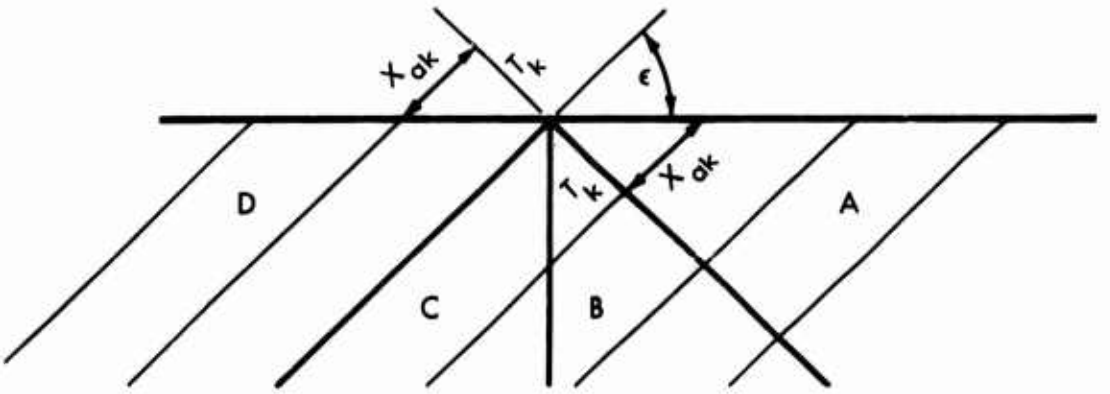

Figure 30. Propagation areas.

Rays in area A are considered real if the condition:

$$\Sigma x_k \leq x_{ak}$$

is met. The previously mentioned rays in areas B, C, and D are considered real if the condition:

$$\Sigma x_k \geq x_{ak}$$

is yielded.

The input to the program is organized in such a manner that the layers of the considered rock body are denoted by a continuous row of arabic numbers starting with "1". The upper boundary layer, generally the geologically youngest layer, is layer number "1".

Summarization of the rules for preparing the geology input:

1. Determine the sign of the inclination angle.

2. Determine the side boundaries of the rock body to be considered by drawing the perpendiculars to the layers through the point of detonation and the location of the structure.

3. Determine the upper and lower boundaries by parallels to the layers in the distance $L_{max} = 0.6R_S + 0.5\,T_D$ from the point of detonation and the location of the structure.

4. Check whether the ground surface substitutes the upper parallel as upper boundary.

5. Divide the layers in which detonation point and structure are located by an imaginary cut into two layers each.

6. Enumerate the layers of the rock body to be considered, starting with "1" for the upper boundary layer (generally the geologically youngest layer).

7. Order the layers penetrated by:

Ray Group I	to the input notation NLF,
Ray Group II	to the input notation NLB1, and
Ray Group III	to the input notation NLB2.

APPENDIX D

DERIVATION OF THE STRESS DISTRIBUTION CAUSED BY AN INCIDENT HARMONIC WAVE

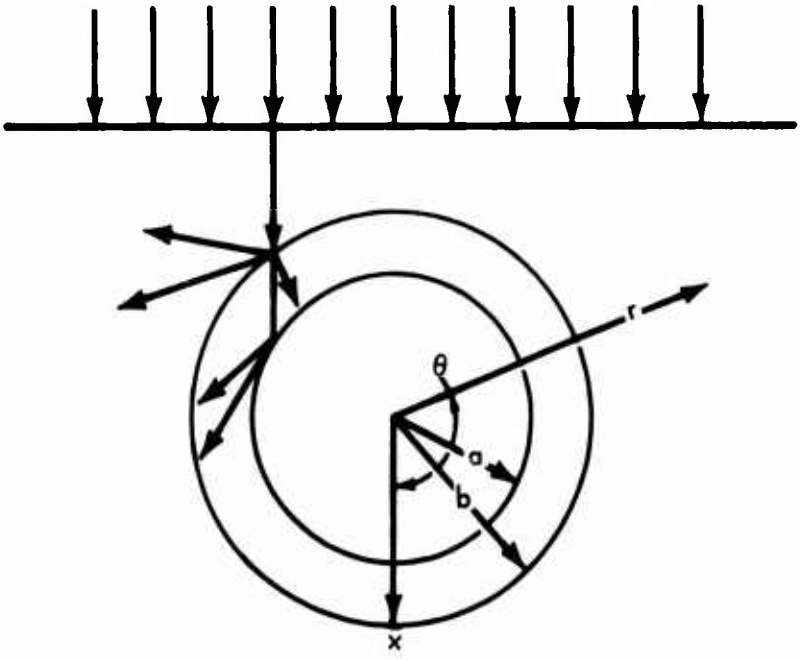

Figure 31. Stress wave intercepting cylinder.

Notation:

r = coordinate radius in meters

a = inner radius of the structure in meters

b = outer radius of the structure in meters

C_{α} = longitudinal seismic velocity in meters per second

C_{β} = transverse seismic velocity in meters per second

σ_r = radial stress in kp/m^2

σ_{θ} = circumferential stress in kp/m^2

$\tau_{r\theta}$ = shear stress in kp/m^2

1 as a subscript denotes the rock medium

2 as a subscript denotes the liner.

STRESS TENSOR

The differential equation governing the motion of an elastic, isotropic, and homogeneous medium is:

$$(\lambda + \mu)\nabla\nabla \cdot \bar{u} + \mu \nabla^2 \bar{u} = \rho \ddot{\bar{u}}$$

where

λ = Lame's 1. constant of the medium

μ = Lame's 2. constant of the medium

ρ = density of the medium

$\bar{u}$ = displacement vector

The displacement vector can be expressed by the derivatives of a scalar potential and a vector potential:

$$\bar{u} = \nabla\phi + \nabla x \bar{\psi}$$

The potentials satisfy the wave equation:

$$\nabla^2 \phi = \frac{1}{C_\alpha^2} \ddot{\phi}$$

$$\nabla^2 \bar{\psi} = \frac{1}{C_\beta^2} \ddot{\bar{\psi}}$$

where

ϕ = longitudinal displacement potential

$\bar{\psi}$ = distortional displacement potential

$C_\alpha = \sqrt{\frac{\lambda + 2\mu}{\rho}}$ = longitudinal seismic velocity

$C_\beta = \sqrt{\frac{\mu}{\rho}}$ = distortional seismic velocity

The stress tensor is related to the displacement vector by:

$$\bar{\bar{\sigma}} = \lambda (\nabla \cdot \bar{u})\, \bar{\bar{I}} + \mu (\nabla \bar{u} + \bar{u} \nabla)$$

where

$\bar{\bar{I}}$ = unit tensor

For the assumed plane strain problem, the vector-displacement potential is directed into the axis of the cylinder:

$$\bar{\psi} = \bar{e}_z \psi$$

The vector potential is the scalar product of the unit vector $\bar{e}_z$ and the magnitude ψ. Substituting the potentials into the stress tensor, the stress equation in cylindrical coordinates can be written as:

$$\sigma_r = \lambda \nabla^2 \phi + 2\mu \left(\frac{\partial^2 \phi}{\partial r^2} + \frac{1}{r} \frac{\partial^2 \psi}{\partial \theta \, \partial r} - \frac{1}{r^2} \frac{\partial \psi}{\partial \theta} \right)$$

$$\sigma_\theta = \lambda \nabla^2 \phi + 2\mu \left(\frac{1}{r^2} \frac{\partial^2 \phi}{\partial \theta^2} + \frac{1}{r} \frac{\partial \phi}{\partial r} - \frac{1}{r} \frac{\partial^2 \psi}{\partial r \, \partial \theta} + \frac{1}{r^2} \frac{\partial \psi}{\partial \theta} \right)$$

$$\tau_{r\theta} = 2\mu \left(\frac{1}{r} \frac{\partial^2 \phi}{\partial r \partial \theta} - \frac{1}{r^2} \frac{\partial \phi}{\partial \theta} + \frac{1}{r} \frac{\partial \psi}{\partial r} + \frac{1}{r^2} \frac{\partial^2 \psi}{\partial \theta^2} - \frac{1}{2} \nabla^2 \psi \right)$$

The equations for the displacement are:

$$u_r = \frac{\partial \phi}{\partial r} + \frac{1}{r} \frac{\partial \psi}{\partial \theta}$$

$$u_\theta = \frac{1}{r}\frac{\partial \phi}{\partial \theta} - \frac{\partial \psi}{\partial r}$$

STRESSES

The potentials of an incident, longitudinal, harmonic wave propagating in the x- direction are:

$$\phi = \phi_o e^{i(\alpha x - \omega t)}$$

$$\psi = 0$$

where

ϕ_o = amplitude

ω = circular frequency

$\alpha = \frac{\omega}{C_\alpha}$ = wave number of the longitudinal wave

The nonzero potential can be written in cylindrical coordinates as:

$$\phi = \phi_o e^{i(\alpha x - \omega t)} = \phi_o \sum_0^\infty \epsilon_n i^n J_n(\alpha r) \cos(n\theta) e^{-i\omega t}$$

where

J_n = Bessel function of first kind of order n

ϵ_n = 1 for n = 0

ϵ_n = 2 for $n \neq 0$

The incident wave is reflected at the liner. The outward-propagating longitudinal and shear waves are determined by:

$$\phi_{(1)}^{(R)} = \sum_{n=0}^{\infty} A_n H_n^{(1)}(\alpha_1 r) \cos n\theta \, e^{-i\omega t}$$

$$\psi_{(1)}^{(R)} = \sum_{n=0}^{\infty} B_n H_n^{(1)} (\beta_1 r) \sin n\theta \, e^{-i\omega t}$$

The waves propagating through the liner towards the inner boundary are represented by:

$$\phi_{(2)}^{(i)} = \sum_{n=0}^{\infty} M_n H_n^{(2)} (\alpha_2 r) \cos n\theta \, e^{-i\omega t}$$

$$\psi_{(2)}^{(i)} = \sum_{n=0}^{\infty} N_n H_n^{(2)} (\beta_2 r) \sin n\theta \, e^{-i\omega t}$$

The refracted wave is reflected at the inner face of the liner. The reflected waves propagate outward:

$$\phi_{(2)}^{(R)} = \sum_{n=0}^{\infty} R_n H_n^{(1)} (\alpha_2 r) \cos n\theta e^{-i\omega t}$$

$$\psi_{(2)}^{(R)} = \sum_{n=0}^{\infty} S_n H_n^{(1)} (\beta_2 r) \cos n\theta e^{-i\omega t}$$

where

$H_n^{(1)}$ = Hankel function of first kind of order n (for inward-propagating waves)

$H_n^{(2)}$ = Hankel function of second kind of order n (for outward-propagating waves)

$\alpha = \frac{\omega}{C_\alpha}$ = wave number of longitudinal wave

$\beta = \frac{\omega}{C_\beta}$ = wave number of shear wave

ω = circular frequency

A_n, B_n, M_n, N_n, R_n, and S_n are coefficients that have to be determined by using the boundary conditions:

At the interface between rock and liner,

$$r = b$$

$$\sigma_{r(1)} = \sigma_{r(2)}$$

$$\tau_{r\theta(1)} = \tau_{r\theta(2)}$$

$$u_{r(1)} = u_{r(2)}$$

$$u_{\theta(1)} = u_{\theta(2)}$$

the innerface of the liner has to be stress-free:

$$r = a$$

$$\sigma_{r(2)} = 0$$

$$\tau_{r\theta(2)} = 0$$

Superposition of the effects of the incident reflected and refracted waves respectively leads to the stress equations:

$$\sigma_{r(1)} = 2\mu_1 r^{-2} \sum_{n=0}^{\infty} \left[\left(\phi_o \epsilon_n i^n {}_1D_{nr}^{(i)} + A_{n1} D_{nr}^{(R)} + B_{n1} \bar{D}_{nr}^{(R)} \right) \times \left(\cos n\theta e^{-i\omega t} \right) \right]$$

$$\sigma_{\theta(1)} = 2\mu_1 r^{-2} \sum_{n=0}^{\infty} \left[\left(\phi_o \epsilon_n i^n {}_1F_{nr}^{(i)} + A_{n1} F_{nr}^{(R)} - B_{n1} \bar{D}_{nr}^{(R)} \right) \times \left(\cos n\theta e^{-i\omega t} \right) \right]$$

$$\tau_{r\theta(1)} = 2\mu_1 r^{-2} \sum_{n=0}^{\infty} \left[\left(\phi_o \epsilon_n i^n {}_1E_{nr}^{(i)} + A_{n1} E_{nr}^{(i)} + B_{n1} \bar{E}_{nr}^{(R)} \right) \left(\sin n\theta e^{-i\omega t} \right) \right]$$

$$\sigma_{r(2)} = 2\mu_2 r^{-2} \sum_{n=0}^{\infty} \left[\left(M_{n2} D_{nr}^{(i)} + N_{n2} \bar{D}_{nr}^{(i)} + R_{n2} D_{nr}^{(R)} + S_{n2} \bar{D}_{nr}^{(R)} \right) \times \left(\cos n\theta e^{-i\omega t} \right) \right]$$

$$\sigma_{\theta(2)} = 2\mu_2 r^{-2} \sum_{n=0}^{\infty} \left[\left(M_{n2} F_{nr}^{(i)} - N_{n2} \bar{D}_{nr}^{(i)} + R_{n2} F_{nr}^{(R)} - S_{n2} \bar{D}_{nr}^{(R)} \right) \times \left(\cos n\theta e^{-i\omega t} \right) \right]$$

$$\tau_{r\theta(2)} = 2\mu_2 r^{-2} \sum_{n=0}^{\infty} \left[\left(M_{n2} E_{nr}^{(i)} + N_{n2} \epsilon_{nr}^{(i)} + R_{n2} \bar{E}_{nr}^{(R)} + S_{n2} \bar{E}_{nr}^{(R)} \right) \times \left(\sin n\theta e^{-i\omega t} \right) \right]$$

where

$${}_1D_{nr}^{(i)} = \left(n^2 + n - \frac{1}{2}\beta_1^2 r^2 \right) J_n(\alpha_1 r) - \alpha_1 r J_{n-1}(\alpha_1 r)$$

$${}_2D_{nr}^{(1)} = \left(n^2 + n - \frac{1}{2}\beta_2^2 r^2 \right) H_n^{(2)}(\alpha_2 r) - \alpha_2 r H_{n-1}^{(2)}(\alpha_2 r)$$

$${}_1D_{nr}^{(R)} = \left(n^2 + n - \frac{1}{2}\beta_1^2 r^2 \right) H_n^{(1)}(\alpha_1 r) - \alpha_1 r H_{n-1}^{(1)}(\alpha_1 r)$$

$${}_2D_{nr}^{(R)} = \left(n^2 + n - \frac{1}{2}\beta_2^2 r^2 \right) H_n^{(1)}(\alpha_2 r) - \alpha_2 r H_{n-1}^{(1)}(\alpha_2 r)$$

$${}_1E_{nr}^{(i)} = (n^2 + n) J_n(\alpha_1 r) - n\alpha_1 r J_{n-1}(\alpha_1 r)$$

$${}_2E_{nr}^{(i)} = (n^2 + n) H_n^{(2)}(\alpha_2 r) - n\alpha_2 r H_{n-1}^{(2)}(\alpha_2 r)$$

$$ {}_1E_{nr}^{(R)} = (n^2 + n)\, H_n^{(1)}(\alpha_1 r) - n\alpha_1 r H_{n-1}^{(1)}(\alpha_1 r) $$

$$ {}_2E_{nr}^{(R)} = (n^2 + n)\, H_n^{(1)}(\alpha_2 r) - n\alpha_2 r H_{n-1}^{(1)}(\alpha_2 r) $$

$$ {}_1F_{nr}^{(i)} = -\left(n^2 + n - \alpha_1^2 r^2 + \tfrac{1}{2}\beta_1^2 r^2\right) J_n(\alpha_1 r) + \alpha_1 r J_{n-1}(\alpha_1 r) $$

$$ {}_2F_{nr}^{(i)} = -\left(n^2 + n - \alpha_2^2 r^2 + \tfrac{1}{2}\beta_2^2 r^2\right) H_n^{(2)}(\alpha_2 r) + \alpha_2 r H_{n-1}^{(2)}(\alpha_2 r) $$

$$ {}_1F_{nr}^{(R)} = -\left(n^2 + n - \alpha_1^2 r^2 + \tfrac{1}{2}\beta_1^2 r^2\right) H_n^{(1)}(\alpha_1 r) + \alpha_1 r H_{n-1}^{(1)}(\alpha_1 r) $$

$$ {}_2F_{nr}^{(R)} = -\left(n^2 + n - \alpha_2^2 r^2 + \tfrac{1}{2}\beta_2^2 r^2\right) H_n^{(1)}(\alpha_2 r) + \alpha_2 r H_{n-1}^{(1)}(\alpha_2 r) $$

$$ {}_1D_{nr}^{(R)} = -(n^2 + n)\, H_n^{(1)}(\beta_1 r) + n\beta_1 r H_{n-1}^{(1)}(\beta_1 r) $$

$$ {}_2D_{nr}^{(R)} = -(n^2 + n)\, H_n^{(1)}(\beta_2 r) + n\beta_2 r\, H_{n-1}^{(1)}(\beta_2 r) $$

$$ {}_2D_{nr}^{(i)} = -(n^2 + n)\, H_n^{(2)}(\beta_2 r) + n\beta_2 r\, H_{n-1}^{(2)}(\beta_2 r) $$

$$ {}_1\bar{E}_{nr}^{(R)} = -\left(n^2 + n - \tfrac{1}{2}\beta_1^2 r^2\right) H_n^{(1)}(\beta_1 r) + \beta_1 r\, H_{n-1}^{(1)}(\beta_1 r) $$

$$ {}_2\bar{E}_{nr}^{(R)} = -\left(n^2 + n - \tfrac{1}{2}\beta_2^2 r^2\right) H_n^{(1)}(\beta_2 r) + \beta_2 r\, H_{n-1}^{(1)}(\beta_2 r) $$

$$ {}_2\bar{E}_{nr}^{(i)} = -\left(n^2 + n - \tfrac{1}{2}\beta_2^2 r^2\right) H_n^{(2)}(\beta_2 r) + \beta_2 r\, H_{n-1}(\beta_2 r) $$

The coefficients A_n, B_n, M_n, N_n, R_n, and S_n can be determined from:

$$\left[a_{ij}\right]\left\{c_j\right\} = \left\{b_i\right\}$$

where

$$\left[a_{ij}\right] = \begin{vmatrix}
\nu_1 D_{nb}^{(R)} & \nu_1 \bar{D}_{nb}^{(R)} & {}_2D_{nb}^{(i)} & {}_2\bar{D}_{nb}^{(i)} & {}_2D_{nb}^{(R)} & {}_2\bar{D}_{nb}^{(R)} \\
\nu_1 E_{nb}^{(R)} & \nu_1 \bar{E}_{nb}^{(R)} & {}_2E_{nb}^{(i)} & {}_2\bar{E}_{nb}^{(i)} & {}_2E_{nb}^{(R)} & {}_2\bar{E}_{nb}^{(R)} \\
\alpha_1 b H_n^{(1)'}(\alpha_1 b) & n H_n^{(1)}(\beta_1 b) & \alpha_2 b H_n^{(2)'}(\alpha_2 b) & n H_n^{(2)}(\beta_2 b) & \alpha_2 b H_n^{(1)'}(\alpha_2 b) & n H_n^{(1)}(\beta_2 b) \\
n H_n^{(1)}(\alpha_1 b) & \beta_1 b H_n^{(1)'}(\beta_1 b) & n H_n^{(2)}(\alpha_2 b) & \beta_2 b H_n^{(2)'}(\beta_2 b) & n H_n^{(1)}(\alpha_2 b) & \beta_2 b H_n^{(1)'}(\beta_2 b) \\
0 & 0 & {}_2D_{na}^{(i)} & {}_2\bar{D}_{na}^{(i)} & {}_2D_{na}^{(R)} & {}_2\bar{D}_{na}^{(R)} \\
0 & 0 & {}_2E_{na}^{(i)} & {}_2\bar{E}_{na}^{(i)} & {}_2E_{na}^{(R)} & {}_2\bar{E}_{na}^{(R)}
\end{vmatrix}$$

and

$$\{c_j\} = \begin{Bmatrix} -A_n \\ -B_n \\ M_n \\ N_n \\ R_n \\ S_n \end{Bmatrix}$$

and

$$\{b_i\} = \phi_0 \cdot \bar{E}_n \cdot i^n = \begin{Bmatrix} \nu_1 D_{nb}^{(i)} \\ \nu_1 E_{nb}^{(i)} \\ \alpha_1 b J_n'(\alpha_1 b) \\ n J_n(\alpha_1 b) \\ o \\ o \end{Bmatrix}$$

The expressions

$$ {}_{j}X^{(y)}_{na} \quad \text{or} \quad {}_{j}X^{(y)}_{nb} $$

denote the values of

$$ {}_{j}X^{(y)}_{nr} $$

for r = a or r = b, respectively.

After determining the coefficients, the stress can be calculated from the stress equation.

APPENDIX E

DERIVATION OF THE FOURIER-TRANSFORMED POTENTIAL OF THE TRIANGULAR PRESSURE PULSE

THE FOURIER TRANSFORM IN GENERAL

The Fourier transform $f(\omega)$ of the pulse $f(t)$ is

$$f(\omega) = \frac{1}{2\pi} \int_{-\infty}^{\infty} f(t)\, e^{i\omega t}\, dt$$

Because the pulse is considered to start on times greater than zero, the one-sided Fourier transform:

$$f(\omega) = \frac{1}{2\pi} \int_{0}^{\infty} f(t)\, e^{i\omega t}\, dt$$

will be used.

If the function $f(t)$ is approximated by straight-line segments in the increments of Δt_j, the function can be written as:

$$f(t) = f_{j-1}(t) + \frac{\Delta f_j(t)}{\Delta t_j} (t - t_{j-1})$$

for

$$t_{j-1} < t \leq t_j$$

where

$$\Delta f_j(t) = f_j(t) - f_{j-1}(t)$$

$$\Delta t_j = t_j - t_{j-1}$$

The first derivative of the approximating function:

$$\frac{df_j(t)}{dt} = \frac{\Delta f_j(t)}{\Delta t_j}$$

is continuous inside the interval Δt_i . At the limit arguments, t_{j-1} and t_j , the first derivative is discontinuous. The function of the first derivative is a step function.

The second derivative inside the interval is zero:

$$\frac{d^2 f(t)}{dt^2} = 0$$

but is undefined in this form for the limiting arguments of the interval. The second derivative for the limiting arguments can be determined by the Dirac impulse:

$$\frac{d^2 f(t)}{dt^2} = \Delta f(t_j)\, \delta\ (t - t_j)$$

if $t = t_j$, where

$$\Delta f'(t_j) = \frac{df_{j+1}(t)}{dt} - \frac{df_j(t)}{dt}$$

Since the Dirac impulse is zero for arguments different from zero:

$$\delta (t-t_j) = 0$$

If $t \neq t_j$,

the second derivative for the interval and its limit on the right may be written:

$$f''(t) = \Delta f'(t_j)\, \delta\ (t - t_j)$$

$$t_{j-1} < t \leq t_j$$

The Fourier transform of $f''(t)$ is:

$$f''(\omega) = \frac{1}{2\pi} \int_0^{\infty} f''(t)\, e^{i\omega t}\, dt$$

$$f''(\omega) = \frac{1}{2\pi} \sum_{j=1}^{n} \int_{t_{j-1}}^{t_j} \Delta f'(t_j)\, \delta(t - t_j)\, e^{i\omega t}\, dt$$

Using the definition of the Dirac function:

$$\int_0^{\infty} e^{i\omega t}\, \delta(t - t_j)\, dt \equiv e^{i\omega t_j}$$

the transform of $f''(t)$ is simplified to:

$$f''(\omega) = \frac{1}{2\pi} \sum_{j=1}^{n} \Delta f'(t_j)\, e^{i\omega t_j}$$

The second derivative of the harmonic wave form is:

$$f''(\omega) = -\omega^2 f(\omega)$$

Therefore, the transform of $f(t)$ can finally be obtained as follows:

$$f(\omega) = -\frac{f''(\omega)}{\omega^2}$$

$$f(\omega) = \frac{1}{2\pi} \sum_{j=1}^{n} \frac{\Delta f'(t_j)\, e^{i\omega t}}{-\omega^2}$$

where, according to prior definition:

$$\Delta f'(t_j) = \frac{f_{j+1}(t) - f_j(t)}{t_{j+1} - t_j} - \frac{f_j(t) - f_{j-1}(t)}{t_j - t_{j-1}}$$

APPLICATION OF FOURIER TRANSFORM

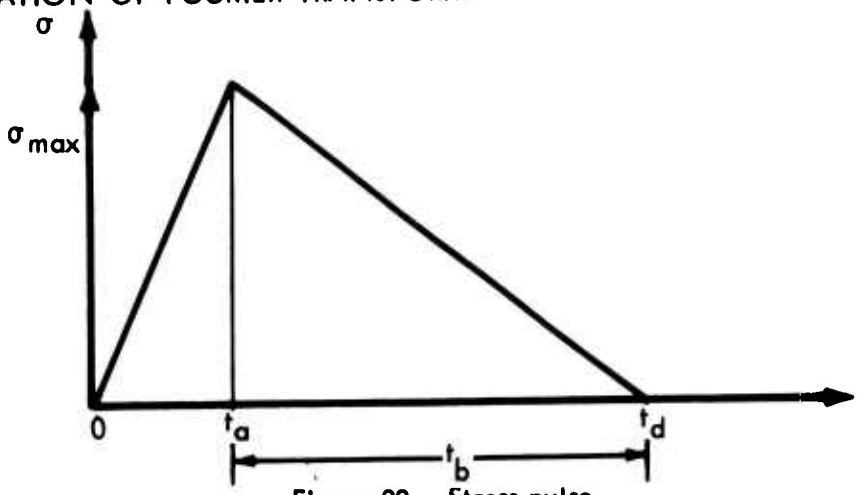

Figure 32. Stress pulse.

The free-field stress $\sigma(t)$ can be approximated:

$$\sigma(t) = \frac{\sigma_{max}^{(i)}}{t_a} \cdot t \qquad 0 \le t \le t_a$$

$$\sigma(t) = \frac{\sigma_{max}^{(1)} (t_d - t)}{(t_d - t_a)} \qquad t_a \le t \le t_d$$

The derivative differences with the arguments $t = t_j$ are:

$$t_j = 0$$

$$\Delta f'(0) = \frac{\sigma_{max}^{(i)}}{t_a}$$

$$t_j = t_a$$

$$\Delta f'(t_a) = \sigma_{max}^{(i)} \left(\frac{1}{t_b} + \frac{1}{t_a} \right)$$

$$t_j = t_d$$

$$\Delta f'(t_d) = \frac{\sigma^{(i)}_{max}}{t_b}$$

The free-field stress as a function of the circular frequency ω now can be expressed by:

$$\sigma(\omega) = \frac{\sigma^{(i)}_{max}}{2\pi \cdot \omega^2}\left[\frac{1}{t_a} \cdot e^{i\omega t_o}\left(\frac{1}{t_b} + \frac{1}{t_a}\right)e^{i\omega t_a} + \frac{1}{t_b} e^{i\omega t_d}\right]$$

$$\sigma(\omega) = \frac{\sigma^{(i)}_{max}}{2\pi \cdot \omega^2}\left[\left(\frac{1}{t_b} + \frac{1}{t_a}\right)e^{i\omega t_a} - \frac{1}{t_b} e^{i\omega t_d} - \frac{1}{t_a}\right]$$

Since the particle velocity is bound to the free-field stress by the relationship:

$$v = \frac{\sigma}{\rho \cdot C_\alpha}$$

where

ρ = density of the free-field medium

C_α = longitudinal seismic velocity of the free-field medium

the particle velocity as a function of the circular frequency can be written:

$$v(\omega) = \frac{\sigma^{(i)}_{max}}{2\pi\ \omega^2 \rho \cdot C_\alpha}\left[\left(\frac{1}{t_b} + \frac{1}{t_a}\right)e^{i\omega t_a} - \frac{1}{t_b} e^{i\omega t_d} - \frac{1}{t_a}\right] .$$

The Fourier transformation delivers:

$$v(t) = \int_0^\infty v(\omega) \cdot e^{i(\alpha x - \omega t)} \, d\omega$$

or, in a more general form:

$$v(t) = \int_0^\infty v(\omega) \cdot e^{i\omega t} \, d\omega$$

and

$$v(t) = \int_0^\infty \frac{\sigma_{max}^{(i)}}{2\pi \, \omega^2 \rho \cdot c_\alpha} \left[\left(\frac{1}{t_b} + \frac{1}{t_a} \right) e^{i\omega t_a} - \frac{1}{t_b} e^{i\omega t_d} - \frac{1}{t_a} \right] e^{i\omega t} d\omega \, .$$

DISPLACEMENT POTENTIAL AS A FUNCTION OF THE CIRCULAR FREQUENCY

The transform between $\phi(t)$ and $\varphi(\omega)$ is:

$$\phi(t) = \frac{1}{2\pi} \int_0^\infty \varphi(\omega) \, e^{i(\alpha x - \omega t)} \, d\omega$$

By taking the partial derivative with respect to x, the displacement equation is:

$$u(t) = \int_0^\infty \varphi(\omega) \, i\alpha \, e^{i(\alpha x - \omega t)} \, d\omega$$

By taking the derivative of the displacement expression with respect to time, the velocity equation is:

$$v(t) = \int_0^\infty \varphi(\omega)\,\alpha\,\omega\, e^{i(\alpha x-\omega t)}\,d\omega$$

and, with $\alpha = \omega/c_\alpha$, the form is:

$$v(t) = \frac{1}{c_\alpha}\int_0^\infty \varphi(\omega)\,\omega^2\, e^{i(\alpha x-\omega t)}\,d\omega$$

By comparing this equation with the last one of the previous section, the frequency-dependent potential now can be determined:

$$\varphi(\omega) = \frac{\sigma^{(i)}_{max}}{2\pi\,\omega^2\rho}\left[\left(\frac{1}{t_b}+\frac{1}{t_a}\right)e^{i\omega t_a} - \frac{1}{t_b}\,e^{i\omega t_d} - \frac{1}{t_a}\right]$$

or

$$\varphi(\omega) = \frac{v_{max}\,c_\alpha}{2\pi\cdot\omega^4}\left[\left(\frac{1}{t_b}+\frac{1}{t_a}\right)e^{i\omega t_a} - \frac{1}{t_b}\,e^{i\omega t_d} - \frac{1}{t_a}\right] .$$

APPENDIX F

DERIVATION OF THE STRESS DISTRIBUTION CAUSED BY A TRIANGULAR-SHAPED PRESSURE PULSE

The potentials of the incident triangular-shaped pulse that propagates in the x- direction are:

$$\varphi = \int_{-\infty}^{\infty} \varphi(\omega)\, e^{i(\alpha x - \omega t)}\, d\omega$$

$$\psi = 0$$

where

$\varphi(\omega)$ = Fourier transform of ϕ

ω = circular frequency

$\alpha = \frac{\omega}{C_\alpha}$ = wave number of the longitudinal wave.

The nonzero longitudinal potential φ can be expressed by a Bessel function series:

$$\varphi = \int_{-\infty}^{\infty} \varphi(\omega) e^{i(\alpha x - \omega t)}\, d\omega = \int_{-\infty}^{\infty} \varphi(\omega) \sum_{0}^{\infty} \left[\epsilon_n i^n \tau_n(\alpha r)\cos(n\theta) e^{-i\omega t}\right] d\omega$$

which yields stresses as follows:

$$\sigma_{r(1)dy} = 2\mu_1 r^{-2} \int_{\infty}^{\infty} \sum_{n=0}^{\infty} \left[\left(\phi_0(\omega)\epsilon_n i^n {}_1D_{nr}^{(i)} + A_{n1} D_{nr}^{(R)} + B_{n1} \bar{D}_{nr}^{(R)}\right) \times \left(\cos n\theta\, e^{-i\omega t}\, d\omega\right)\right]$$

$$\sigma_{\theta(1)dy} = 2\mu_1 r^{-2} \int_{\infty}^{\infty} \sum_{n=0}^{\infty} \left[\left(\phi_o(\omega) \epsilon_n i^n {}_1 F_{nr}^{(i)} + A_{n1} F_{nr}^{(R)} - B_{n1} \bar{D}_{nr}^{(R)} \right) \right.$$

$$\left. \times \left(\cos n\theta \, e^{-i\omega t} \, d\omega \right) \right]$$

$$\tau_{r\theta(1)dy} = 2\mu_1 r^{-2} \int_{\infty}^{\infty} \sum_{n=0}^{\infty} \left[\left(\phi_o(\omega) \epsilon_n i^n {}_1 E_{nr}^{(i)} + A_{n1} E_{nr}^{(R)} + B_{n1} \bar{E}_{nr}^{(R)} \right) \right.$$

$$\left. \times \left(\sin n\theta \, e^{-i\omega t} \, d\omega \right) \right]$$

$$\sigma_{r(2)dy} = 2\mu_2 r^{-2} \int_{\infty}^{\infty} \sum_{n=0}^{\infty} \left[\left(M_{n2} D_{nr}^{(i)} + N_{n2} \bar{D}_{nr}^{(i)} + R_{n2} D_{nr}^{(R)} + S_{n2} \bar{D}_{nr}^{(R)} \right) \right.$$

$$\left. \times \left(\cos n\theta \, e^{-i\omega t} \, d\omega \right) \right]$$

$$\sigma_{\theta(2)dy} = 2\mu_2 r^{-2} \int_{\infty}^{\infty} \sum_{n=0}^{\infty} \left[\left(M_{n2} F_{nr}^{(i)} - N_{n2} \bar{D}_{nr}^{(i)} + R_{n2} F_{nr}^{(R)} - S_{n2} \bar{D}_{nr}^{(R)} \right) \right.$$

$$\left. \times \left(\cos n\theta \, e^{-i\omega t} \, d\omega \right) \right]$$

$$\tau_{r\theta(2)dy} = 2\mu_2 r^{-2} \int_{\infty}^{\infty} \sum_{n=0}^{\infty} \left[\left(M_{n2} E_{nr}^{(i)} + N_{n2} \bar{E}_{nr}^{(i)} + R_{n2} E_{nr}^{(R)} + S_{n2} \bar{E}_{nr}^{(R)} \right) \right.$$

$$\left. \times \left(\sin n\theta \, e^{-i\omega t} \, d\omega \right) \right] .$$

APPENDIX G

DERIVATION OF THE ALLOWABLE STRESSES FOR ROCK

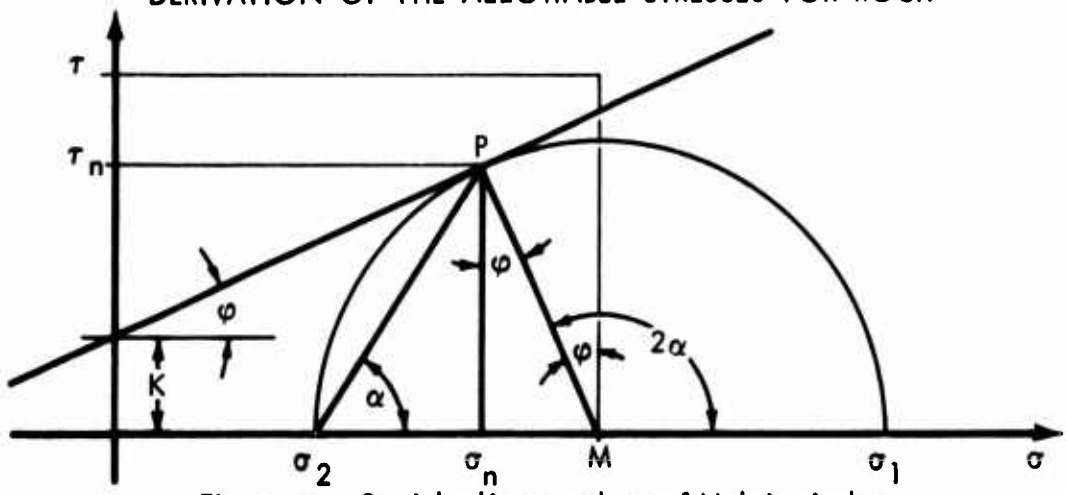

Figure 33. Straight-line envelope of Mohr's circles.

Notation:

K = cohesive strength in kp/m^2

φ = angle of internal friction

σ_1 = major principal stress

σ_2 = minor principal stress

σ_r = radial stress

σ_θ = circumferential stress

$\tau_{r\theta}$ = shear stress.

ALLOWABLE MAXIMUM PRINCIPAL STRESS IN AN ISOTROPIC MEDIUM

According to Mohr-Coulomb-Navier's Theory, the envelope of Mohr's circles is the straight line:

$$\tau = \operatorname{tg}\varphi \cdot \sigma + K$$

From Figure 32, it can be read:

$$\tau_n = \frac{\sigma_1 - \sigma_2}{2} \cos\varphi$$

$$\sigma_n = \frac{\sigma_1 + \sigma_2}{2} - \frac{\sigma_1 - \sigma_2}{2} \sin\varphi$$

$$\frac{\sigma_1 - \sigma_2}{2} \cos\varphi = \frac{\sin\varphi}{\cos\varphi}\left(\frac{\sigma_1 + \sigma_2}{2} - \frac{\sigma_1 - \sigma_2}{2} \sin\varphi\right) + K$$

Manipulations lead to the representation of the envelope related to the principal stresses:

$$\sigma_1 = \frac{2K\cos\varphi}{1 - \sin\varphi} + \frac{1 + \sin\varphi}{1 - \sin\varphi}\sigma_2$$

The last equation means that for a certain σ_2, the value of σ_1 is just the allowable limit. Therefore, the equation should be written:

$$\sigma_{allowable} = \frac{2K\cos\varphi}{1 - \sin\varphi} + \frac{1 + \sin\varphi}{1 - \sin\varphi}\sigma_2$$

The actual, maximum, principal stress σ_1 has to yield the condition:

$$\sigma_1 < \sigma_{allowable}.$$

APPENDIX H

DERIVATION OF THE SINGLE-SHOT SURVIVABILITY

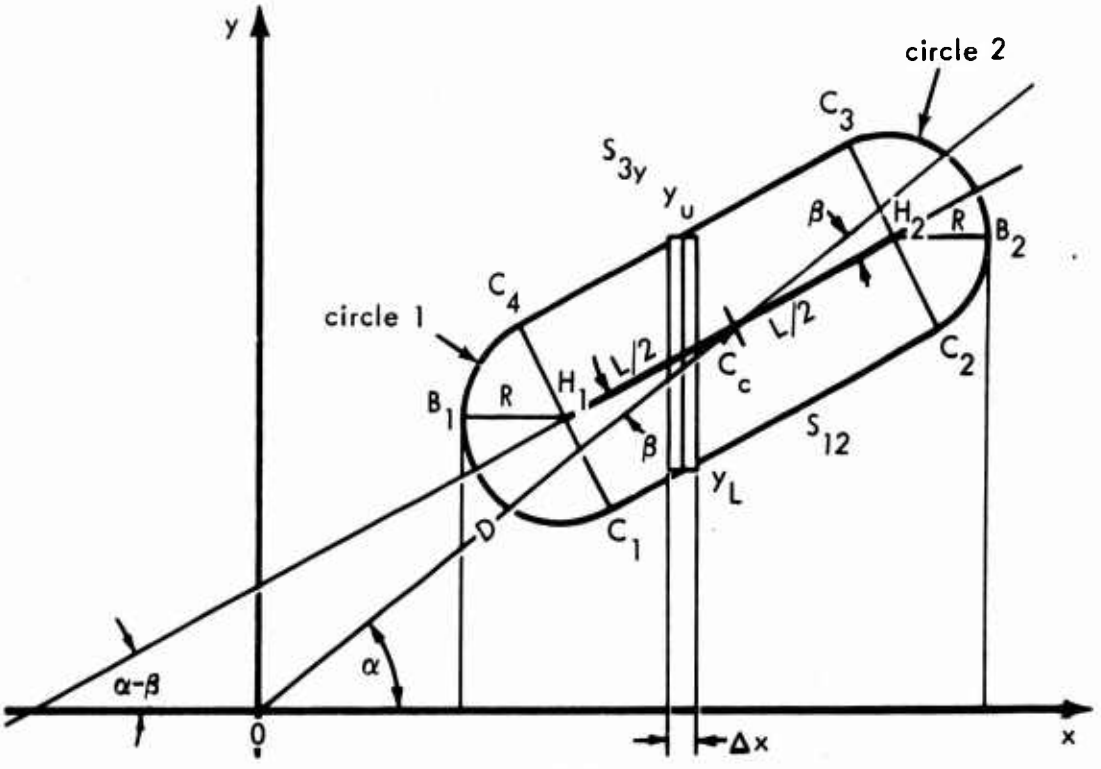

Figure 34. Plan for probability analysis.

Notation:

Desired ground zero is the origin 0 of the coordinate system

D = distance between desired ground zero and the center of the structure in meters

α = location angle for the center of the structure in degrees

L = length of the tunnel in meters

β = angle between tunnel direction and D direction in degrees

R = failure distance of the tunnel from GZ

σ_x = standard deviation in x direction

σ_y = standard deviation in y direction

P = probability of failure

S = probability of survival (survivability)

The idea is to determine the target area, to divide the target area in narrow rectangles of width Δx and of length $y_u - y_L$ to determine the probability of failure for the narrow rectangles, to find the probability of failure over the entire target area by summation of the probabilities of all the rectangles, and to determine the survivability out of the probability of failure.

DETERMINATION OF THE TARGET AREA

Center C_c:

$$x_{C_c} = D \cdot \cos \alpha$$

$$y_{C_c} = D \cdot \sin \alpha$$

Point H_1:

$$x_{H_1} = x_{C_c} - \frac{L}{2} \cdot \cos (\alpha - \beta)$$

$$y_{H_1} = y_{C_c} - \frac{L}{2} \cdot \sin (\alpha - \beta)$$

Point H_2:

$$x_{H_2} = x_{H_1} + L \cdot \cos (\alpha - \beta)$$

$$y_{H_2} = y_{H_1} + L \cdot \sin (\alpha - \beta)$$

Point C_1:

$$x_{C_1} = x_{H_1} + R \cdot \sin (\alpha - \beta)$$

$$y_{C_1} = y_{H_1} - R \cdot \cos (\alpha - \beta)$$

Point C_2:

$$x_{C_2} = x_{H_2} + R \cdot \sin(\alpha - \beta)$$

$$y_{C_2} = y_{H_2} - R \cdot \cos(\alpha - \beta)$$

Point C_3:

$$x_{C_3} = x_{H_2} - R \cdot \sin(\alpha - \beta)$$

$$y_{C_2} = y_{H_2} + R \cdot \cos(\alpha - \beta)$$

Point C_4:

$$x_{C_4} = x_{H_1} - R \cdot \sin(\alpha - \beta)$$

$$y_{C_4} = y_{H_1} + R \cdot \cos(\alpha - \beta)$$

BOUNDARIES

Equation of circle 1:

$$y = \left[R^2 - (x - x_{H_1})^2\right]^{1/2} + y_{H_1}$$

Equation of circle 2:

$$y = \left[R^2 - (x - x_{H_2})^2\right]^{1/2} + y_{H_2}$$

Equation of straight line S_{12}:

$$y = \frac{y_{C_2} - y_{C_1}}{x_{C_2} - y_{C_1}} (x - x_{C_1}) + y_{C_1}$$

Equation of straight line S_{34}:

$$y = \frac{y_{C_3} - y_{C_4}}{x_{C_3} - x_{C_4}} (x - x_{C_4}) + y_{C_4}$$

PARTITION OF THE TARGET AREA IN NARROW RECTANGLES

The width of the rectangles is:

$$\Delta x = \frac{\sigma_x}{A}$$

The divisor A determines the width of the rectangles in relation to the weapon accuracy expressed by the standard deviation in the x - direction. The usual problems for the resultant accuracy (probability result) was found to be sufficient if A was chosen:

$$A = 100$$

$$\Delta x = \frac{\sigma x}{100}$$

and the error was less than one percent.

To get the length of the rectangles the target-area boundary is divided into a lower boundary $B_1C_1C_2B_2$ and an upper boundary $B_2C_3C_4B_1$ (Figure 34). The length of rectangle 1 then is:

$$L = y_u \left(x + \frac{\Delta x}{2}\right) - y_L \left(x + \frac{\Delta x}{2}\right)$$

Because of the different functions, the y_u - and y_L - values are calculated differently over the x - range:

$$(x_{H_1} - R) < x < x_{C_4}$$

$$y_u = + \left[R^2 - (x - x_{H_1})^2\right]^{1/2} + y_{H_1}$$

$$x_{C_4} \leq x \leq x_{C_3}$$

$$y_u = \frac{y_{C_3} - y_{C_4}}{x_{C_3} - x_{C_4}} \cdot (x - x_{C_4}) + y_{C_4}$$

$$x_{C_3} < x \leq (x_{H_2} + R)$$

$$y_u = +\left[R^2 - (x - x_{H_2})^2\right]^{1/2} + y_{H_2}$$

$$(x_{H_1} - R) < x < x_{C_1}$$

$$y_L = -\left[R^2 - (x - x_{H_1})^2\right]^{1/2} + y_{H_1}$$

$$x_{C_1} \leq x \leq x_{C_2}$$

$$y_L = \frac{y_{C_2} - y_{C_1}}{x_{C_2} - y_{C_1}} \cdot (x - x_{C_1}) + y_{C_1}$$

$$x_{C_2} < x \leq (x_{H_2} + R)$$

$$y_L = -\left[R^2 - (x - x_{H_2})^2\right]^{1/2} + y_{H_2} .$$

PROBABILITY FUNCTION

The cumulative normal distribution function is used to represent the single-shot probability in military targeting (Figure 35). Since the

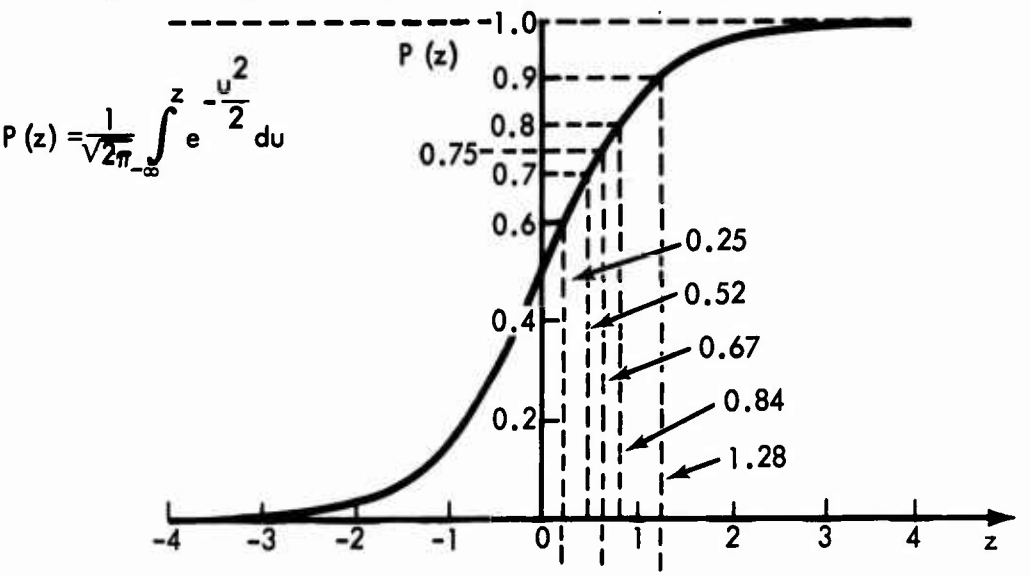

Figure 35. Normal distribution function.

integral in this function cannot be solved by the direct integration method, numerical values were obtained by series approximations and established and published in tables in References 11, 12, and 13. Using the table of Reference 13, four series functions were developed to substitute the probability function in the range from $z = .00$ to $z = +00$. The error made by using the approximation functions is less than one percent:

$$1.95 \leq z$$

$$P(z) = 1 - 0.399 \cdot \frac{1}{e^{\frac{z^2}{2}}} \left(\frac{1}{z} - \frac{1}{z^3} \right)$$

$$0 < z < 1.95$$

$$P(z) = 0.841 + 0.242 \left[(z - 1) - \frac{(z - 1)^2}{2} + \frac{(z - 1)^4}{12} \right]$$

$$(-1.95) < z \leq 0$$

$$P(z) = 0.159 - 0.242 \left[(z - 1) - \frac{(z - 1)^2}{2} + \frac{(z - 1)^4}{12} \right]$$

$$z \leq (-1.95)$$

$$P(z) = 0.399 \cdot \frac{1}{e^{\frac{z^2}{2}}} \left(- \frac{1}{z^3} - \frac{1}{z} \right)$$

The independent variable z is measured in standard deviations. In targeting, the standard deviation is expressed in a length unit. To introduce them, the length values x, Δx, y_u, and y_L have to be divided by the appropriate standard deviation:

$$z_1 = \frac{x}{\sigma x}$$

$$z_2 = \frac{x + \Delta x}{\sigma x}$$

$$z_3 = \frac{y_u}{\sigma y}$$

$$z_4 = \frac{y_L}{\sigma y}$$

The single-shot probability for the stripe of infinite length between y_u and y_L is:

$$P_y = P(z_3) - P(z_4)$$

Similarly, the single-shot probability for the stripe of infinite length and width Δx is:

$$P_x = P(z_2) - P(z_1)$$

The single-shot probability of the rectangle $x \cdot (y_u - y_L)$ is:

$$P_{\square} = P_y \cdot P_x$$

Summation of the whole target area leads to the single-shot probability for the target:

$$P = \sum P_{\square}$$

$$P = \sum_{(x_{H_1} - R)}^{(x_{H_2} + R)} \left[P\left(\frac{x + \Delta x}{\sigma x}\right) - P\left(\frac{x}{\sigma x}\right) \right]$$

$$\times \left[P\left(\frac{y_u\left(x + \frac{\Delta x}{2}\right)}{\sigma y}\right) - P\left(\frac{y_L\left(x + \frac{\Delta x}{2}\right)}{\sigma y}\right) \right]$$

The survivability S is obtained by:

$$S = 1 - P$$

APPENDIX I

COST AND COST-EFFECTIVENESS COMPUTATION

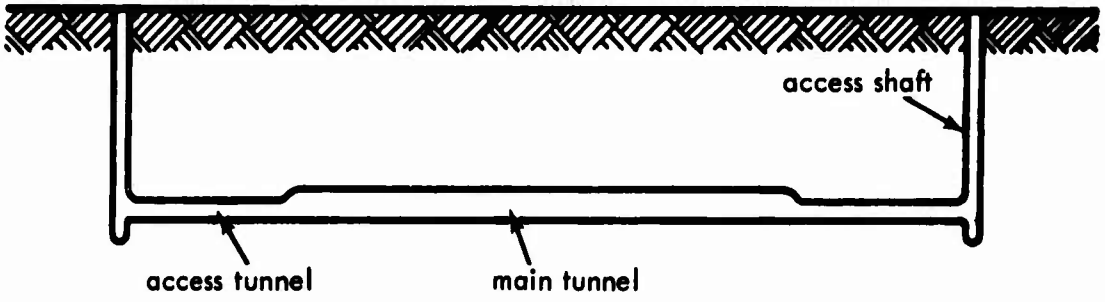

Figure 36. Tunnel section for example problem.

Notation:

K	=	cohesive rock strength, in kp/cm^2
$C_{\alpha 2}$	=	seismic velocity of liner material, in meters per second
L	=	length of main tunnel, in meters
L_{Tu}	=	length of access tunnel, in meters
a_{Tu}	=	inner radius of access tunnel, in meters
a	=	inner radius of tunnel, in meters
a_{Sh}	=	inner radius of access shaft, in meters
b	=	outer radius of tunnel, in meters
b_{Tu}	=	outer radius of access tunnel, in meters
b_{Sh}	=	outer radius of access shaft, in meters
H	=	depth of main tunnel, in meters

p_ℓ = percentage of longitudinal reinforcement

p_θ = percentage of circumferential reinforcement

p_w = percentage of web reinforcement

E_L = cost adjust factor for labor costs

E_E = cost adjust factor for underground equipment

E_{Em} = cost adjust factor for energy

E_{Ex} = cost adjust factor for explosives

E_{Dr} = cost adjust factor for drill material

E_{Co} = cost adjust factor for concrete

E_{St} = cost adjust factor for reinforcement steel

E_{StCy} = cost adjust factor for steel liner

F = cost factor for shafts

C_{Tot} = total structure costs (dollars) for conventional excavation in rock

$C_{Tot\ mach}$ = total structure costs (dollars) for machine excavation in rock

V_{us} = usable volume

C_{Space} = structure costs per usable volume in rock ($/m^3) for conventional excavation

$C_{Space\ mach}$ = structure cost per usable volume in rock ($/m^3) for machine excavation

C_{eff} = cost effectiveness for conventional excavation

$C_{eff\ mach}$ = cost effectiveness for machine excavation

The cost equations, compiled here, are based upon figures in Reference 14.

LABOR COSTS

The labor costs, given in dollars per lineal meter, comprise costs for excavating and dumping in the vicinity of the tunnel portal:

Dry, massive, moderately jointed or dry, intact rock:

$K \geq 200\ kp/cm^2$

$b < 2.30\ m$

$$C_L = E_L \cdot (88.1 \cdot b^2 - 244.1 \cdot b + 450.1)$$

$b \geq 2.30\ m$

$$C_L = E_L\ (41.6 \cdot b^2 - 91.8 \cdot b + 394.1)$$

Dry, stratified or schistose rock:

$200\ kp/cm^2 > K \geq 100\ kp/cm^2$

$b < 2.30\ m$

$$C_L = E_L\ (55.4 \cdot b^2 - 153.7 \cdot b + 355.0)$$

$b \geq 2.30\ m$

$$C_L = E_L\ (43.3 \cdot b^2 - 120.1 \cdot b + 395.0)$$

Dry, moderately blocky and seamy rock:

$100\ kp/cm^2 > K \geq 50\ kp/cm^2$

$b < 2.30\ m$

$$C_L = E_L \cdot (88.1 \cdot b^2 - 254.4 \cdot b + 438.0)$$

$b \geq 2.30\ m$

$$C_L = E_L \cdot (57.7 \cdot b^2 - 192.8 \cdot b + 504.0)$$

Dry, very blocky and seamy rock:

$50\ kp/cm^2 > K$

$b < 2.30\ m$

$$C_L = E_L \cdot (65.5 \cdot b^3 - 192.7 \cdot b + 416.0)$$

$b \geq 2.30\ m$

$$C_L = E_L\ (44.8 \cdot b^2 - 96.3 \cdot b + 364.0)\ .$$

UNDERGROUND EQUIPMENT COSTS

Underground equipment includes:

1. Drill jumbos, drills, mucking machines, cars, locomotives, compressors, ventilator fans, ~~small~~ miscellaneous equipment, and
2. Pipes and tracts.

A write-off rate of 15 percent per month is taken into account for the first group. This rate covers depreciation and maintenance. The monthly costs were reduced to unit costs in dollars per lineal meter. The second group of equipment items could be related directly to the tunnel length.

Dry, massive, moderately jointed or dry intact rock:

$K \geq 200\ kp/cm^2$

$b < 1.8\ m$

$$C_E = E_E\ (13.6 \cdot b + 144.0)$$

$1.8\ m \leq b < 2.75\ m$

$$C_E = E_E\ (32.2 \cdot b + 195.1)$$

$2.75\ m \leq b$

$$C_E = E_E\ (64.4 \cdot b + 160.8)$$

Dry, stratified or schistose rock:

$200\ kp/cm^2 > K \geq 100\ kp/cm^2$

$b < 1.8\ m$

$C_E = E_E \cdot 154.1$

$1.8\ m \leq b < 2.75\ m$

$C_E = E_E\ (32.2 \cdot b + 165.6)$

$2.75\ m \leq b$

$C_E = E_E\ (57.3 \cdot b + 141.0)$

Dry, moderately blocky and seamy rock:

$100\ kp/cm^2 > K \geq 50\ kp/cm^2$

$b < 1.8\ m$

$C_E = E_E \cdot 157.4$

$1.8\ m \leq b < 2.75\ m$

$C_E = E_E\ (32.2 \cdot b + 175.5)$

$2.75\ m \leq b$

$C_E = E_E\ (64.5 \cdot b + 134.8)$

Dry, very blocky and seamy rock:

$50\ kp/cm^2 > K$

$b < 1.8\ m$

$C_E = E_E \cdot 164.0$

$1.8\ m \leq b < 2.75\ m$

$$C_E = E_E \ (48.4 \cdot b + 145.0)$$

$2.75 \text{ m} \leq b$

$$C_E = E_E \ (71.6 \cdot b + 131.1) \ .$$

ENERGY COSTS

The energy costs given in dollars per lineal meters are based on a unit price of 1 cent per horsepower hour:

Dry, massive, moderately jointed or dry, intact rock:

$K \geq 200 \text{ kp/cm}^2$

$b < 1.8 \text{ m}$

$$C_{En} = E_{En} \cdot 14.9$$

$1.8 \text{ m} \leq b < 2.75 \text{ m}$

$$C_{En} = E_{En} \ (5.9 \cdot b + 4.3)$$

$2.75 \text{ m} \leq b$

$$C_{En} = E_{En} \ (4.6 \cdot b + 10.5)$$

Dry, stratified or schistose rock:

$200 \text{ kp/cm}^2 > K \geq 100 \text{ kp/cm}^2$

$b < 1.8 \text{ m}$

$$C_{En} = E_{En} \cdot 13.1$$

$1.8 \text{ m} \leq b < 2.75 \text{ m}$

$$C_{En} = E_{En} \ (3.1 \cdot b + 7.3)$$

$2.75 \text{ m} \leq b$

$$C_{En} = E_{En} \cdot (4.1 \cdot b + 6.8)$$

Dry, moderately blocky and seamy rock:

$100\ kp/cm^2 > k \geq 50\ kp/cm^2$

$b < 1.8\ m$

$$C_{En} = E_{En} \cdot 13.4$$

$1.8\ m \leq b < 2.75\ m$

$$C_{En} = E_{En} \cdot (4.3 \cdot b + 5.6)$$

$2.75\ m \leq b$

$$C_{En} = E_{En} \cdot (5.0 \cdot b + 5.9)$$

Dry, very blocky and seamy rock:

$50\ kp/cm^2 > K$

$b < 1.8\ m$

$$C_{En} = E_{En} \cdot 14.1$$

$1.8\ m \leq b < 2.75\ m$

$$C_{En} = E_{En}\ (4.8 \cdot b + 5.9)$$

$2.75\ m \leq b$

$$C_{En} = E_{En}\ (6.1 \cdot b + 4.9)\ .$$

COSTS FOR EXPLOSIVES

The costs per lineal meter are:

Dry, massive,moderately jointed or dry intact rock:

$K \geq 200\ kg/cm^2$

$b < 1.0\ m$

$$C_{Ex} = 0$$

$1.0\ m \leq b < 2.0\ m$

$$C_{Ex} = E_{Ex} \cdot (33.6 \cdot b - 21.3)$$

$2.0\ m \leq b$

$$C_{Ex} = E_{Ex}\ (7.5 \cdot b^2 - 3.4 \cdot b + 22.2)$$

Dry, stratified or schistose rock:

$200\ kp/cm^2 > K \geq 100\ kp/cm^2$

$b < 1.0\ m$

$$C_{Ex} = 0$$

$1.0\ m \leq b < 2.0\ m$

$$C_{Ex} = E_{Ex} \cdot (25.1 \cdot b - 14.4)$$

$2.0\ m \leq b$

$$C_{Ex} = E_{Ex} \cdot (4.1 \cdot b^2 + 4.2 \cdot b + 10.5)$$

Dry, moderately blocky and seamy rock:

$100\ kp/cm^2 > K \geq 50\ kp/cm^2$

$b < 1.0\ m$

$$C_{Ex} = 0$$

$1.0\ m \leq b < 2.0\ m$

$$C_{Ex} = E_{Ex} \cdot (26.9 \cdot b - 15.8)$$

$2.0\ m \leq b$

$$C_{Ex} = E_{Ex} \cdot (5.0 \cdot b^2 + 1.1 \cdot b + 15.1)$$

Dry, very blocky and seamy rock:

$50\ kp/cm^2 > K$

$b < 1.0\ m$

$C_{Ex} = 0$

$1.0\ m \leq b < 2.0\ m$

$C_{Ex} = E_{Ex}\ (21.5 \cdot b - 11.4)$

$2.0\ m \leq b$

$C_{Ex} = E_{Ex} \cdot (3.0 \cdot b^2 + 5.9 \cdot b + 7.6)$.

COST FOR DRILL BITS AND RODS

The costs for drill bits and rods are as follows:

carbide inset bits–$14.20 each

drill rods–$15.00 each

The unit costs are dimensioned in dollars per lineal meters. They are for all kinds of rocks:

$$C_{Dr} = E_{Dr} \cdot (3.3 \cdot b - 1.2)\ .$$

EXCAVATION COSTS

The sum of the labor, equipment, energy, explosive, and drill material costs establishes a subtotal of the excavation costs:

$$C_{Sub} = C_L + C_E + C_{En} + C_{Ex} + C_{Dr}$$

For engineering, overhead, and contingencies, 25 percent of the subtotal is added. For profits, 15 percent of the subtotal is added. In addition to these costs, expenses for miscellaneous items are to be taken into account. So, the excavation costs in dollars per lineal meter are:

$$C_{EC} = 1.4 \cdot C_{Sub} + C_M$$

where C_M is the miscellaneous cost:

$$C_M = E_M \cdot 9.35 \cdot b^2 .$$

LINER COSTS

The tunnels might be lined in plain concrete, reinforced concrete, or steel. The seismic velocity of the liner is distinguishing in the program when concrete or steel is to be considered in the cost-computation subroutine. If the seismic velocity $C_{\alpha 2}$ of the liner equals or is less than 4,500 meters per second, control is given to the calculation of the costs of reinforced concrete liner. If the seismic velocity exceeds 4,500 meters per second, the costs for a steel liner are computed.

REINFORCED CONCRETE LINER

The amount of reinforcement steel is:

$$A_{St} = \frac{3.14}{100}\left[\left(p_\ell + p_\theta\right)\left(b^2 - a^2\right) + 2 \cdot a \cdot p_w \cdot \left(b - a\right)\right]$$

The amount of concrete is:

$$A_{Co} = 3.14\left[\left(0.15 + b\right)^2 - a^2\right] - A_{St}$$

The costs for the concrete are based on a unit price of $40.00 per cubic yard in place. The costs for the reinforcement steel are based on:

$0.30 per pound

$$C_{Co} = E_{Co} \cdot A_{Co} \cdot \frac{40}{0.76}$$

$$C_{St} = E_{St} \cdot A_{St} \cdot 7.85 \cdot 2204.6 \cdot 0.30$$

The costs per lineal meter for a reinforced concrete liner are:

$$C_{Li} = C_{Co} + C_{St}$$

If plain concrete is used, the costs are obtained by setting:

$$p_{\ell} = p_{\theta} = p_{w} = 0$$

The costs for steel liner consist of the costs for steel and Gunite between rock and steel liner. The basic unit prices are:

$0.44 per pound for steel in place

$3.95 per cubic foot for Gunite in place

$$C_{Li} = E_{StCy} (b^2 - a^2) \cdot 3.14 \cdot 2204.6 \cdot 0.44$$

$$+ E_{Co} \cdot 6.28 \cdot b \cdot 0.05 \cdot 35 \cdot 3.95 \ .$$

TOTAL STRUCTURE COSTS

The sum of the excavation costs and the liner costs furnishes the total structure costs per lineal meter:

$$C_{Str} = C_{El} + C_{Li}$$

The protective underground structure consists usually of the main tunnel, access tunnels, and access shafts. The costs of the access structures can be calculated with the previously given cost equations, as well as the costs of the main structure. For the access structures, the pertaining radii are to be introduced:

Access tunnel:

$$C_{Tu} = C_{Str} (a = a_{Tu} , b = b_{Tu})$$

Access shaft:

$$C_{Sh} = C_{Str} (a = a_{Sh} , b = b_{Sh}) \cdot F$$

The factor F in the cost equation for the shaft brings into account that a shaft is more expensive than a tunnel of the same diameter. In general, $F = 1.5$. The total costs in dollars for the access structures are:

$$C_{AcTu} = L_{Tu} \cdot C_{Tu}$$

$$C_{AcSh} = (H + b + 3) \cdot C_{Sh}$$

The access costs are:

$$C_{Ac} = C_{AcTu} + C_{AcSh}$$

The total costs for the entire protective structure are:

$$C_{Tot} = C_{Str} \cdot L + C_{Ac} \cdot$$

SPECIFIC STRUCTURE COSTS

In many application cases, an estimation of the total structure cost is insufficient. Very often specific costs must be made available for economic comparisons—cost related to usable volume:

$$V_{us} = L \cdot 3.14 \cdot a^2$$

is:

$$C_{Space} = \frac{C_{Tot}}{V_{us}}$$

The effectiveness and the cost of a structure are measured in the expression of the cost effectiveness:

$$C_{eff} = \frac{C_{Tot}}{V_{us} \cdot S} \cdot$$

APPENDIX J

DESCRIPTION, FLOW CHART, AND LISTING OF THE MAIN PROGRAM

A flow chart for the computer program is given in Figure 37. The arrangement of the program can be understood and followed by using the flag "NPAS" as a guide. Prior to setting "NPAS" to one, the Input is read from five cards:

Card 1: Format: 2F10.0, 2F5.0, SE 10.6

Cols 1-10	Specif. gravity of media	(no units)
Cols 11-20	Specif. gravity of liner	(no units)
Cols 21-25	Poisson's ratio of media	(no units)
Cols 26-30	Poisson's ratio of liner	(no units)
Cols 31-40	Elastic modulus of media	(kp/m^2)
Cols 41-50	Elastic modulus of liner	(kp/m^2)
Cols 51-60	Radius of inside liner	(meters)
Cols 61-70	Radius of outside liner	(meters)
Cols 71-80	Depth of cylinder center	(meters)

Card 2: Format: 7E10.6, F5.0, I5

Cols 1-10	Tangent of phi of media	(no units)
Cols 11-20	Cohesive strength of media	(kp/m^2)
Cols 21-30	Tensile strength of media	(kp/m^2)
Cols 31-40	Constant "L" of liner	(kp/m^2)
Cols 41-50	Constant "M" of liner	$(\frac{kp}{m^2}) \cdot (\frac{m^2}{kp})^{1.37}$
Cols 51-60	Constant "N" of liner	(no units)
Cols 61-70	Tensile strength of liner	(kg/m^2)

Cols 71-75	Nominal Weapon Yield	(KT)
Cols 76-80	Number of weapon type*	(no units)

Card 3: Format: 8F10.0

Cols 1-10	Distance from cylinder to target	(meters)
Cols 11-20	Length of cylinder	(meters)
Cols 21-30	Angle alpha	(degree)
Cols 31-40	Angle beta	(degree)
Cols 41-50	Standard deviation in "X"	(meters)
Cols 51-60	Standard deviation in "Y"	(meters)
Cols 61-70	Effect longitudinal seismic velocity between GZ and structure	(meters per second)
Cols 71-80	Adjustment factor for labor cost	(no units)
Alpha:	Location of cylinder from target	
Beta:	Orientation of cylinder. . . direction	

Standard Deviation: Range at which 40% of shots fall inside.

Card 4: Format: 8F10.0

Cols 1-10	Radius inside liner of access tunnel	(meters)
Cols 11-20	Radius outside liner of access tunnel	(meters)
Cols 21-30	Access tunnel length	(meters)
Cols 31-40	Radius inside liner of access shaft	(meters)
Cols 41-50	Outside liner of access shaft	(meters)
Cols 51-60	Ratio of longitudinal reinforcement	(percent)
Cols 61-70	Ratio of circumferential reinforcement	(percent)
Cols 71-80	Ratio of web reinforcement	(percent)

* Number of weapon type: "1" Contact surface burst, "2" true surface burst, "3" fully buried detonation (nominal weapons yield = effective weapons yield).

Card 5: Format: 8F10.0

Cols 1-10	Adjustment factor for equipment cost	(no units)
Cols 11-20	Adjustment factor for power	(no units)
Cols 21-30	Adjustment factor for explosives	(no units)
Cols 31-40	Adjustment factor for drill bits and rods	(no units)
Cols 41-50	Adjustment factor for concrete	(no units)
Cols 51-60	Adjustment factor for reinforcement steel	(no units)
Cols 61-70	Miscellaneous	(no units)
Cols 71-80	Adjustment factor for steel liner	(no units)

NPAS = 1.

The static stresses, the principal stresses, and the yield stresses are computed for inside the liner. A yield check is made. If yielding does not occur, then it is:

NPAS = 2.

The procedure under NPAS = 1 will be repeated for the interface for both liner and rock. If no yielding exists, the weapon values will be computed. The horizontal distance, incremented by one diameter, is set to zero. The peak free-field dynamic stress is determined and checked against a preliminary yield:

$$\text{preliminary} = \frac{2K \cdot \cos\varphi}{1 - \sin\varphi}$$

where, in accordance with the notation of Appendix G,

K = cohesive strength of rock in kp/m^2

φ = angle of internal friction in degrees

If yielding occurs, the horizontal distance will be increased as long as the check against the preliminary yield is negative. The application of

the preliminary check shortens considerably the run time since the dynamic stresses and the appropriate strength values need not be computed for each new horizontal distance.

If the preliminary yield check is negative, then it will be:

NPAS = 3.

The pressure pulse is computed. The frequency values for the integration are established:

NPAS = 4.

Static and dynamic stresses and the pertaining yield values are computed for rock and liner at the interface. If either rock or liner yields, the horizontal distance is increased and the dynamic part is resolved:

NPAS = 5.

The procedure of NPAS = 4 is repeated for the inside of the liner. If it yields no longer, then it will be:

NPAS = 6.

Where the failure occurred first, in the interface or at the inside of the liner, is checked. The horizontal distance is moved into the safe area by increasing it by one diameter. The survivability and the economic features are computed. Then a sixth card, containing information about the type of the next problem, is read in:

Card 6: Format: I1.

Only one value occurs in Col. 1:

"0" All data have been run and the program calls an exit and prints "Job Completed."

"1" A new problem is to be run in which new data cards (1-6) will be read.

"2" Only new data cards (3-6) will be read. This allows a change in the cost of probability programs: one change in the length of the cylinder or distance to the target.

The output data are the static stresses for the:

1. Inside liner,

2. Interface liner, and
3. Rock at the interface for 13 angles from 0 to 180 degrees.

Other output data include:

1. Total stresses for 13 angles and 10 time steps,
2. Minimum survival distance,
3. Probability of failure,
4. Survivability,
5. Total cost for conventional tunneling,
6. Total cost for machine tunneling, and
7. Cost per usable volume per unit increment of survivability.

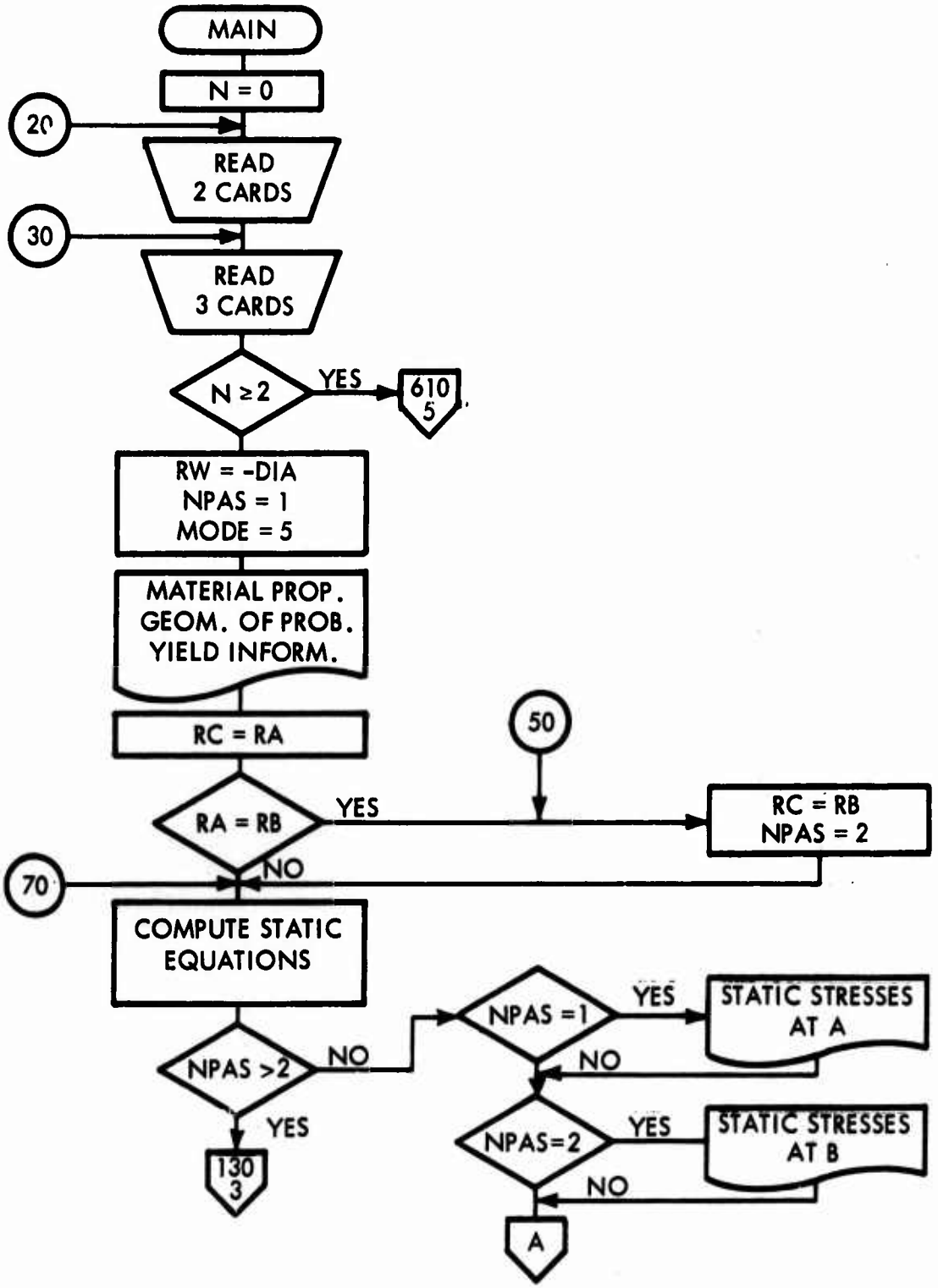

Figure 37. Flow diagram for the computer program.

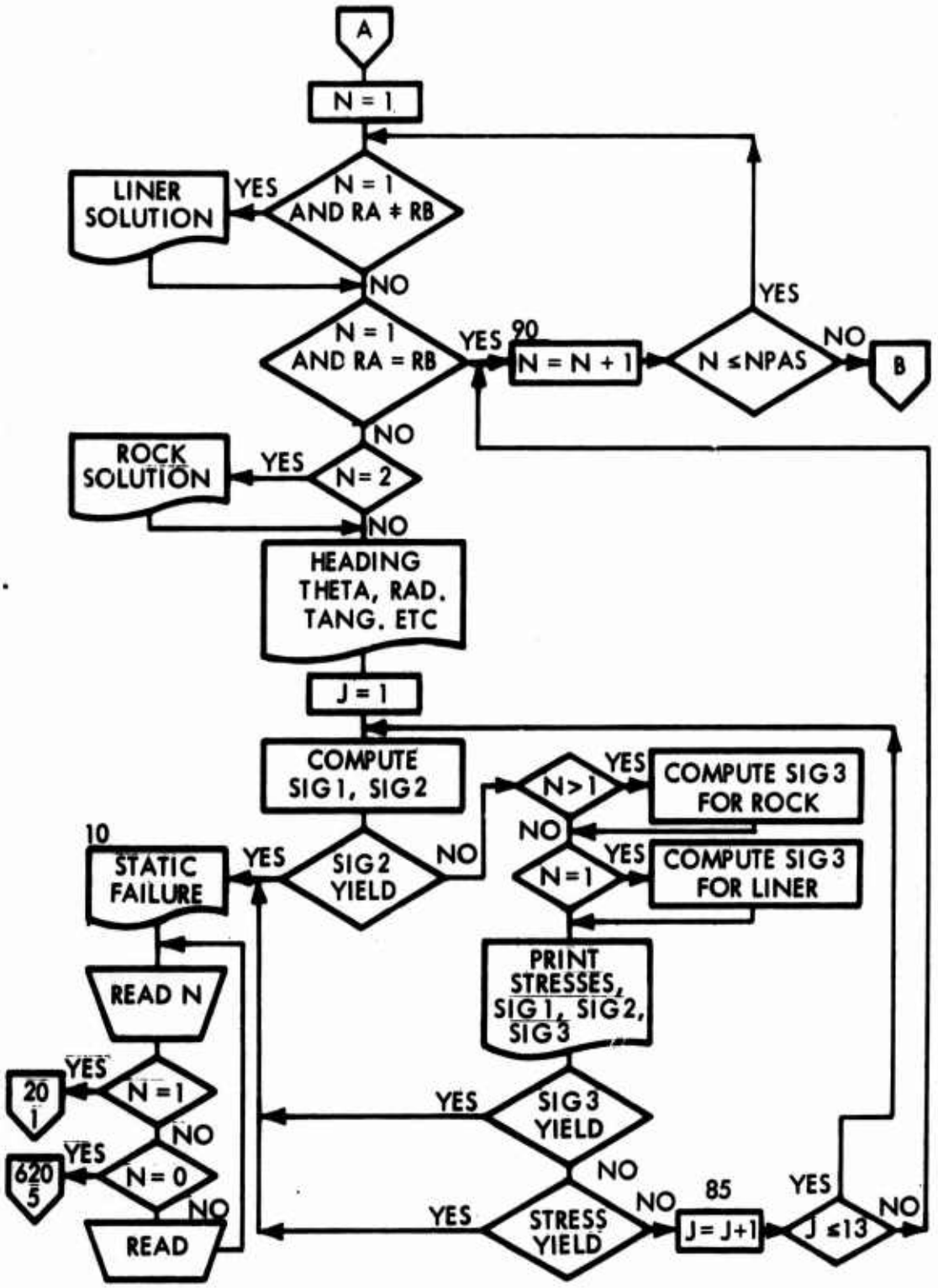

Figure 37—continued.

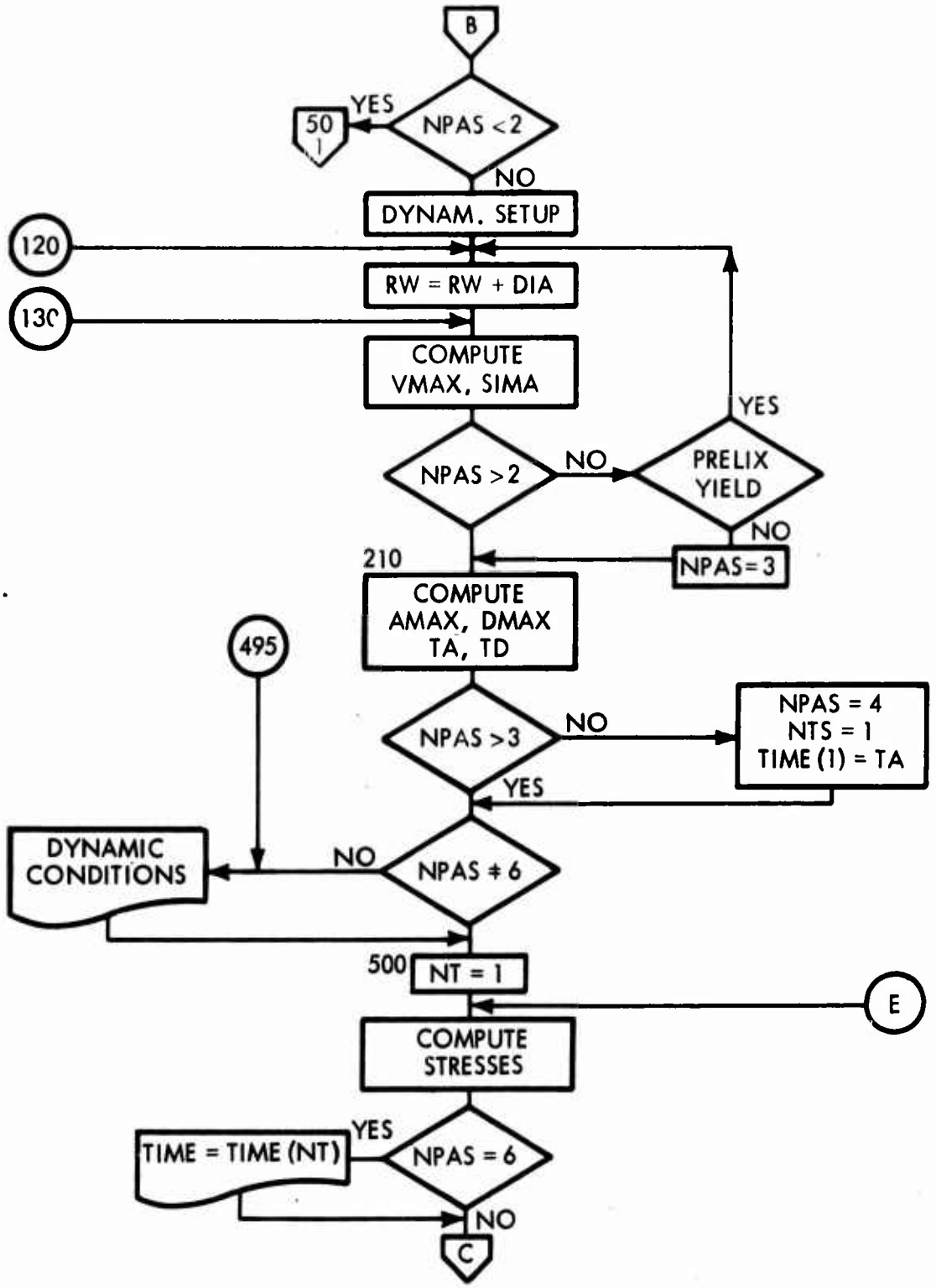

Figure 37—continued.

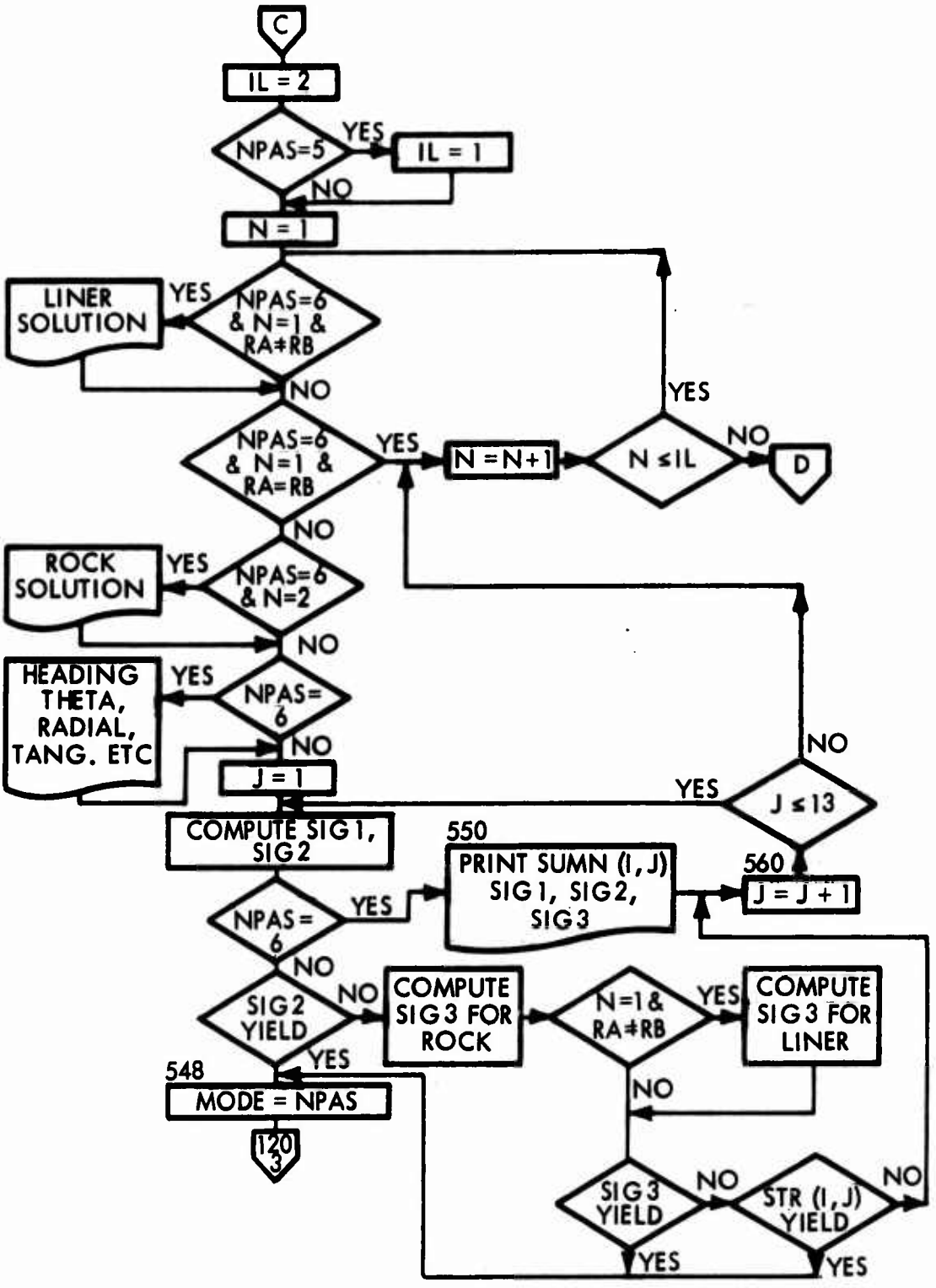

Figure 37—continued.

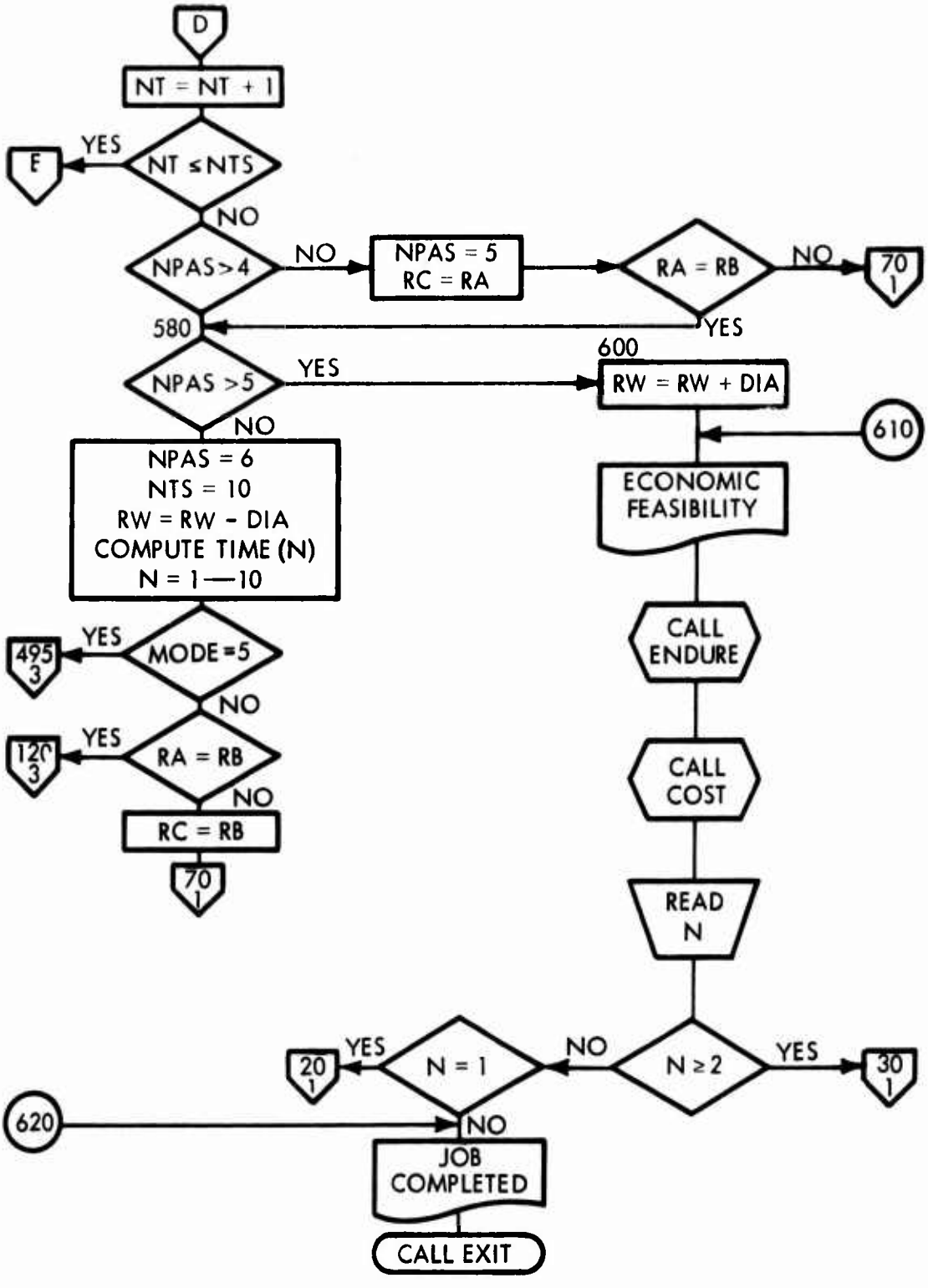

Figure 37—continued.

DISTRIBUTION LIST

Capt. F. L. Brand, NAVELEX PME 117-21, Main Navy Building, Washington, D. C. 20360 (1)

Mr. W. J. Bobisch, Code 04B, Naval Facilities Engineering Command, Navy Department, Washington, D. C. 20390 (1)

Mr. J. E. Don Carlos, NAVELEX PME 117T, Main Navy Building, Washington, D. C. 20360 (1)

Capt. R. S. Gardiner, OPNAV, The Pentagon, Room 5D786, Washington, D. C. 20350 (1)

Dr. D. H. Blumberg, CSC Systems Division, 6565 Arlington Blvd., Falls Church, Virginia 22046 (1)

Mr. N. Christofilos, I. D. A., 400 Army Navy Drive, Arlington, Virginia 22202 (1)

Dr. B. Kruger, NAVELEX PME 117-21A, Main Navy Bldg., Washington, D. C. 20360 (1)

LCDR. W. J. Laufersweiler, Code 054D, Naval Facilities Engineering Command, Navy Department, Washington, D. C. 20390 (1)

Mr. J. Merrill, Code 2004, NUSL Fort Trumbull, New London, Conn. 06320 (1)

Dr. T. P. Quinn, ONR 4101, Main Navy Bldg., Washington, D. C. 20360 (1)

Dr. H. L. Yudkin, M. I. T. Lincoln Laboratory, 244 Wood Street, Lexington, Mass. 02173 (1)

Mr. J. G. Lewis, Defense Atomic Support Agency, Washington, D. C. 20305 (2)

Dr. Henry Cooper, Air Force Weapons Laboratory, Kirtland Air Force Base, New Mexico 87117 (1)

Dr. N. M. Newmark and Assoc., Head, Civil Eng. Depart., University of Illinois, Urbana, Illinois 46990 (1)

Code SMQNM, Space and Missile Systems Organization, Norton Air Force Base, San Bernardino, Calif. 92409 (1)

Agbabian-Jacobsen Associates, 8939 S. Sepulveda Blvd., Los Angeles, Calif. 90045 (1)

Mr. J. R. Allgood, Naval Civil Eng. Laboratory, Structures Division, Port Hueneme, Calif. 93041 (1)

Defense Documentation Center, Bldg. 5, Cameron Station, Alexandria, Va. 22314 (20)

Naval Civil Engineering Laboratory
OPTIMUM POSITIONING OF DEEP UNDERGROUND TUNNELS IN ROCK (U), by J. Rottgerkamp
TR-677 115 p. illus April 1970 Confidential

1. Underground facilities—Design criteria I. YF 008.08.02.108

(U) The objective of this study was to define the limit survival distances from ground zero for deep underground protective structures in rock and to formalize a methodology for defining the cost of such systems. To achieve this objective, a computer program was developed and subsequently was exercised for representative tunnels with concrete and steel liners in sandstone or granite.

Limit distance contours were obtained for a range of effective seismic velocities. They show that there are optimum depths which, if exceeded, will increase the survival distance and decrease the survivability. The optimum site profile consists of a thick soil layer over a strong basement rock.

Steel liners provide greater survivability and lower cost than concrete liners. Interestingly, the type of enveloping rock appears to be more significant to survival for smaller yield weapons than for larger ones. It is apparent from the results that deep underground protective structures can be designed for high degrees of survivability.

Naval Civil Engineering Laboratory
OPTIMUM POSITIONING OF DEEP UNDERGROUND TUNNELS IN ROCK (U), by J. Rottgerkamp
TR-677 115 p. illus April 1970 Confidential

1. Underground facilities—Design criteria I. YF 008.08.02.108

(U) The objective of this study was to define the limit survival distances from ground zero for deep underground protective structures in rock and to formalize a methodology for defining the cost of such systems. To achieve this objective, a computer program was developed and subsequently was exercised for representative tunnels with concrete and steel liners in sandstone or granite.

Limit distance contours were obtained for a range of effective seismic velocities. They show that there are optimum depths which, if exceeded, will increase the survival distance and decrease the survivability. The optimum site profile consists of a thick soil layer over a strong basement rock.

Steel liners provide greater survivability and lower cost than concrete liners. Interestingly, the type of enveloping rock appears to be more significant to survival for smaller yield weapons than for larger ones. It is apparent from the results that deep underground protective structures can be designed for high degrees of survivability.

Naval Civil Engineering Laboratory
OPTIMUM POSITIONING OF DEEP UNDERGROUND TUNNELS IN ROCK (U), by J. Rottgerkamp
TR-677 115 p. illus April 1970 Confidential

1. Underground facilities—Design criteria I. YF 008.08.02.108

(U) The objective of this study was to define the limit survival distances from ground zero for deep underground protective structures in rock and to formalize a methodology for defining the cost of such systems. To achieve this objective, a computer program was developed and subsequently was exercised for representative tunnels with concrete and steel liners in sandstone or granite.

Limit distance contours were obtained for a range of effective seismic velocities. They show that there are optimum depths which, if exceeded, will increase the survival distance and decrease the survivability. The optimum site profile consists of a thick soil layer over a strong basement rock.

Steel liners provide greater survivability and lower cost than concrete liners. Interestingly, the type of enveloping rock appears to be more significant to survival for smaller yield weapons than for larger ones. It is apparent from the results that deep underground protective structures can be designed for high degrees of survivability.

Naval Civil Engineering Laboratory
OPTIMUM POSITIONING OF DEEP UNDERGROUND TUNNELS IN ROCK (U), by J. Rottgerkamp
TR-677 115 p. illus April 1970 Confidential

1. Underground facilities—Design criteria I. YF 008.08.02.108

(U) The objective of this study was to define the limit survival distances from ground zero for deep underground protective structures in rock and to formalize a methodology for defining the cost of such systems. To achieve this objective, a computer program was developed and subsequently was exercised for representative tunnels with concrete and steel liners in sandstone or granite.

Limit distance contours were obtained for a range of effective seismic velocities. They show that there are optimum depths which, if exceeded, will increase the survival distance and decrease the survivability. The optimum site profile consists of a thick soil layer over a strong basement rock.

Steel liners provide greater survivability and lower cost than concrete liners. Interestingly, the type of enveloping rock appears to be more significant to survival for smaller yield weapons than for larger ones. It is apparent from the results that deep underground protective structures can be designed for high degrees of survivability.

Unclassified

Security Classification

DOCUMENT CONTROL DATA - R & D

(Security classification of title, body of abstract and indexing annotation must be entered when the overall report is classified)

1. ORIGINATING ACTIVITY (Corporate author)	2a. REPORT SECURITY CLASSIFICATION
Naval Civil Engineering Laboratory Port Hueneme, California 93041	Confidential
	2b. GROUP 1

3. REPORT TITLE

OPTIMUM POSITIONING OF DEEP UNDERGROUND TUNNELS IN ROCK (U)

4. DESCRIPTIVE NOTES (Type of report and inclusive dates)

Not final; September 1968 – September 1969

5. AUTHOR(S) (First name, middle initial, last name)

J. Rottgerkamp

6. REPORT DATE	7a. TOTAL NO. OF PAGES	7b. NO. OF REFS
April 1970	115	15

8a. CONTRACT OR GRANT NO.	9a. ORIGINATOR'S REPORT NUMBER(S)
b. PROJECT NO. YF 008.08.02.108	TR-677
c.	9b. OTHER REPORT NO(S) (Any other numbers that may be assigned this report)
d.	

10. DISTRIBUTION STATEMENT

11. SUPPLEMENTARY NOTES	12. SPONSORING MILITARY ACTIVITY
	Naval Facilities Engineering Command Washington, D. C. 20390

13. ABSTRACT

(U) The objective of this study was to define the limit survival distances from ground zero for deep underground protective structures in rock and to formalize a methodology for defining the cost of such systems. To achieve this objective, a computer program was developed and subsequently was exercised for representative tunnels with concrete and steel liners in sandstone or granite.

Limit distance contours were obtained for a range of effective seismic velocities. They show that there are optimum depths which, if exceeded, will increase the survival distance and decrease the survivability. The optimum site profile consists of a thick soil layer over a strong basement rock.

Steel liners provide greater survivability and lower cost than concrete liners. Interestingly, the type of enveloping rock appears to be more significant to survival for smaller yield weapons than for larger ones. It is apparent from the results that deep underground protective structures can be designed for high degrees of survivability.

DD FORM 1 NOV 65 1473 (PAGE 1)

S/N 0101-807-6801

Unclassified

Security Classification

14 KEY WORDS	LINK A		LINK B		LINK C	
	ROLE	WT	ROLE	WT	ROLE	WT
Computer programs						
Design criteria						
Cost engineering						
Positioning						
Tunnels						
Underground facilities						
Subsurface structures						
Shelters						
Survival						
Velocity						
Seismic waves						
Tunnel linings						
Rock mechanics						